DEVELOPMENT AND CHARACTERIZATION OF ANTI-INFLAMMATORY COATINGS FOR IMPLANTED NEURAL PROBES

A Dissertation
Presented to
The Academic Faculty

by

Yinghui Zhong

In Partial Fulfillment
of the Requirements for the Degree
Doctor of Philosophy in the
School of Biomedical Engineering

Georgia Institute of Technology
December 2006

DEVELOPMENT AND CHARACTERIZATION OF ANTI-INFLAMMATORY COATINGS FOR IMPLANTED NEURAL PROBES

Approved by:

Dr. Ravi V. Bellamkonda, Advisor
School of Biomedical Engineering
Georgia Institute of Technology

Dr. Julia E. Babensee
School of Biomedical Engineering
Georgia Institute of Technology

Dr. Michelle C. LaPlaca
School of Biomedical Engineering
Georgia Institute of Technology

Dr. Todd C. McDevitt
School of Biomedical Engineering
Georgia Institute of Technology

Dr. Robert J. McKeon
Department of Cell Biology
Emory University School of Medicine

Georgia Institute of Technology

Date Approved: Noverber 20, 2006

ACKNOWLEDGEMENTS

First of all, I would like to thank my advisor Dr. Ravi Bellamkonda, who always guides, supports and encourages me through my entire Ph.D. study. He not only gave me the opportunity to receive the advanced education and to work on this exciting project, but also provided me of his instructions, experiences and knowledge to help me go through all the difficulties and challenges I have met in the past years. I would like to express my sincere appreciation to the member of my thesis committee, Dr. Robert J. McKeon, Dr. Julia E. Babensee, Dr. Michelle C. LaPlaca, and Dr. Todd C. McDevitt, for taking the time to guide me through my dissertation. I would like to express my appreciation to their valuable comments and suggestions to my project.

I want to thank all the past and present members of the Bellamkonda Group, who have helped created a friendly and supportive research environment. In particular, I wish to thank Xiaojun Yu, Nancy Meilander, Ryan Gilbert, Justin Saul, Mahesh Dodla, Anjana Jain, Katie McNeeley, Chenyu Kao, Rupal Thazhath, Wei He, Yong-tae Kim, and George McConnell. I would like to express my sincere gratitude to Jim Ross, Kacy Cullen, Matt Davis, Peter Crapo, Matthew Ward, and Thomas Schneider for their help in my research.

Finally, to my family, who always support me and make my work meaningful.

TABLE OF CONTENTS

LIST OF TABLES

LIST OF FIGURES

SUMMARY

Stable single-unit recordings from the nervous system using microelectrode arrays can have significant implications for the treatment of a wide variety of sensory and movement disorders. However, the long-term performance of the implanted neural electrodes is compromised by the formation of glial scar around these devices, which is a typical consequence of the inflammatory tissue reaction to implantation-induced injury in the CNS. The glial scar is inhibitory to neurons and forms a barrier between the electrode and neurons in the surrounding brain tissue. Therefore, to maintain long-term recording stability, reactive gliosis and other inflammatory processes around the electrode need to be minimized.

This work has succeeded in the development of neural electrode coatings that are capable of sustained release of anti-inflammatory agents while not adversely affecting the electrical performance of the electrodes. The effects of coating methods, initial drug loadings on release kinetics were investigated to optimize the coatings. The physical properties of the coatings and the bioactivity of released anti-inflammatory agents were characterized. The effect of the coatings on the electrical property of the electrodes was tested. Two candidate anti-inflammatory agents were screened by evaluating their anti-inflammatory potency *in vitro*. Finally, neural electrodes coated with the anti-inflammatory coatings were implanted into rat brains to assess the anti-inflammatory potential of the coatings *in vivo*. This work represents a promising approach to attenuate astroglial scar around the implanted silicon neural electrodes, and may provide a

promising strategy to improve the long-term recording stability of silicon neural electrodes.

CHAPTER I

INTRODUCTION AND BACKGROUND

Introduction

Stable single-unit recordings from the nervous system using microelectrode arrays can have significant implications for the treatment of a wide variety of sensory and movement disorders. However, the long-term performance of the implanted neural electrodes is compromised by the formation of glial scar around these devices, which is a typical consequence of the inflammatory tissue reaction to implantation-induced injury in the CNS. The glial scar is inhibitory to neurons and forms a barrier between the electrode and neurons in the surrounding brain tissue (Cui et al., 2003; Schwartz, 2004; Turner et al.; 1999). Therefore, to maintain long-term recording stability, reactive gliosis and other inflammatory processes around the electrode need to be minimized.

The overall goal of this research was to develop and characterize coatings capable of local release of anti-inflammatory agents to reduce the reactive cellular and molecular brain responses, while not adversely affecting the electrical performance of the electrodes. This strategy may help stabilize the electrode-brain interface and potentially facilitate long-term recording from neural electrodes *in vivo*. The first objective of this research was the development of coatings for sustained release of anti-inflammatory drugs. Nitrocellulose is a biocompatible polymer with high binding capacity for proteins and nucleic acids. The capacity of nitrocellulose as the polymer matrix for incorporation of anti-inflammatory agents was explored. The anti-inflammatory neuropeptide α-

melanocyte stimulating hormone (α-MSH) was used to investigate the effects of coating methods, initial drug loadings on release kinetics. The physical properties of the coatings and the bioactivity of released α-MSH were characterized. The effect of the coatings on the electrical properties of the electrodes was tested (Chapter II). Dexamethasone (DEX) is a potent anti-inflammatory agent that has been used clinically to treat many inflammatory responses. The capacity of nitrocellulose coatings to be used for sustained delivery of DEX was explored in Chapter III. The next step towards the overall objective was selection of an effective anti-inflammatory agent to be used in the electrode coatings for *in vivo* evaluation. The anti-inflammatory potency of α-MSH and DEX was evaluated *in vitro*, and DEX was shown to be a more powerful anti-inflammatory agent than α-MSH. The anti-inflammatory effects and neurotoxicity of DEX at various dosages were further investigated *in vitro* (Chapter IV). Neural electrodes coated with nitrocellulose-DEX coatings were then implanted into rat brains, and the anti-inflammatory potential of the coatings was evaluated using histological analysis (Chapter V). This work represents a promising approach to attenuate astroglial scar around the implanted silicon neural electrodes, and may provide a promising strategy to improve the long-term recording stability of silicon neural electrodes.

Application of Cortical Neural Prosthetics in Pathological Disorders

Cortical neural prosthetics (CNPs) are a subset of neural prosthetics, a larger category that includes stimulating, as well as recording, electrodes. Stimulation-based devices have now been used extensively in applications to restore hearing functions and alleviate the symptoms of Parkinson's disease by activating neurons in different parts of

the CNS (Schwartz, 2004; Pesaran et al., 2006). Recording-based devices are called brain-computer interfaces (BCIs). The BCI is an interface in which a brain accepts and controls a mechanical device as a natural part of its representation of the body. By reading signals from an array of neurons and using computer chips and programs to translate the signals into action, these devices provide possibility for paralyzed patients to control a motorized wheelchair or a prosthetic limb through thought (Donoghue, 2002; Schwartz, 2004, Pesaran et al., 2006). An example is the implantable microelectrodes embedded chronically in the cerebral cortex that can link the brain to the external world by processing the recoded neural signals to extract the subject's command to control an external device as shown in Figure 1.1.

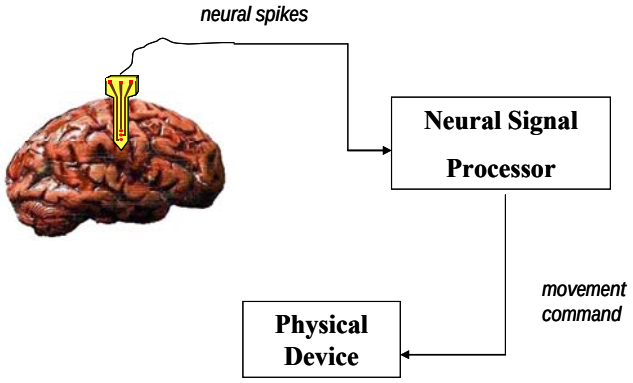

Figure 1.1: The organization of a brain-computer interface (BCI). In the output BCI, the implanted microelectrode detects the neural-coded intent, which is processed and decoded into a movement command. The command drives a physical device such as a computer or an artificial limb so that the intent becomes action.

This technology holds great promise for patients with impaired movement functions, which can be caused by stroke, cervical spine injuries, and neurodegenerative diseases such as multiple sclerosis and amyotrophic lateral sclerosis (ALS). However,

despite the clinical success of the stimulation-based CNPs, the recording-based CNPs are still in research stage due to the problem of long term recording stability (Schwartz, 2004; Ludwig et al., 20006; Donoghue, 2002; Santhanam et al., 2006). When these devices are implanted into brain tissue for long-term recording, they lose the ability to record neural activity a few days to weeks after implantation (Cui et al., 2003; Schwartz, 2004). The major cause of this problem is the formation of glial scar around the Si-microelectrodes, which is a typical consequence of the inflammatory tissue reaction caused by the injuries and implants in the CNS. The glial scar forms an inhibitory barrier for axon re-growth and functions as a diffusive barrier that is thought to reduce the ability of implanted devices to communicate with neurons by insulating the device from the surrounding brain tissue (Properzi et al., 2003; Cui et al., 2003; Schwartz, 2004; Turner et al., 1999, Biran et al., 2005).

Multiple Recording Electrode Types

Investigators are currently working on developing multi-channel recording microelectrode arrays for long-term cortical neuronal recordings (Kipke et al., 2003; Polikov et al., 2005, Schwartz, 2004). Numerous types of microelectrode arrays have been developed, including microwires (Williams et al., 1999; Kralik et al., 2001; Nicolelis et al., 1999), silicon micromachined microprobes (Hetke and Anderson, 2002; Jones et al., 1992, Ludwig et al., 2006, Drake et al., 1988; Campbell et al., 1991), and polymer-substrate probes (Rousche et al., 2001, Stieglitz et al., 2000). Among the different electrode types, microwire electrode arrays and silicon micromachined

microprobes are the two main types of electrode arrays currently being explored (Polikov et al., 2005, Schwartz, 2004) because they are easy to process and fabricate.

The first chronic recording electrodes were microwires (Figure 1.2A). Microwire electrodes consist of fine wires 20 to 50 microns in diameter (Schwartz, 2004). The wires are generally made of conductive medals including platinum, gold, tungsten, iridium, and stainless steel, that are insulated with teflon or polyimide (Polikov et al., 2005, Schwartz, 2004). The tips of the wires are not insulated and are used for recording neuronal signals (Polikov et al., 2005). The wires can be arranged as arrays by soldering them to a small connector to acquire more accessibility to neurons necessary for neuroprosthetic control (Williams et al., 1999; Nicolelis et al., 1999; Polikov et al., 2005, Schwartz, 2004).

Compared with silicon micromachined microprobes, microwire electrodes have the advantages of ease in fabrication as well as low electrode impedance. Impedance is proportional to both thermal noise and signal loss, and consequently, low impedance improves signal transport across the neural interface and helps to increase the detection sensitivity to neural activity (Ludwig et al., 2006; Cui et al., 2001; Robinson et al., 1968). One of the causes of the failure of microelectrode arrays in long-term recording is the increase of electrode impedance over time due to tissue reaction (Liu et al., 1999; Schwartz, 2004, Cui et al., 2003). It has been shown that electrode impedance was well correlated with tissue reactivity around the implanted electrodes (Williams, 2001). Therefore the low impedance of microwire electrodes potentially leads to chronic recording stability. However, there have been studies showing that the number of functional electrodes declines with time for microwire electrode arrays (Nicolelis et al.,

2003), indicating that long term recording stability is also an issue for microwire electrodes. The recording sites for microwire electrodes are the tips of the wires, and the arrays are glued to the skull, so the depth of the electrode tip relative to the skull is fixed. If the cortical surface moves after the surgery, the relative position of the electrode tip to the brain tissue will change. This may cause it to move to a different cortical layer or white matter, and fail to record neural signals of interest (Schwartz, 2004; Polikov et al., 2005). As a result, the same individual neurons can not be "tracked" longer than about six weeks (Rousche et al., 2001; Williams et al., 1999; Nicolelis et al., 1997)

Silicon micromachined microprobes are the next generation of electrode arrays. Silicon photolithographic processing allows for unsurpassed control over electrode size, shape, texture, and spacing; allowing multiple recording sites to be placed on a single electrode shank (Polikov et al., 2005). A number of silicon-based microelectrode arrays have been developed; nevertheless, two particular designs have attained prominence in the field (Schwartz, 2004; Polikov et al., 2005, vetter et al., 2004). The first is planar electrode arrays developed by the University of Michigan Center for Neural Communication Technology (Figure 1.2C). The Michigan probes have several important advantages over microwires including batch fabrication, high reproducibility of geometrical and electrical characteristics, precise and repeatable relative electrode locations; high density recording sites; and the ability to integrate circuits directly on the probes (Vetter et al., 2004; Kewley et al., 1997; Polikov et al., 2005). The shanks of the Michigan probes are 15 microns thick and 100 to 500 microns wide, with the length ranging from 3 mm to 1 cm. Compared with microwire arrays, the Michigan probes have more accessibility to neurons of interest because the multiple recordings sites are placed

along the probe, at least some of the sites will be situated at cortical depths desirable for good extracellular recordings (Schwartz et al., 2004).

The other prominent silicon electrode design comes from University of Utah, which is now commercially available through Cyberkinetics (Figure 1.2B). The Utah Electrode Array (UEA) is fabricated from a single block of silicon which, through etching, doping, and heat treatment, results in a three-dimensional, 5 x 5 or 10 x 10 arrays of needles on a 4 x4 mm squire. The array has a recording site at the tip of each shank. The shank length ranges from 1.0 to 1.5 mm, the diameter ranges from 100 micron at its base to less than 1 micron at the tip (Schwartz, 2004; Polikov et al., 2005). This design has the advantage of placing a relatively large number of recording sites in a compact volume of cortex. However, with a single recording site at a fixed cortical depth, the UEAs suffer from the same positioning problem as microwires that lead to the failure of recording the same group of neurons over time (Schwartz, 2004).

This common drawback of the microwire electrodes and UEAs reduces the attractiveness of these two types of electrodes for long-term chronic implant. The Michigan probes have unique advantages over the other two types of electrode arrays in that it has more accessibility to neurons and flexible designs. However, the scar tissue encapsulation, which raises the electrode impedance, is a more severe problem for the Michigan probes because of their high electrode impedance. The Michigan probes are usually capable of recording good action potentials for the first one to three weeks after implantation, after which time the signal degrades (Schwartz, 2004). Therefore the research of this dissertation was focused on reducing the tissue reaction to the Michigan

probes. The methods developed in this research, however, is also applicable to other types of electrodes.

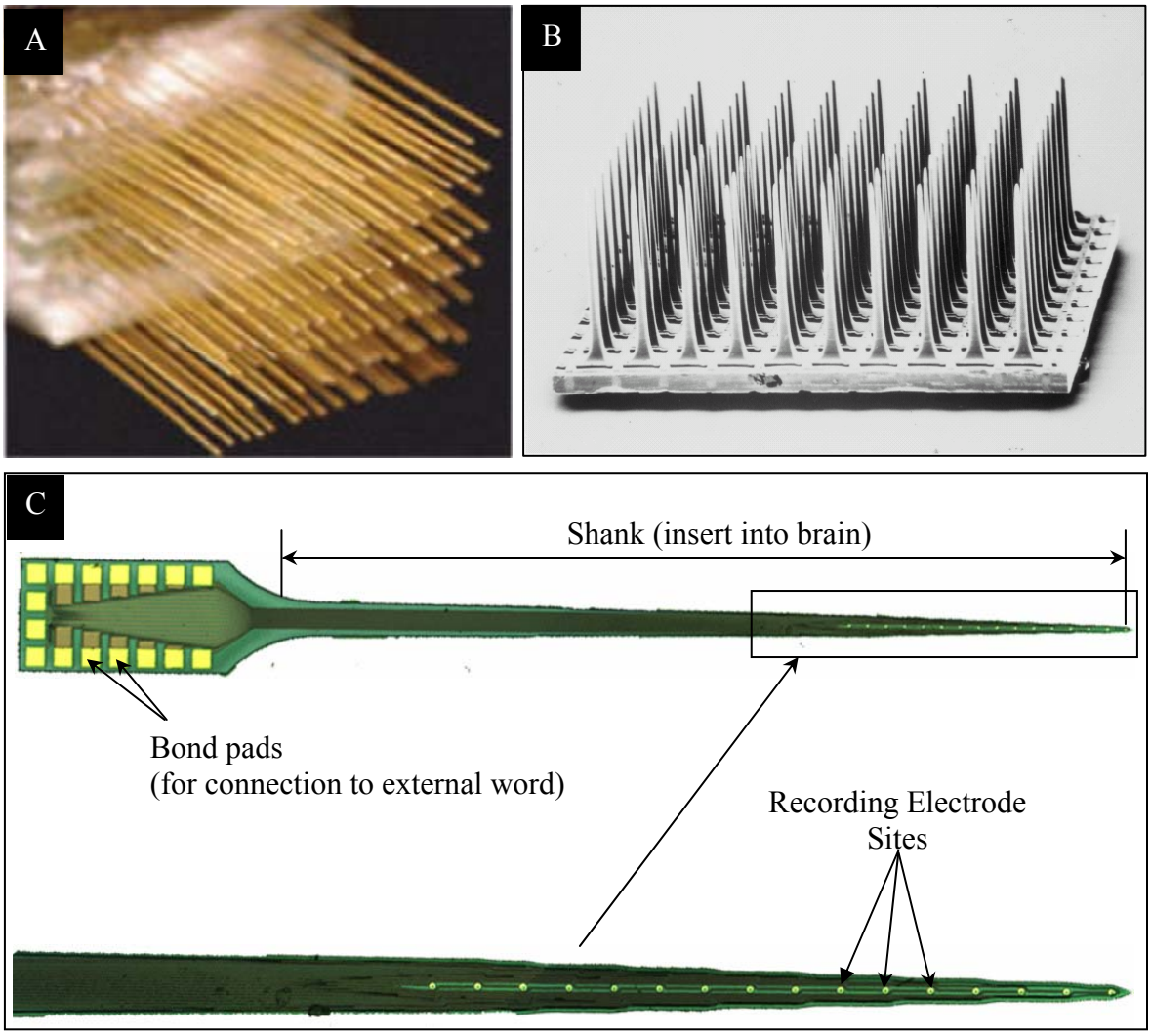

Figure 1.2: Various designs of electrode types. (A) An example of a microwire electrode array formed by Teflon coated stainless microwires. (from Nicolelis et al, 2003). (B) Utah Electrode Array formed from a single block of silicon. (from Rousche and Normann, 1998). (C) A 16 channel, single shank Michigan recording probe. The probe part in the box is magnified in to show the 16 recording electrode sites.

Factors Affecting Tissue Reaction to the Implanted Neural Electrodes

Factors that affect the brain tissue reaction to the implanted neural electrodes include the mechanical trauma during insertion, foreign body reaction, electrode insertion and implantation methods, and physical properties of the electrodes (size, shape, as well as surface characteristics).

When a neural probe is inserted into the brain, neurons and glial cells are killed or injured during insertion, blood vessels are disrupted and the blood-brain barrier (BBB) is damaged. This mechanical trauma and the presence of neural probe as foreign material initiates the cellular and molecular cascades of the central nervous system (CNS) wound healing response. The tissue injury and breakdown of BBB cause release of cytokines and neurotoxic free radicals, as well as invasion of blood-borne macrophages (Fitch and Silver, 1997; Schwartz, 2004). Insertion induced accumulation of fluid and necrotic nervous tissue cause edema, further adding the pressure surrounding the probe. The main cell types involved in the inflammatory and wound healing response to the brain injury and materials implanted in the CNS are microglia/blood-borne macrophages, oligodendrocyte precursors (OPCs), and astrocytes (Fawcett and Asher, 1999; Norton, 1999; Hampton et al, 2004, Polikov et al., 2005). Microglia/macrophages and OPCs respond very rapidly to brain injuries (Fawcett and Asher, 1999; Hampton et al, 2004, Kato and Walz, 2000). Following injury to the adult CNS, a large number of microglia/macrophages and OPCs were recruited to the injury site. The microglia/macrophages are activated upon adherence to the material surface (Anderson, 2001). The activated microglia/blood-borne macrophages release neurotoxic molecules such as free radicals, nitric oxide (NO), as well as proinflammatory cytokines including interleukin-1 (IL-1), tumor necrosis factor-α (TNF-α) and interleukin-6 (IL-6)

(Kyrkanides et al, 2001; Hays, 1999; Bruccoleri et al, 1998; Takeuchi et al, 2001), which subsequently activate the astrocytes (Merrill and Benveniste, 1996; John et al, 2005). The activation of astrocytes is also mediated by blood-borne factors including growth factors and hormone, albumin, thrombin, angiotensin II and cAMP (Logan and Berry, 2002) The reactive astrocytes undergo hypertrophy, proliferation, and upregulate trophic factors, cytokines, as well as extracellular matrix (Fawcett and Asher, 1999; Polikov et al., 2005).

Chondroitin sulfate proteoglycans (CSPGs) are important inhibitory molecules in glial scar (Properzi and Fawcett, 2004; Fawcett and Asher, 1999). Astrocytes produce neurocan, phosphacan, and brevican; microglia/macrophages produce NG2; and OPCs produce neurocan, NG2, and versican (Properzi and Fawcett, 2004; Fawcett and Asher, 1999; Tang et al., 2003; Tatsumi et al, 2005; Hampton et al, 2004). It has recently been suggested that part of NG2 positive cells proliferating in the injury site differentiate into the glial scar astrocytes (Alonso et al, 2005; Tatsumi et al 2005). The CSPGs and other glial scar associated inhibitory molecules create an inhibitory environment that blocks the regrowth of neural processes and may potentially cause the exclusion of neural cells by their presence.

Several research groups have been investigating the effects of insertion speed and implantation method on tissue reaction to implanted neural probes. One study using microwire electrode arrays shows that slow insertion rate (100 μm/s) may contribute to the unusually large number of single units recorded in this study (Nicolelis et al., 2003). In contrast, the silicon-based UEAs require a minimum insertion rate of 8.3 m/s for a complete, safe insertion of all 100 electrodes in the array to a depth of 1.5 mm into the

cortex (Rousche and Normann, 1991). Other groups use insertion rates in between these two extremes on the planar silicon electrode arrays (i.e. the Michigan probes and probes with similar design) (Turner et al., 1999; Szarowski et al., 2003). However, the effects of different insertion rates on tissue reaction to the planar silicon electrode arrays remain unknown.

There are two insertion methods that are currently in use. Some groups insert the electrodes by hand (Kipke et al., 2003; Szarowski et al., 2003; Liu et al., 1999; Biran et al., 2005), while other groups use microdrives with controlled speed and positioning that either custom-built or commercially available (Spataro et al., 2005; Turner et al., 1999; Szarowski et al., 2003; Nicolelis et al., 2003). UEAs can not be inserted by hand because of the high insertion rate required for a complete and safe insertion. The other two types of electrodes can be inserted either by hand or a microdrive. There is no experimental evidence showing which implantation method is optimal for the microwire electrode arrays and planar silicon electrode arrays. A study on planar silicon electrode arrays using both implantation methods suggests that the implantation method does not influence the long-term tissue reaction (Szarowski et al., 2003).

The physical properties of the microelectrode arrays (size, shape, as well as surface characteristics) are other factors that may contribute to the tissue reaction to implanted microelectrodes. It has been suggested that the prosthesis with small size, smooth surfaces and round corners are likely to create less tissue damage at the time of insertion (Edell et al., 1992). However, a recently study compared the tissue response to the planar silicon electrode arrays of different sizes, shapes, and surface characteristics through GFAP, vimentin, and ED-1 staining. The histological evidence indicated that

although these factors made a difference in the tissue reaction around the implanted devices in the first one week after implantation, responses observed after four weeks were similar for all devices (Szarowski et al., 2003).

Strategies to Minimize Tissue Reaction to the Implanted Neural Electrodes

A number of Research groups are working on different approaches to reduce the inflammatory tissue response around the implanted neural electrodes. These approaches can be divided into two categories: the materials science strategies and the bioactive molecule strategies (Polikov et al., 2005). The materials science strategies include modifying the size and shape of the electrodes (Edell et al., 1992; Szarowski et al., 2003), or using alternative materials such as polymers (Rousche et al., 2001, Stieglitz et al., 2000) or ceramics (Moxon et al., 2004; Singh et al., 2003). However, none of these efforts showed any significant reduction of the inflammatory tissue reaction.

The bioactive molecules strategies have focused on administration of anti-inflammatory agents through electrode coatings (Kim and Martin, 2006), direct injection through microchannels fabricated into the electrodes (Retterer et al., 2004), or systemic injection (Spataro et al., 2005). Systemic injections or local release of anti-inflammatory agents from non-functional polymers has been shown to reduce the reactive tissue reaction to the neural implants (Spatara et al., 2005; Shain et al., 2003). Systemic injection, though effective and easy to operate, is not a viable option because of the sides effects associated with peripheral metabolism and chronic use, and the difficulty for the drugs to cross the blood-brain barrier (Kim and Martin, 2006; Retterer et al., 2004).

Several research groups are seeking to integrate the microfluidic drug delivery systems into the functioning electrical devices in device fabrication (Chen et al., 1997; Rathnasingham et al., 2004; Retterer et al., 2004). Microfluidic channels capable of releasing biomolecules have been successfully integrated into silicon neural prosthetics. The diffusion of test biomolecules from the microfluidic channels was investigated both *in vitro* and *in vivo* (Retterer et al., 2004). In some designs, the drug releasing rate can be controlled by pumps and valves (Papargeorgiou et al., 2001). These studies represent preliminary steps toward developing a viable clinical intervention strategy to improve the biocompatibility and chronic stability of silicon-based multielectrode arrays (Retterer et al., 2004).

An alternative strategy for local drug delivery is through electrode coatings. To date three types of anti-inflammatory bioactive coatings for neuroprosthetics have been reported, poly(ethylene-co-vinyl) acetate (EVAc) coatings capable of releasing anti-inflammatory agent monocycline (Bjornsson et al., 2003), alginate hydrogel matrices embedded with dexamethasone (DEX) loaded PLGA nanoparticles (Kim and Martin, 2006), and conducting polymer polypyrrole coatings using dexamethasone phosphate as the negative dopant (Wadhwa et al., 2006).

EVAc as a drug releasing polymer has been well studied. It has been successfully used for slow release of proteins as well as small molecule drugs (Saltzman et al., 1999; Cypes et al., 2003). However, *In vivo* study showed that EVAc-monocycline coated neural prosthetic devices generated more severe tissue reaction than uncoated devices (Bjornsson et al., 2003). It remains unclear that the failure of this coating is due to EVAc polymer matrix or the drug monocycline.

Conducting polymer polypyrrole was electrochemically deposited onto the electrode sites of the Michigan neural probes using dexamethasone phosphate as the negatively charged dopant (Wadhwa et al., 2006). The drug release can be controlled by electrical stimulation. *In vitro* studies showed that the released drug remained bioactive. However, the efficacy of the coatings was not tested *in vivo* yet. As the total area of the electrode sites is less than 0.5% of the total neural probe area, and the conducting polymer can only be deposited on the electrode sites, less than 0.5% probe surface is coated. Therefore the potency of the anti-inflammatory effects of the coating is in question.

DEX loaded PLGA nanoparticles embedded in alginate hydrogel were coated on the Michigan probes by dip coating (Kim and Martin, 2006). Sustained release has been observed for up to 3 weeks *in vitro*. *In vivo* study showed that the impedance amplitude for the DEX coated electrodes did not change while that of the control electrodes increased 3 times about 2 weeks after implantation. However, the authors didn't perform a histological study to correlate the improved impedance with tissue reaction.

In summary, local administration of anti-inflammatory drugs from microfluidic channels or bioactive coatings of the neural prosthetics has the capacity to manage the cellular and tissue responses around the implanted devices, and therefore holds great promise to solve the long-term stability problem of chronically implanted neural electrodes. Thus the research of this dissertation will be focused on the bioactive coatings strategy.

Nitrocellulose is a biocompatible polymer which has high binding capacity for proteins and nucleic acids. Although the mechanism of binding is not yet completely

understood, it appears to depend mainly on hydrophobic and electrostatic interactions that are caused by the nitrate dipole (Tijssen, 1993; Harlow and Lane, 1988; Wallis et al., 1979; Handman and Jarvis, 1988). Since nitrocellulose is a convenient substrate for rapid non-covalent attachment of proteins (Lagenaur and Lemmon, 1987), it is commonly used to attach extracellular matrix proteins to investigate cell adhesion and growth *in vitro* (Lagenaur and Lemmon, 1987; Snow et al., 1990; Vielmetter et al., 1990). NGF or laminin treated nitrocellulose has also been used *in vivo* to induce extensive axon growth after spinal cord injury in both adult and neonatal rats (Schreyer and Jones, 1987; Houle and Ziegler , 1994; Houle and Johnson, 1989). Although the high protein binding capacity of nitrocellulose has enabled its extensive use both *in vitro* and *in vivo* for cell adhesion, growth and tissue regeneration, its potential for drug release has yet to be explored. In this study, we proposed to use nitrocellulose as the polymer coating matrix for local release of anti-inflammatory agents.

Candidates of Anti-inflammatory Agents

Nuclear Factor Kappa B (NF-κB) is a crucial transcription factor that is essential to the expression of a large number of genes involved in cellular inflammation including MHC-1, IL-1, IL-6, IL-8, TNF-α, granulocyte colony-stimulating factor, chemokines, cylco-oxygenase, lipoxygenase, and nitric oxide synthase (Ichiyama et al., 1999; Manna and Aggarwal, 1998). Most types of inflammation require activation of NF-κB (Manna and Aggarwal, 1998). It has been shown in a number of model systems that NF-κB levels increase as a consequence of brain injury (Salminen et al., 1995; Yang et al., 1995). According to these models, it is possible that injury leads to an increase in production of

IL-1 or TNF, which then activate NF-κB, leading to induction of the expression of a range of pro-inflammatory genes (O'Neill and Kaltschmidt, 1997). Therefore, suppression of NF-κB action downregulates the expression of genes that are involved in inflammation. The advantage of targeting inflammation at the nuclear factor level is that the activation passways of many known (IL-1, TNF) and unknown inflammatory agents converge at this level, intervention at this level enables suppressing inflammation that may be caused by a variety of cytokines in response to neural injury.

A number of studies suggest that the neuropeptide α-melanocyte stimulating hormone (α-MSH) inhibits the production of proinflammatory cytokines and mediators via the modulation of NF-κB activation (Ichiyama et al., 1999; Manna and Aggarwal, 1998; Starowicz and Przewlcka, 2003). α-MSH is a tridecapeptide derived from a lager precursor molecule pro-opiomelanocortin (POMC) and found in pituitary, brain, skin, and circulation (Lipton and Catania, 1997; Oktar and Alican, 2002). The amino acid sequence of α-MSH is N-Acetyl-Ser-Tyr-Ser-Met-Glu-His-Phe-Arg-Trp-Gly-Lys-Pro-Val-NH_2. It has been shown that α-MSH inhibits the production and activity proinflammatory cytokines such as of IL-1β, IL-6, IFN-γ, and TNFα; downregulates the expression of co-stimulatory molecule such as CD86 and CD40, modulates the expression of nitric oxide synthase, and induces the production of suppressor factors such as the cytokine synthesis inhibitory factor IL-10 (Starowicz and Przewlcka, 2003; Luger et al., 1999, Oktar and Alican, 2002; Lipton et al., 2000; Star et al., 1995). The suppression of NF-κB by α-MSH was not cell type specific and was mediated through generation of cAMP and activation of PKA (Manna and Aggarwal, 1998). α-MSH has no known pharmacologic toxicity and is able to suppress NF-κB by various stimuli.

Therefore it is an excellent candidate as a powerful anti-inflammatory agent in the CNS, due to its pleiotropic effects on inflammation (Starowicz and Przewlcka, 2003).

Another anti-inflammatory drug candidate is dexamethasone (DEX). DEX is a synthetic glucocorticoid hormone that is used clinically to treat many inflammatory responses. Glucocorticoids in turn exert anti-inflammatory effects on many cell types including T cells, macrophages, eosinophils, neutrophils, mast cells, endothelial and epithelial cells, thereby creating a classical endocrine feedback loop (Smoak and Cidlowski, 2004). Most potent anti-inflammatory effects of glucocorticoids result from protein-protein interactions between glucocorticoid receptor (GR) and transcription factors, particularly NF-κB and activator protein-1 (AP-1) (Smoak and Cidlowski, 2004; Yamazaki et al., 2005). In CNS, systematic injection of DEX was shown to reduce tissue reaction around neural implants (Shain et al., 2003; Spataro et al., 2005). Addition of DEX to activated microglia-neuron cocultures protects neurons by down-regulating nitric oxide (NO) production (Golde et al., 2003). Its anti-inflammatory effects have usually been attributed to its effects on microglia/macrophages, which knowingly express high levels of glucocorticoid receptors (Tanaka et al., 1997). DEX has been show to inhibit proliferation, iNOS synthesis, and cytokine expression of microglia (Golde et al., 2003; Chao et al, 1992; Tanaka et al, 1997). A recently study showed that DEX inhibited proliferation of NG2 positive cells, which may differentiate into astrocytes in injured brain (Alonso, 2005). As these NG2 positive cells do not express the glucocorticoid receptors, the authors suggested that DEX may have indirect effects on these cells via modification of glutamate release and/or interaction with microglia. DEX also directly inhibits astrocyte proliferation (Crossin et al, 1997). It's very possible that DEX exerts

its anti-inflammatory effects on the glial cells through direct interactions with cells as well as the interactions among different types of cells. As DEX modulates the inflammatory responses of multiple types of glial cells, it is a promising drug candidate for controlling the reactive tissue response to the implanted neural electrodes.

CHAPTER II

DEVELOPMENT AND CHARACTERIZATION OF COATINGS CAPABLE OF RELEASING ALPHA-MSH FOR SILICON NEURAL PROBES[1]

Abstract

Si-multi-electrode arrays implanted into brain tissue for long-term recording lose electrical connectivity due to the post-implantation inflammatory reaction. This inflammatory reaction creates a physical and electrical gap between the electrode site and the surrounding neurons. In this study, novel nitrocellulose-based coatings were developed for the sustained delivery of the anti-inflammatory neuropeptide α-melanocyte stimulating hormone (α-MSH). α-MSH was incorporated in micron-scale nitrocellulose coatings and slow, sustained release over 21 days was attained *in vitro*. The α-MSH released on day 21 was still bioactive, and successfully inhibited nitric oxide (NO) production by lipopolysacchride (LPS) stimulated microglia. The amount of initial drug loading directly affected the release rate, with higher initial loading increasing the mass released but not the percent of drug released. The surface morphology and thickness of the coatings was examined by scanning electron microscopy (SEM) and profilometry. In

---

[1] Zhong Y., Bellamkonda R.V., 2005. Controlled release of anti-inflammatory agent alpha-MSH from neural implants. J Control Release. 106(3), 309-318.

addition, impedance measurement showed that the α-MSH loaded nitrocellulose coatings reduced the magnitude of electrode impedance at the biologically relevant frequency of 1 kHz. In conclusion, nitrocellulose-based, bioactive coatings that release anti-inflammatory agents and do not increase the impedance of the electrode were successfully fabricated. These coatings have the potential to reduce inflammation at the electrode-brain interface in *vivo*, and facilitate long-term recordings from Si-multi-electrode arrays.

Introduction

Stable single-unit recordings from the nervous system using Si-microelectrode arrays can have significant implications for the treatment of a wide variety of sensory and movement disorders. However, when these devices are implanted into neural tissue for long-term recording, they quickly (a few days to weeks) lose the ability to record from neurons. Histological evidence shows that a cellular sheath surrounds the insertion site of Si-microelectrodes, which is a typical consequence of inflammatory reaction resulting from physical injury to the CNS. In the CNS, this process of sheath formation is termed 'reactive gliosis' or astroglial scarring. This astroglial scar is inhibitory to neurons and forms a barrier between the electrode and neurons in the surrounding brain tissue. This problem is particularly apparent for the Michigan probes, which has relatively small recording sites and hence bigger impedance compared to the so-called Utah arrays and microwires (Cui et al., 2003; Schwartz, 2004; Turner et al., 1999).

To maintain long-term recording stability, reactive gliosis and other inflammatory processes around the electrode need to be minimized. The neuropeptide α-melanocyte

stimulating hormone (α-MSH) exerts powerful anti-inflammatory effects through inhibition of proinflammatory cytokine production and related mediators of inflammation (Ichiyama et al., 1999). A number of studies suggest that α-MSH inhibits the production of proinflammatory cytokines via the modulation of nuclear transcription factor-κB (NF-κB) activation, and the inhibition of NF-κB is a focal point in the mediation of the effects of melanocortins on cells of the immune system. α-MSH is an excellent candidate as a powerful anti-inflammatory agent in the CNS, due to its pleiotropic effects on inflammation and energy homeostasis (Starowicz and Przewlocka, 2003). In this study, the fabrication of nitrocellulose-based coatings on oxidized Si substrates for the sustained release of α-MSH is reported.

Conventional drug delivery systems such as microspheres are not ideal, as the limited surface area (about 1 mm^2) of the microelectrodes does not allow for sufficient loading of drug carriers to facilitate sustained release. Nitrocellulose is a biocompatible polymer which has high binding capacity for proteins and nucleic acids. Although the mechanism of binding is not yet completely understood, it appears to depend mainly on hydrophobic and electrostatic interactions that are caused by the nitrate dipole (Tijssen, 1993; Harlow and Lane, 1988; Wallis et al., 1979; Handman and Jarvis, 1988). Since nitrocellulose is a convenient substrate for rapid non-covalent attachment of proteins (Lagenaur and Lemmon, 1987), it is commonly used to attach extracellular matrix proteins to investigate cell adhesion and growth *in vitro* (Lagenaur and Lemmon, 1987; Snow et al., 1990; Vielmetter et al., 1990). NGF or laminin treated nitrocellulose has also been used *in vivo* to induce extensive axon growth after spinal cord injury in both adult and neonatal rats (Schreyer and Jones, 1987; Houle and Ziegler , 1994; Houle and

Johnson, 1989). Although the high protein binding capacity of nitrocellulose has enabled its extensive use both *in vitro* and *in vivo* for cell adhesion, growth and tissue regeneration, its potential for drug release has yet to be explored. In this study, α-MSH was incorporated into nitrocellulose coatings and sustained release of α-MSH over three weeks *in vitro* was achieved.

Polymer-based controlled release systems are normally classified as either reservoir (membrane) delivery systems or matrix (monolithic) delivery systems. In the former type release is controlled by a polymeric membrane that surrounds a drug containing reservoir, whereas in matrix devices the drug is either dissolved in or dispersed homogeneously throughout a polymer matrix (Richards, 1985; Saltzman, 2001; Polishchuk and Zaikov, 1997). Both delivery methods were investigated in this study using nitrocellulose as the polymer. The anti-inflammatory activity of α-MSH released from this nitrocellulose-based delivery system was tested through nitrite production by primary microglial cells, and impedance measurement was used to characterize the contribution of the coatings to electrode impedance.

Materials and Methods

Fabrication of α-MSH Loaded Nitrocellulose Coatings

Polished Si wafers of 1 cm^2 with a 10,000 Å oxide layer (University Wafer, MA) were cleaned by ultrasonification in deionized water and ethanol, and stored in 70% ethanol for sterilization. The wafers were dried under nitrogen and adhered to the spindle of a microcentrifuge (IEC) by a double-sided adhesive tape. 33.3 mg (5 cm^2) nitrocellulose (Schleicher & Schuell BioScience) was dissolved in 12 ml methanol; the

solution (20 µl) was then added to the surface of a wafer, followed by spinning at 2000 rpm for 30 s to enable spin coating.

Matrix delivery method. 100 or 400 µg α-MSH (Sigma) powder was mixed thoroughly with 20 µl nitrocellulose (NC) and evaporated on 1 cm^2 Si wafers. This α-MSH-NC layer was subsequently coated with 6 additional layers of pure nitrocellulose generated in the following manner- 3 layers of evaporation and 3 layers of spin coating (2000 rpm, 30 s). The α-MSH containing layer was termed as Matrix 100 and Matrix 400 based on the amount of α-MSH added to the nitrocellulose layer.

Reservoir delivery method. 100 or 400 µg α-MSH in water solution was evaporated on 1 cm^2 Si wafers. This α-MSH layer was subsequently coated with 6 additional layers of pure nitrocellulose as previously mentioned in the matrix delivery method, as Reservoir 100 and Reservoir 400.

In Vitro α-MSH Release Assay

Si wafers coated with α-MSH and nitrocellulose were incubated at 37°C either in PBS for quantification of α-MSH release, or in microglial cell culture medium (DMEM-F12 media supplemented with 10% fetal bovine serum) for bioactivity analysis with microglia cultures. The release medium (PBS or microglial cell culture medium) was changed every 24 h. The amount of α-MSH released every 24 h from triplicate samples (n = 3) was determined by the subtraction of the UV adsorption at 215 and 225 nm with a microplate reader (Bio-Tek instruments, VT). The α-MSH containing microglial cell culture medium collected every 24 h was stored at -20°C until bioactivity was performed.

Isolation of Cortical Microglia

All procedures involving animals were approved by the Institutional Animal Care and Use Committee (IACUC) of the Georgia Institute of Technology. Postnatal (day 0-1) Sprague-Dawley rats (Harlan) were anesthetized using isoflurane and rapidly decapitated. The cerebral cortices were isolated, separated from meninges, and minced in calcium- and magnesium-free Hanks' balanced salt solution (HBSS) (Invitrogen, Carlsbad, CA). The tissue was dissociated in 0.25% trypsin and 1mM EDTA (Invitrogen) for 20 min at 37°C. The trypsinization was stopped by adding Dulbecco's modified Eagle's medium with Ham's F12 (1:1) (DMEM/F12, Invitrogen) supplemented with 10% heat inactivated fetal bovine serum (FBS) (Invitrogen), and the tissue was triturated through a fire polished glass pipette. The dissociated cells were centrifuged at 1000 rpm for 3 minutes, and the supernatant was removed. The cells were resuspended in DMEM/F12 medium supplemented with 10% FBS, 2 mM L-glutamine, and 1% penicillin/streptomycin, and plated in 75 cm^2 poly-L-lysine (0.1 mg/ml, Sigma) coated tissue culture flasks (Fisher) at a density of one brain per flask. Three days later, the culture medium was changed with DMEM/F12 medium supplemented with 20% FBS, 2 mM L-glutamine, and 1% penicillin/streptomycin to enrich for microglial cells. After 14 d, flasks were lightly shaken to release microglial cells into the media supernatant, and these floating microglia were subsequently centrifuged into a pellet, and resuspended in DMEM-F12 medium supplemented with 10% FBS. The cells were seeded in 96-well culture plates at a density of 3×10^4 cells per well. Twenty-four hours after seeding, microglial cells were treated with 100 pg/ml lipopolysaccaride (LPS, Sigma) and incubated in the microglial cell culture medium containing α-MSH released every 24 h for 48 h.

The purity of the microglial culture was assessed by standard immunocytochemistry. Briefly, cells were fixed in Histochoice^{TM}MB (Electron Microscopy Sciences, PA) for 20 min, rinsed with PBS and blocked with 4% normal goat serum for 1h at room temperature. Primary antibody Iba-1 (Wako Chemicals, 1:500) was added at 4°C overnight. After rinsing, goat anti-rabbit IgG Alexa 488 (Molecular Probes) was added for 1 h at room temperature. Cell nuclei were counterstained with 10 4'-6-Diamidino-2-phenylindole (DAPI). The purity of microglia culture was 98.2 ± 1.3% as assessed by quantifying the number of Iba-1^{+} cells versus the total number of cells (n = 6).

Determination of Nitric Oxide Production

Nitric oxide (NO) production by the microglial cultures was determined by measuring the accumulated levels of nitrite in the supernatant with Griess reagent (Promega). Briefly, after incubation with LPS and the release medium collected from α-MSH containing nitrocellulose coatings every 24 h for 48 h, 50 µl cell culture supernatant was incubated with 50 µl sulphanilamide and 50 µl N-1-napthylethylenediamine dihydrochloride (NED) for 10 min each at room temperature. The optical density was measured at 540 nm using a microplate reader (Bio-Tek instruments, VT). NO production with and without α-MSH containing culture medium collected from triplicate nitrocellulose coating samples was determined (n = 3).

Surface Analysis by Scanning Electron Microscopy (SEM) and Profilometry

The surface morphology of the nitrocellulose coatings were investigated by SEM. Si wafers were coated with α-MSH loaded nitrocellulose coatings and mounted onto metal stubs using double sided adhesive tape, vacuum-coated with a gold film, and analyzed under a LEO 1530 thermally-assisted FEG scanning electron microscope. Coating thickness before and after drug was released was measured using a DEKTAK3 profilometer (Veeco Instruments Inc.). The thickness was determined by measuring 3 random areas on each sample for triplicate samples (n = 3).

Impedance Measurement

Micromachined silicon probes (single shank, 16 recording sites) were provided by the University of Michigan Center for Neural Communication Technology. The impedance magnitude of the 14 recording sites was measured before and after Matrix 400 coating (n = 14). A custom built impedance spectroscopy device was used for this study (Ross et al., 2004). A Tektronix TDS 3014B oscilloscope and a HP function generator were also included. The system was operated under computer control using a MATLAB program. A solution of Hank's balanced saline solution (HBSS) was used as the electrolyte. An AC sinusoid with 5 mV of amplitude was used as the input signal with the DC potential set to 0 V. The value of the impedance was determined at the biologically relevant frequency 1 kHz.

Data Analysis

Data are represented as the average value ± the standard error of the mean (S.E.M). A general linear ANOVA model was used to compare mean values of the different conditions. Pairwise comparisons were conducted using Tukey 95%

simultaneous confidence intervals, and $P < 0.05$ was used to indicate statistical significance.

Results

Effect of Coating Methods on Release Kinetics

Nitrocellulose coatings containing α-MSH were prepared using two delivery methods: (1) evaporated α-MSH-nitrocellulose layer coated with nitrocellulose as reservoir method and (2) α-MSH-nitrocellulose mixture coated with nitrocellulose as matrix method (Figure 2.1.1). Active α-MSH was released from nitrocellulose coatings in both delivery methods at different rates (Figure 2.1.2). For a given initial peptide loading concentration, the matrix method had a slower release rate compared to the reservoir method. As shown in Fig. 2 and 3, α-MSH was depleted at day 11 and 13 for Reservoir 100 and Reservoir 400 respectively. However, α-MSH was continuously released from both Matrix 100 and Matrix 400 coatings for over 18 days. α-MSH release from both types of coatings follows a similar release profile - an initial burst followed by a slow, steady release. For each type of coating, the 100 μg initial loading demonstrated a slower release rate than 400 μg initial loading.

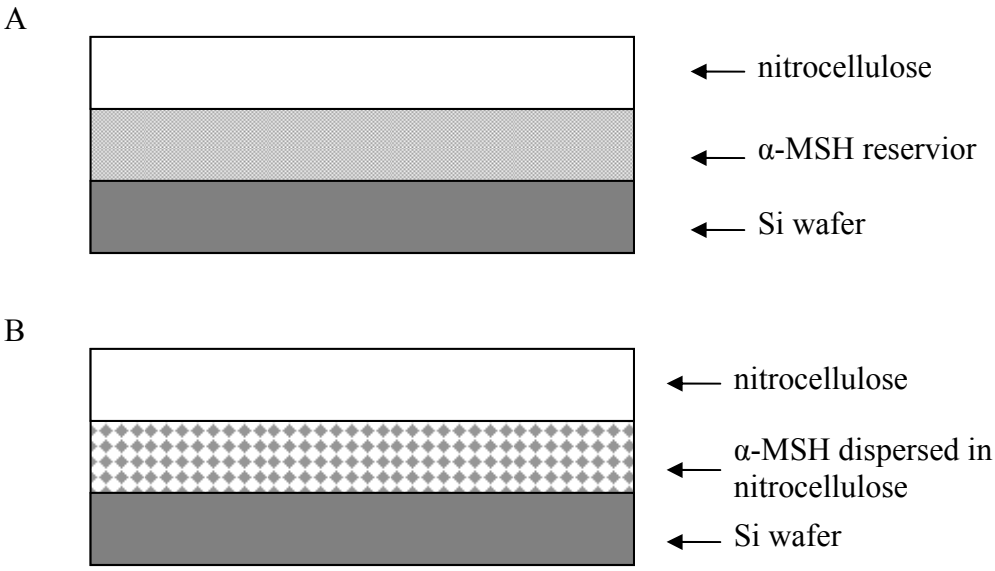

Figure 2.1.1: Two nitrocellulose-based drug delivery methods were studied as shown in (A) reservoir delivery method and (B) matrix delivery method.

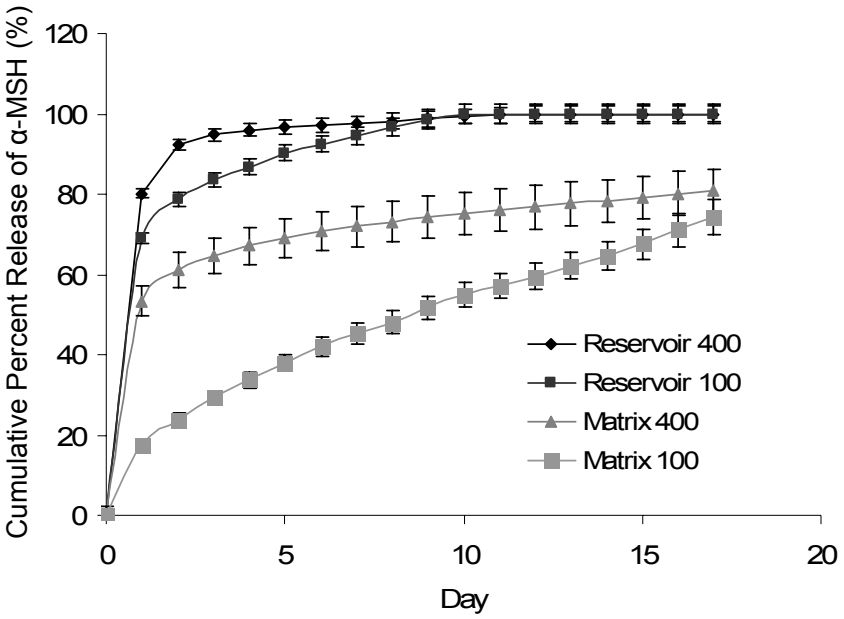

Figure 2.1.2: Effect of coating types on the cumulative release profile. Data shown are the average ± S.E.M. (n = 3).

Effects of Initial α-MSH Loading on Mass Release

α-MSH released daily from nitrocellulose loaded with 100 μg or 400 μg peptide was calculated as mass released (Figure 2.2). For the reservoir coating method, the mass released was not statistically significant different between 100 μg and 400 μg of peptide loading conditions. However, for the matrix coatings, the mass released increased with the increase in initial loading, and the release from 100 μg and 400 μg loading was significantly different ($P < 0.05$) after day 3. In fact, the mass release from Matrix 400 was always significantly higher ($P < 0.05$) than all the other three groups starting from day 3. In contrast, on days 1-2 there was significantly less ($P < 0.05$) mass release from the matrix coatings, compared to the reservoir coatings when the initial loadings are the same, indicating slower release rate from the matrix coatings.

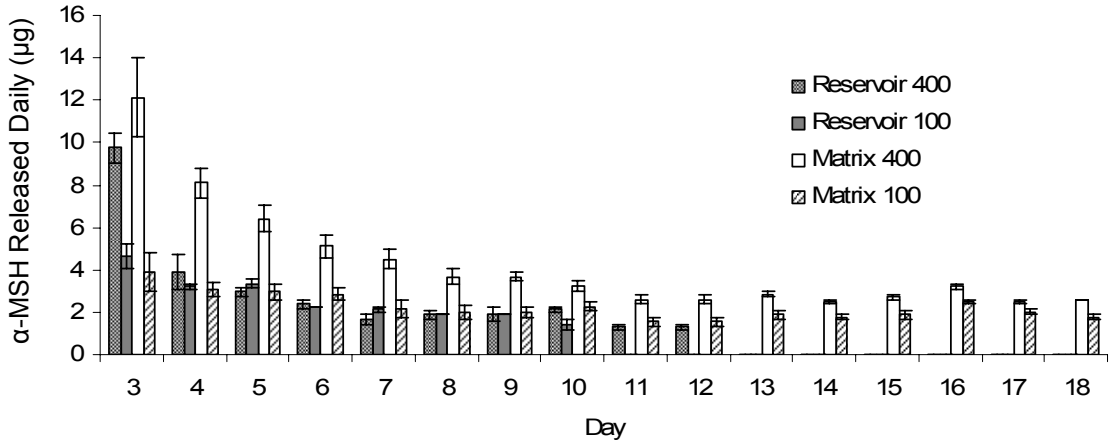

Figure 2.2: Effect of initial peptide loading on mass released daily. Data shown are the average ± S.E.M. (n = 3). The mass released from Matrix 400 was statistically significant ($P < 0.05$) with respect to release from the other three coatings starting from day 4 (the initial burst release on days 1 and 2 is not shown).

Effects of Initial α-MSH Loading on Percent Release

α-MSH released daily from nitrocellulose loaded with 100 μg or 400 μg peptide was calculated as the percent of initially loaded peptide released (Figure 2.3). For both the reservoir coatings and matrix coatings, the percent release from 400 μg initial loading was statistically higher than release from 100 μg on days 1 and 2. In contrast, starting from day3, the percent release from 400 μg was statistically lower than release from 100 μg till day 18. This data suggests that the initial peptide loading affects the release rate; with the lower initial loading generating a slower release rate. The percent release for Matrix 100 was always significantly higher ($P < 0.05$) than the other three groups after day 3.

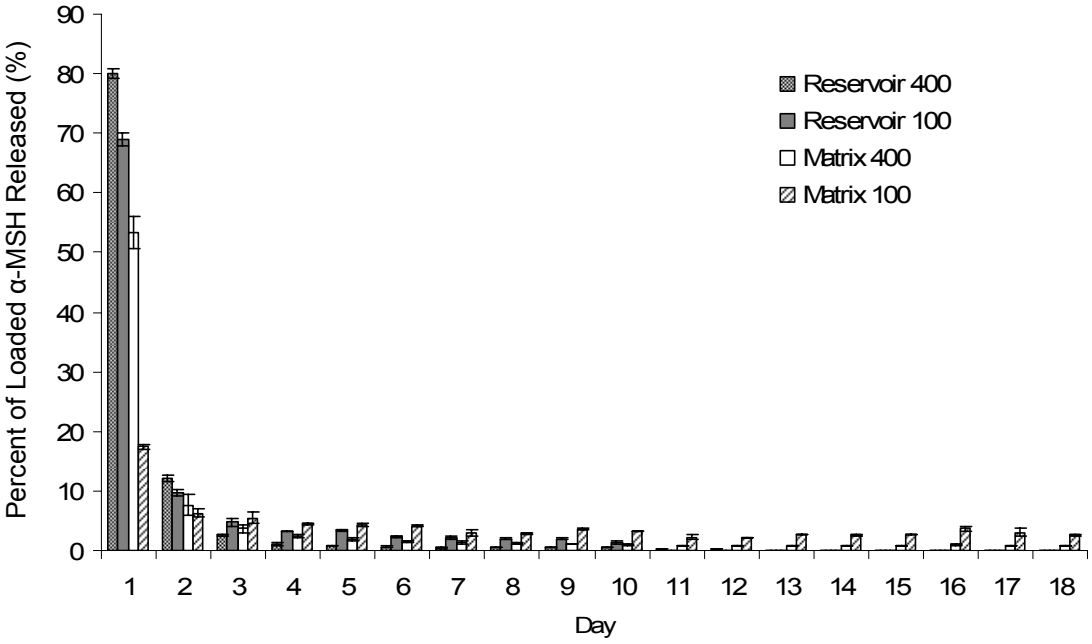

Figure 2.3: Effect of initial peptide loading concentration on percent of protein released daily. Data shown are the average ± S.E.M. (n = 3).

Bioactivity of Released α-MSH

Primary microglial cells were treated with LPS and α-MSH released into microglial culture medium from nitrocellulose coatings (Matrix 400). As shown in Figure 2.4, after 21 days of release, α-MSH is still bioactive, and the level of NO was reduced by 35 to 41% when incubated with the release medium collected every 24 h till day 21.

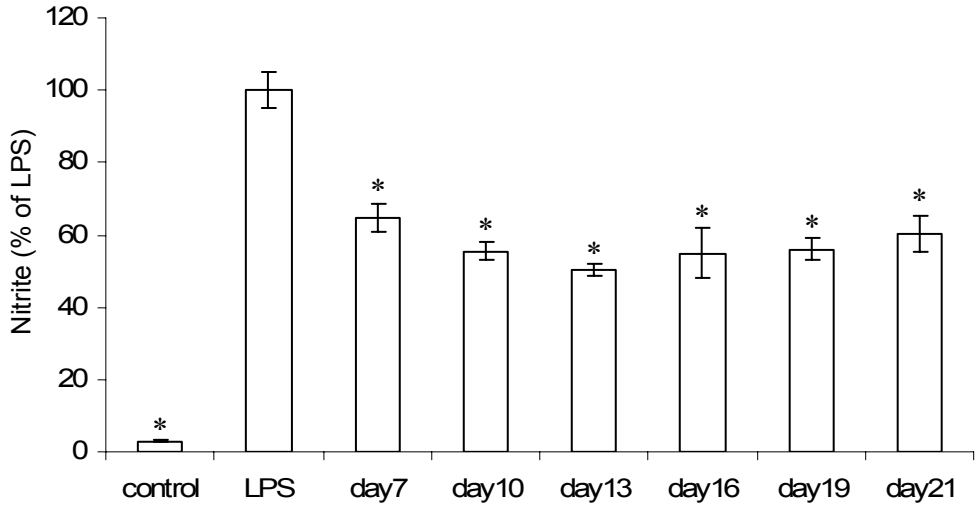

Figure 2.4: Effect of α-MSH released from nitrocellulose coatings on LPS-induced production of nitrite production. Data shown are the average ± S.E.M. (n = 3). Microglia were treated with LPS, or LPS and α-MSH released on day7, 10, 13, 16, 19 and 21 for 48 h, cells without LPS treatment served as control. $*P < 0.05$ compared with LPS-treated cultures.

Physical Characterization by SEM and Profilometry

The surface morphology of α-MSH-nitrocellulose (Figure 2.5A and B), α-MSH-nitrocellulose coated with pure nitrocellulose (Figure 2.5C and D) before and after drug release, and plain Si wafer were investigated by SEM. As shown in Figure 2.5, before α-MSH was released, both α-MSH-nitrocellulose and nitrocellulose have porous structure, with α-MSH-nitrocellulose being less porous than pure nitrocellulose. After α-MSH was released, the morphology of α-MSH-nitrocellulose coating was very similar to pure nitrocellulose coatings, and the surface roughness was greatly reduced for both types of coatings.

The thickness of Matrix 400 coatings before and after α-MSH was released was characterized. The coating thickness before drug release is 2236 ± 499 nm, and the thickness after drug depletion is 1166 ± 143 nm.

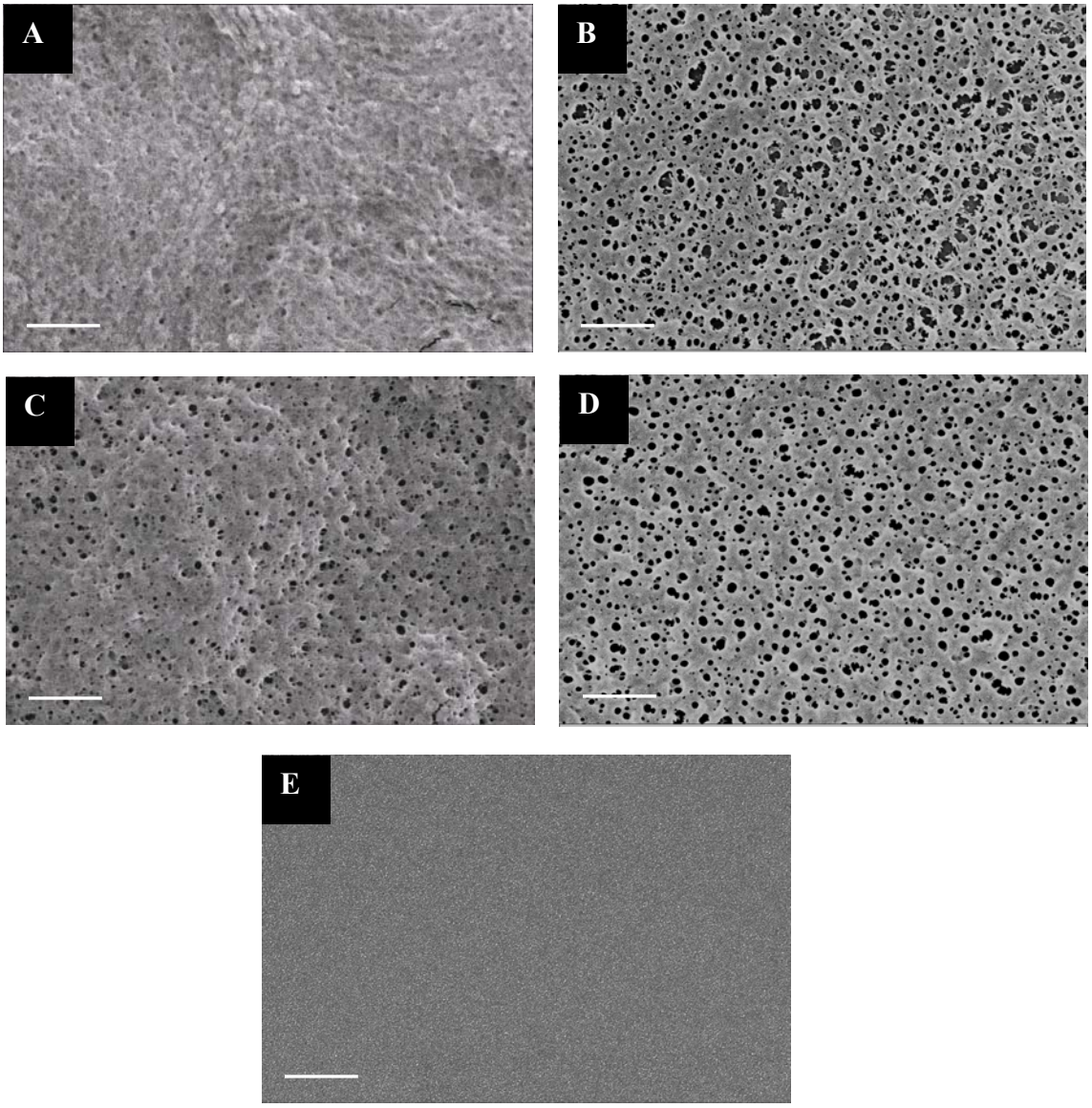

Figure 2.5: Surface morphology of (A) 400 μg α-MSH-nitrocellulose (α-MSH-NC) before drug release, and (B) after drug release; (C) 400 μg α-MSH-nitrocellulose coated with nitrocellulose (α-MSH-NC+NC) before drug release and (D) after drug release; (E) Uncoated oxidized Si surface as analyzed by SEM. Scale bar = 1 μm.

Electronic Properties

To determine the effects of the coatings on the electrical property of the electrodes, the electrical impedance of the 16 recording sites on the Michigan single shank acute probes was measured. Due to the instrument design for impedance measurement, only 14 out of the 16 recording sites could be measured. The magnitude of impedance was measured before and after coating at the biologically relevant frequency 1 kHz. As shown in Figure 2.6A, the impedance magnitude of the recordings sites was significantly reduced after being coated with nitrocellulose-DEX coatings compared to uncoated recording sites at 1 kHz.

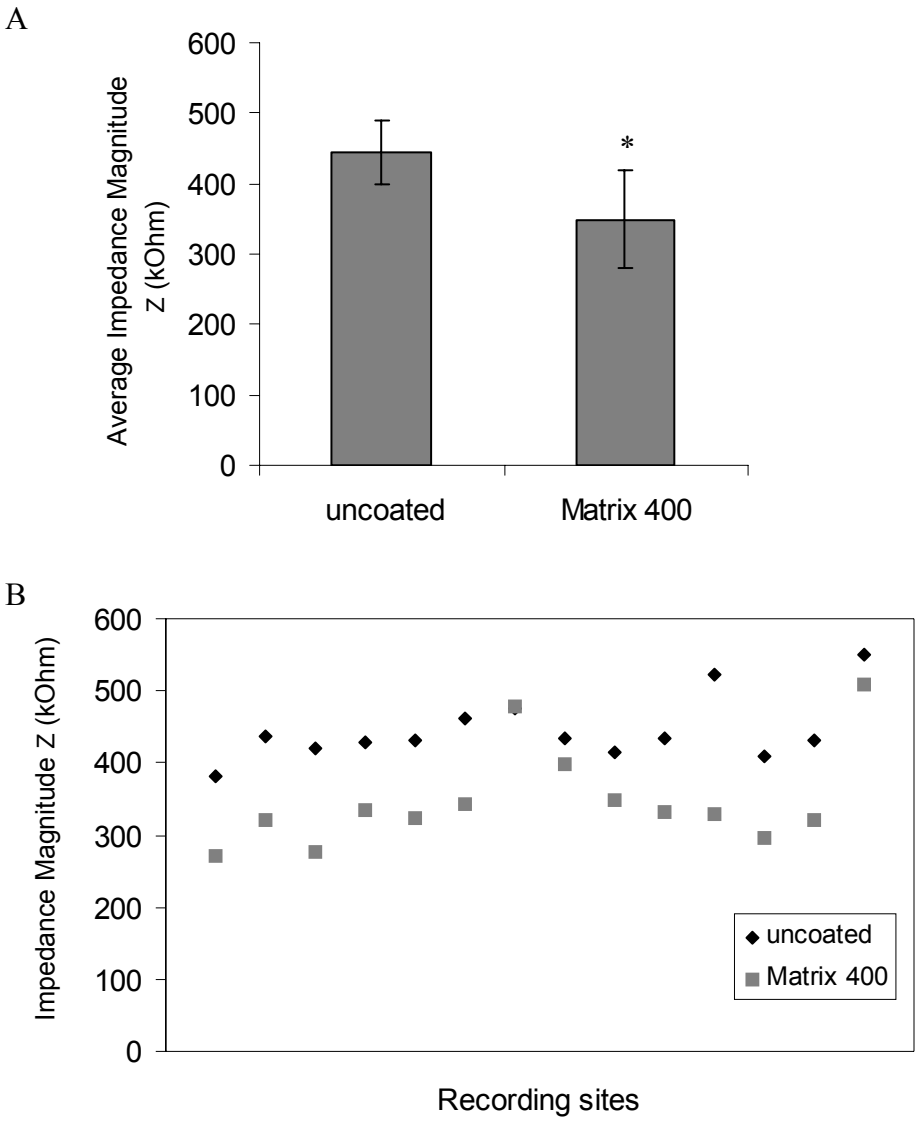

Figure 2.6: Impedance measurement. (A) Average impedance magnitude for the 14 recording sites before and after coating at 1 kHz. The magnitude of impedance for Matrix 400 was statistically significantly lower (*$P < 0.05$) compared to the impedance of uncoated electrode sites (n = 14). (B) Impedance magnitude for the 14 recording sites before coating (◆) and after coating (■).

Discussion

α-melanocyte stimulating hormone (α-MSH) inhibits inflammation by acting on peripheral inflammatory cells, glial inflammatory cells that activate descending anti-inflammatory neural passways (Lipton et al., 1999; Lipton and Catania et al., 1997). Therefore it is a promising agent for the treatment of the inflammatory response resulting from the implantation wound and micromotion induced scarring by chronically implanted electrodes. In this study, α-MSH was successfully incorporated in a nitrocellulose matrix, sustained release was achieved, and the bioactivity of α-MSH was retained after release.

When a matrix type loading method was used, the initial peptide loading directly affected both the mass of peptide released daily and the release rate. Higher initial loading caused a higher mass of peptide to be released every day. However, for the reservoir delivery method, higher initial loadings only caused a significantly higher mass release in the first three days, and then there was no significant difference of the mass released between initial loading amount of 400 μg and 100 μg in the following days of release. Increasing the initial loading caused a higher release rate for both coating methods.

Initial bursts of release for Reservoir 400, Reservoir 100, and Matrix 400 were observed. For the reservoir delivery method, the only barrier to slow drug release was the limiting nitrocellulose layers on top of the drug, and as shown in Figure 2.6C, and the nitrocellulose layers are porous, which allow for water penetration. For the matrix delivery method, the drug was dispersed in the nitrocellulose matrix, making this layer less porous (Figure 2.6A). Therefore it is not surprising that the reservoir samples have a

higher initial burst compared with matrix samples when the initial loadings are the same. Also, the drug/nitrocellulose ratio is higher for the reservoir method compared to the matrix method, and this could contribute to the higher initial burst for the reservoir samples.

Given a coating method (reservoir and matrix method), higher initial drug loading caused higher initial release. This is most likely due to the fact that the higher drug loading increased the drug/nitrocellulose ratio, potentially increasing the relative water permeability into the coating. In addition, higher initial loading also provided a higher concentration gradient between coatings and the release medium, which increased the driving force for drug release.

The data also demonstrates that α-MSH released from the nitrocellulose-based drug delivery system remains biologically active. Any implant inserted into the brain causes tissue injury and an inflammatory response (Schwartz, 2004; Fournier et al., 2003). The initial response to CNS injury is mediated by microglia. Microglia produce inflammatory molecules such as nitric oxide (NO), various cytokines, and prostaglandins, which induce neuronal cell death and trigger the activation of astrocytes, which finally result in the formation of an astroglial scar (Fawcett and Asher, 1999; Liberto et al., 2004; , McGraw et al., 2001; Kim et al., 2003). NO produced by expression of inducible nitric oxide synthase (iNOS) is an important mediator of inflammation and neuronal cell death (Kim et al., 2003; Golde et al., 2003). α-MSH has been shown to inhibit pro-inflammatory cytokines and NO production (Delgado et al., 1999; Galimberti et al., 1999). This study demonstrates that α-MSH can be successfully released for over 21

days, and remains bioactive and inhibits NO production by LPS-stimulated primary microglia (Figure 2.5).

To investigate the effects of these micron-scale coatings on the electrical properties of the electrodes, impedance measurement was conducted on Michigan single-shank neural recording probes. The Michigan probes are silicon-based electrodes with 16-channel recording electrode arrays made from gold. The impedance magnitude of the electrode sites before and after being coated with Matrix 400 was measured at the biologically relevant frequency of 1 kHz. There was a significant reduction of impedance for the coated electrode sites, and consequently, improved the signal transport across the neural interface and helped to increase the detection sensitivity to neural activity (Cui et al., 2001; Cui et al., 2003; Robinson, 1968). It is interesting that nitrocellulose coatings can reduce the impedance of the gold electrodes, because nitrocellulose is a non-conductive material with the dielectric constant at 6.2-7.5. This may be related to the porous structure of the nitrocellulose coatings, which provide a high interfacial area for charge transport, helping to lower the impedance.

Several parameters of these nitrocellulose-based coatings can be altered to customize release profiles to the application of interest. The results have shown that a higher nitrocellulose-drug ratio produced a slower release profile. As the nitrocellulose coatings have porous structure, there are two strategies to further slow drug release. First, the thickness of the nitrocellulose coatings could be increased to increase the diffusion barrier. Second, the parameters of nitrocellulose deposition such as concentration, solvent and rate of evaporation can be changed to vary the average pore size of nitrocellulose coatings to change the release rate.

Conclusions

This work developed and characterized nitrocellulose-based coatings for Si-substrates/electrodes. Anti-inflammatory neuropeptide α-MSH was incorporated in this system and slow, sustained release over 21 days was achieved. The α-MSH released on day 21 was still bioactive and successfully inhibited NO production. Compared with conventional polymer-matrix delivery systems, this novel delivery system is simple, inexpensive, and does not affect the electrical property of the substrate. In conclusion, these novel biocompatible coatings that release anti-inflammatory agents may help stabilize the electrode-brain interface to facilitate long-term recording and stimulation from Si-multi-electrode arrays *in vivo*.

CHAPTER III

DEVELOPMENT AND CHARACTERIZATION OF COATINGS CAPABLE OF RELEASING DEXAMETHASONE FOR SILICON NEURAL PROBES

Abstract

The long-term stability of implanted micromachined neural probes is compromised due to the glial scar formation at the insertion site. In this study, we developed a novel nitrocellulose-based coating for the sustained local delivery of the anti-inflammatory drug dexamethasone (DEX), a synthetic glucocorticoid that effectively reduces inflammation in the CNS. *In vitro* DEX release was observed over 16 days, with a high initial burst in the first three days and relatively slow, stable release thereafter. The released DEX remained bioactive. Impedance spectroscopy showed that the dexamethasone-loaded nitrocellulose coatings significantly reduce the magnitude of electrode impedance at the biologically relevant frequency of 1 kHz through an increase of capacitance. Coating stability test demonstrated that the coatings remained intact during the insertion procedure.

In conclusion, a nitrocellulose-based coating capable of sustained release of anti-inflammatory agent DEX was fabricated and characterized. This coating has the potential to reduce the inflammatory responses to the implanted neural probes without adversely affecting the electrical performance of the electrodes.

Introduction

As discussed in Chapter I, both α-melanocyte stimulating hormone (α-MSH) and dexamethasone (DEX) are powerful anti-inflammatory agents that are promising candidates for modulating the tissue reaction around the implanted neural electrodes. To maintain long-term recording stability, reactive gliosis and other inflammatory processes around the electrode need to be minimized. The fundamental solution to this problem lies in better integration between the implanted electrode and the host nervous tissue. DEX has unique advantage over α-MSH in that it has been widely used clinically to treat various inflammatory responses. In CNS, DEX was shown to reduce tissue reaction around neural implants, and protect neurons by down-regulating nitric oxide (NO) production (Shain et al., 2003; Golde et al., 2003). However, systemic administration of DEX may cause serious side effects including myopathy and diabetes (Kaal and Vecht, 2004; Koehler, 1995; Twycross, 1994). Therefore local delivery of DEX is highly desired. In this study, we propose to design a nitrocellulose-based coating for neural probes that is capable of sustained local release of DEX.

We have demonstrated in Chapter II that nitrocellulose as a polymer matrix is capable of sustained release of neuropeptide α-MSH, which might be attributed to its high protein binding capacity and hydrophobic nature. The goal of this study was to fabricate and evaluate nitrocellulose-based coatings capable of sustained release of DEX. Studies have shown that in some drug delivery systems the molecular weight of loaded drug affects the rate of drug release, with drugs of higher molecular weight having a slower release rate (Meilander et al., 2001). The molecular weight of α-MSH and DEX are 1665 and 392 Da respectively, therefore the capacity of nitrocellulose as the polymer

matrix for sustained release of DEX need to be investigated. α-MSH release study has demonstrated that Matrix 100 has the most steady release rate (see Chapter II and Zhong and Bellamkonda, 2005), therefore we fabricated nitrocellulose coatings loaded with DEX based on this method. The release profile of the nitrocellulose-DEX coatings were investigated in this study. The anti-inflammatory activity of DEX released from this nitrocellulose-based delivery system was tested through its ability to inhibit lipopolysaccharide (LPS) – stimulated nitric oxide (NO) production in primary microglia culture. The surface morphology was characterized by scanning electron microscopy (SEM). The effect of the anti-inflammatory coatings on the electrical performance of the electrodes was evaluated by impedance measurement.

Materials and Methods

Fabrication of DEX Loaded Nitrocellulose Coatings

Polished Si wafers of 1 cm^2 with a 10,000 Å oxide layer (University Wafer, MA) were cleaned by ultrasonification in deionized water and ethanol, and stored in 70% ethanol for sterilization. 33.3 mg (5 cm^2) nitrocellulose (Schleicher & Schuell BioScience) was dissolved in 12 ml methanol. 100 μg dexathasone (Sigma) powder was dissolved in 20 μl nitrocellulose (NC) solution and evaporated on 1 cm^2 Si wafers. This DEX-nitrocellulose layer was subsequently coated with 3 additional layers of pure nitrocellulose by evaporation.

Micromachined silicon neural recording probes (single shank, 16 recording sites, 5mm) were provided by Center for Neural Communication Technology (CNCT) at the university of Michigan (Figure 3.1). The size parameters of the probe are listed in Table 3.1. The neural probes were mounted on polished Si wafers of 1 cm^2 and coated with dexmathasone and nitrocellulose as described above.

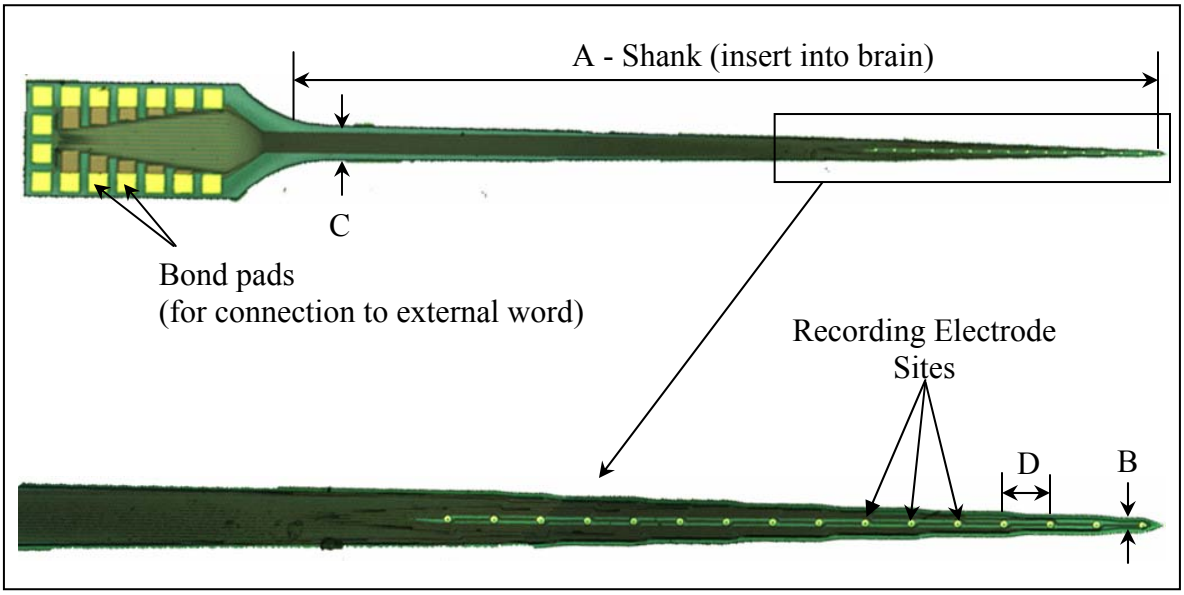

Figure 3.1: A 16 channel, single shank Michigan recording probe. The probe part in the box is magnified in to show the 16 recording electrode sites.

Table 3.1: Size parameters of a 16 channel, single shank Michigan recording probe.

NUMBER OF SITES	SHANK LENGTH (A)	SHANK WIDTH (B → C)	SITE SPACING (D)	SITE AREA
16	5 mm	33 – 200 μm	100 μm	177 μm^2

In Vitro DEX Release Assay

Nitrocellulose-DEX coated Si wafers were incubated at 37°C in PBS for quantification of DEX release. Every 24 h, the PBS was removed and replaced with fresh PBS. The amount of DEX released every 24 h from triplicate samples (n = 3) was determined by the UV adsorption at 242 nm with a microplate reader (Bio-Tek instruments, VT). The DEX containing PBS was then stored at 4°C until bioactivity assay was performed.

In Vitro Diffusion Study

The evaporation method used in this study only allows for coating one side of the Si neural probe. To test the diffusibility of DEX to the other side (uncoated side) of the neural probe, we developed a diffusion chamber using 0.6% agarose gel as an *in vitro* surrogate for the brain tissue. Agarose gel at a 0.6% concentration closely resembles *in vivo* brain tissue with respect to several critical physical characteristics (Chen et al., 2004) and is commonly used to mimic the brain during drug trials. As shown in Figure 3.2, Si wafer with one side coated with DEX was inserted into a 3 mm thick block of agarose gel. The width of the Si wafer is 2 mm, which is 10 times the width of a Si neural probe. Therefore the 3 mm thick agarose is corresponding to 300 μm brain tissue *in vivo*. DEX released into agarose on both sides of the Si wafer diffused into the two PBS chambers and quantified at 1, 2 and 15 h time points (n = 3).

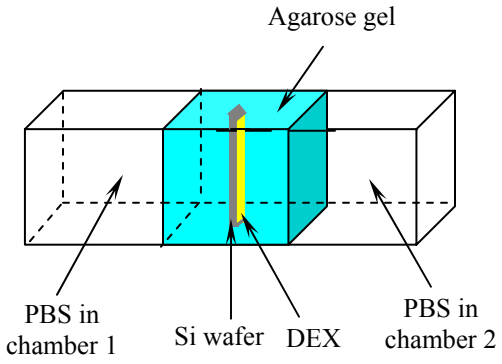

Figure 3.2: Schematic of an *in vitro* DEX diffusion chamber. A Si wafer with one side coated with nitrocellulose-DEX (indicated by yellow color) was inserted into the agarose gel. DEX released into the agarose gel on both sides of the Si wafer was measured in the two PBS chambers.

Isolation of Cortical Microglia

All procedures involving animals were approved by the Institutional Animal Care and Use Committee (IACUC) of the Georgia Institute of Technology. Postnatal (day 0-1) Sprague-Dawley rats (Harlan) were anesthetized using isoflurane and rapidly decapitated. The cerebral cortices were isolated, separated from meninges, and minced in calcium- and magnesium-free Hanks' balanced salt solution (HBSS) (Invitrogen, Carlsbad, CA). The tissue was dissociated in 0.25% trypsin and 1mM EDTA (Invitrogen) for 20 min at 37°C. The trypsinization was stopped by adding Dulbecco's modified Eagle's medium with Ham's F12 (1:1) (DMEM/F12, Invitrogen) supplemented with 10% heat inactivated fetal bovine serum (FBS) (Invitrogen), and the tissue was triturated through a fire polished glass pipette. The dissociated cells were centrifuged at 1000 rpm for 3 minutes, and the supernatant was removed. The cells were resuspended in DMEM/F12 medium supplemented with 10% FBS, 2 mM L-glutamine, and 1% penicillin/streptomycin, and

plated in 75 cm^2 poly-L-lysine (0.1 mg/ml, Sigma) coated tissue culture flasks (Fisher) at a density of one brain per flask. Three days later, the culture medium was changed with DMEM/F12 medium supplemented with 20% FBS, 2 mM L-glutamine, and 1% penicillin/streptomycin to enrich for microglial cells. After 14 d, flasks were lightly shaken to release microglial cells into the media supernatant, and these floating microglia were subsequently used in bioactivity assay. The purity of microglia culture was 98.2 ± 1.3% as assessed by quantifying the number of Iba-1^+ cells versus the total number of cells (n=6).

Bioactivity Assay

The bioactivity of released DEX was tested by its ability to inhibit LPS-stimulated NO production in microglia. Primary rat cortical microglial cells were suspended in DMEM/F12 medium supplemented with 10% FBS, 2 mM L-glutamine, and 1% penicillin/streptomycin, and seeded in 96-well culture plates at a density of 3×10^4 cells per well. Twenty-four hours after seeding, LPS (1 ng/ml) and DEX released from day 1 to day 5 was added to the cell culture medium at a final concentration of 0.5 μg/ml (n = 3). After 48 h, NO production was determined by measuring the accumulated levels of nitrite in the cell culture medium with Griess reagent (Promega). Cells without LPS treatment served as a negative control (n = 3), cells treated with LPS (n = 3) and 0.5 μg/ml DEX served as a positive control (n = 3).

Surface Analysis by Scanning Electron Microscopy (SEM) and Profilometry

The surface morphology of the nitrocellulose coatings were investigated by SEM. Si wafers were coated with DEX loaded nitrocellulose coatings and mounted onto metal stubs using double sided adhesive tape, vacuum-coated with a gold film, and analyzed

under a LEO 1530 thermally-assisted FEG scanning electron microscope. Coating thickness before and after drug was released was measured using a DEKTAK3 profilometer (Veeco Instruments Inc.). The thickness was determined by measuring 3 random areas on each sample for triplicate samples (n = 3).

Coating Stability Test

A Sprague Dawley rat between 275-299 g was anesthetized with ketamine (1 mL/kg), xylazine (0.17 mL/kg), and acepromazine (0.37 mL/kg). Then the rat was perfused transcardially with 0.1 M PBS (pH7.4). The brain was removed carefully for the neural probe coating stability test. The purpose of PBS perfusion was to remove the blood so that the coating surface morphology was not affected by the blood components. To test the effect of insertion step on coating stability, nitrocellulose-DEX coated probes were inserted into the rat brain and immediately pulled out. The integrity of the coatings was subsequently examined with SEM, and compared with coated probes without insertion step.

Impedance Spectroscopy

Micromachined silicon probes (single shank, 16 recording sites) were provided by the University of Michigan Center for Neural Communication Technology. The impedance magnitude of the recording sites was measured before and after Matrix 400 coating (n = 8). A custom built impedance spectroscopy device was used for this study (Ross et al., 2004). A Tektronix TDS 3014B oscilloscope and a HP function generator were also included. The system was operated under computer control using a MATLAB program. A solution of Hank's balanced saline solution (HBSS) was used as the electrolyte. An AC sinusoid with 5 mV of amplitude was used as the input signal with

the DC potential set to 0 V. The value of the impedance was determined over the range of 10-10^5 Hz.

Data Analysis

Data are represented as the average value ± the standard error of the mean (S.E.M). A general linear ANOVA model was used to compare mean values of the different conditions. Pairwise comparisons were conducted using Tukey 95% simultaneous confidence intervals, and $P < 0.05$ was used to indicate statistical significance.

Results

***In Vitro* DEX Release**

DEX released from nitrocellulose coatings was quantified via UV-absorbance at 242 nm and plotted as the cumulative percent of DEX released. The cumulative release profile showed an initial burst in the first three days followed by a relatively slow, steady release over 16 days (Figure 3.3.1). The mass release profile showed that the amount of DEX released daily decreased over time from 36 μg on day 1 to 0.2 μg on day 16 (Figure 3.3.2). The suggested normal dosage for DEX in cell culture is 1 μM (0.5 μg/ml). However, studies have shown that the inhibitory effect of DEX on astrocyte proliferation is similar over the range from 10 nM to 10 μM (Crossin et al., 1997), and DEX at 20 nM effectively inhibited microglia proliferation (Tanaka et al., 1997). Therefore 0.2 μg of DEX should still be therapeutically effective.

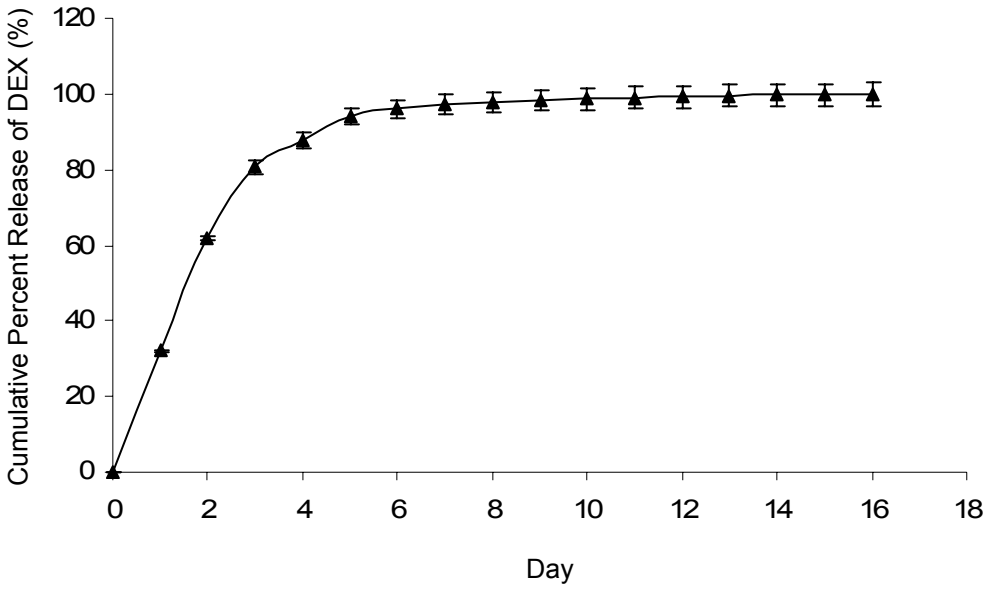

Figure 3.3.1: Cumulative release profile of DEX from nitrocellulose coatings. The cumulative release of DEX was plotted as the percent of initially loaded DEX. Data shown are the average ± S.E.M. (n = 3).

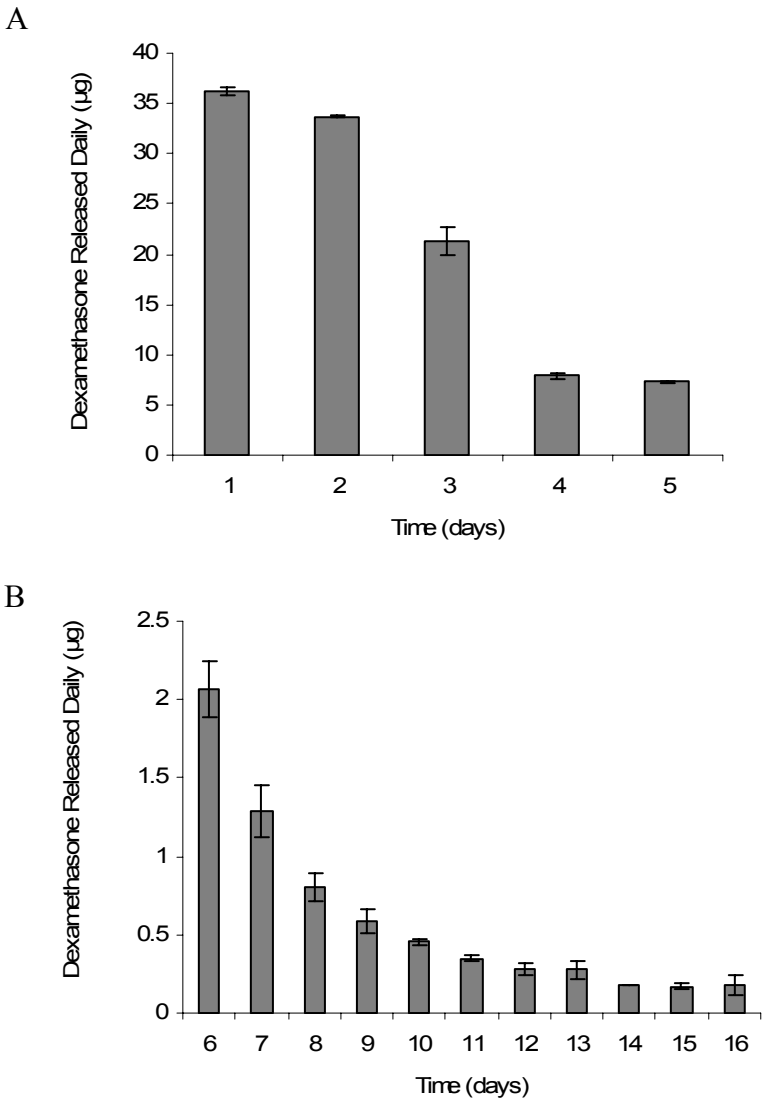

Figure 3.3.2: Mass of DEX released daily. (A) DEX release from day 1 to day 7. (B) DEX release from day 6 to day16. Data shown are the average ± S.E.M. (n = 3).

In Vitro Diffusion Study

The quantity of DEX released from the coated side of the Si wafers into the agarose gel on both sides of the Si wafers was assessed by measuring the quantity of DEX in the two PBS chambers at 1, 2, and 15 h. As shown in Figure 3.4, although only one side of the Si wafer was coated, there was no significant difference between the quantity of DEX released into the PBS chamber on both sides of the Si wafers (n = 3).

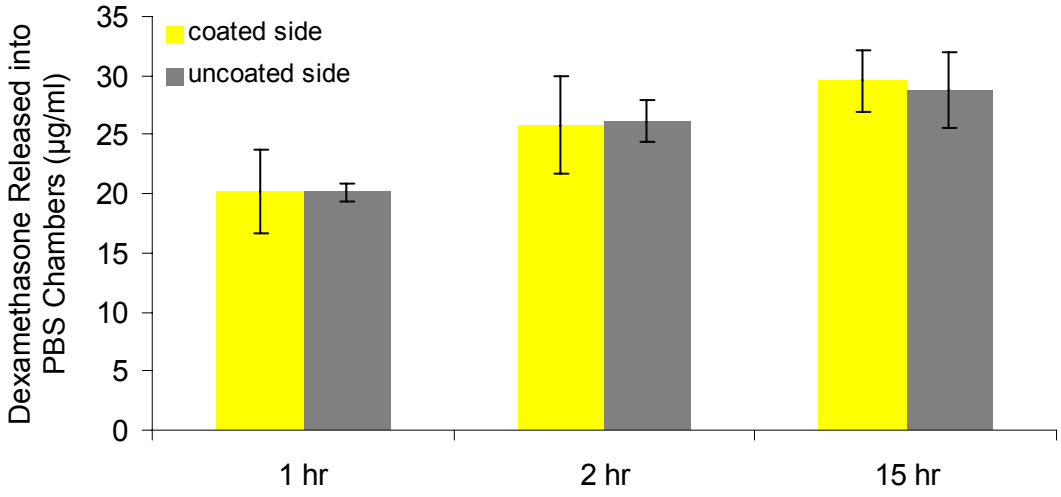

Figure 3.4: Quantity of DEX released into the PBS chambers on both sides of the Si wafer. There was no significant difference between the quantities of DEX released into both chambers. Data shown are the average ± S.E.M. (n = 3).

Bioactivity of Released DEX

Primary microglia culture was activated by LPS (1 ng/ml), DEX released on day 1,2,3,4 and 5 were added to the culture medium at a final concentration of 0.5 μg/ml (1 μM). As shown in Figure 3.5, LPS treatment significantly increased NO production in microglia, and NO level was reduced to normal level when incubated with DEX released every 24 h, indicating that the released DEX is still biologically active. There was no significant difference between the activity of released DEX and fresh DEX.

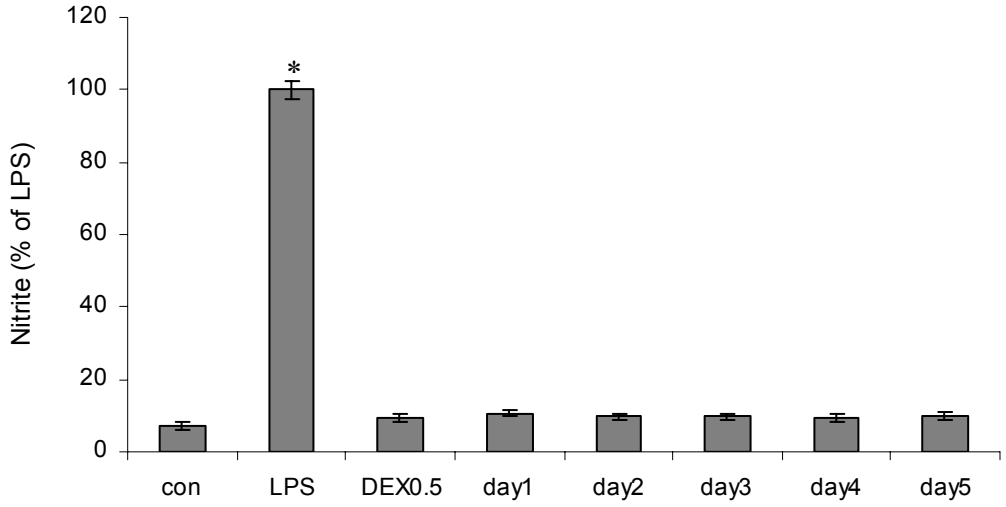

Figure 3.5: Effect of DEX released from nitrocellulose coatings on LPS-induced NO production. Microglia were treated with LPS, LPS and 0.5 μg/ml fresh DEX, or LPS and DEX released on day1, 2, 3, 4, and 5 for 48 h, cells without LPS treatment served as negative control. *$P < 0.05$ compared with control culture (con). Data shown are the average ± S.E.M. (n = 3).

Coating Stability Test

Since neural probes are eventually going to be inserted into brain tissue, the probe coatings are required to be able to resist the shear force during insertion. Neural probes coated with nitrocellulose-DEX coatings were inserted into a PBS perfused rat brain and immediately pulled out. The surface morphology of the coatings before (Figure 3.6A) and after insertion (Figure 3.6B) were characterized by SEM. The coatings remained intact after probe insertion. The surface morphology of nitrocellulose-DEX coatings deposited on Si wafer (Figure 3.6C) was similar to those on Si neural probes (Figure 3.6A), indicating that Si wafers can be used as an alternative in coating characterizations when larger sample area is required. Compared with the relatively smooth Si surface (Figure 3.6D), the coatings have porous structure.

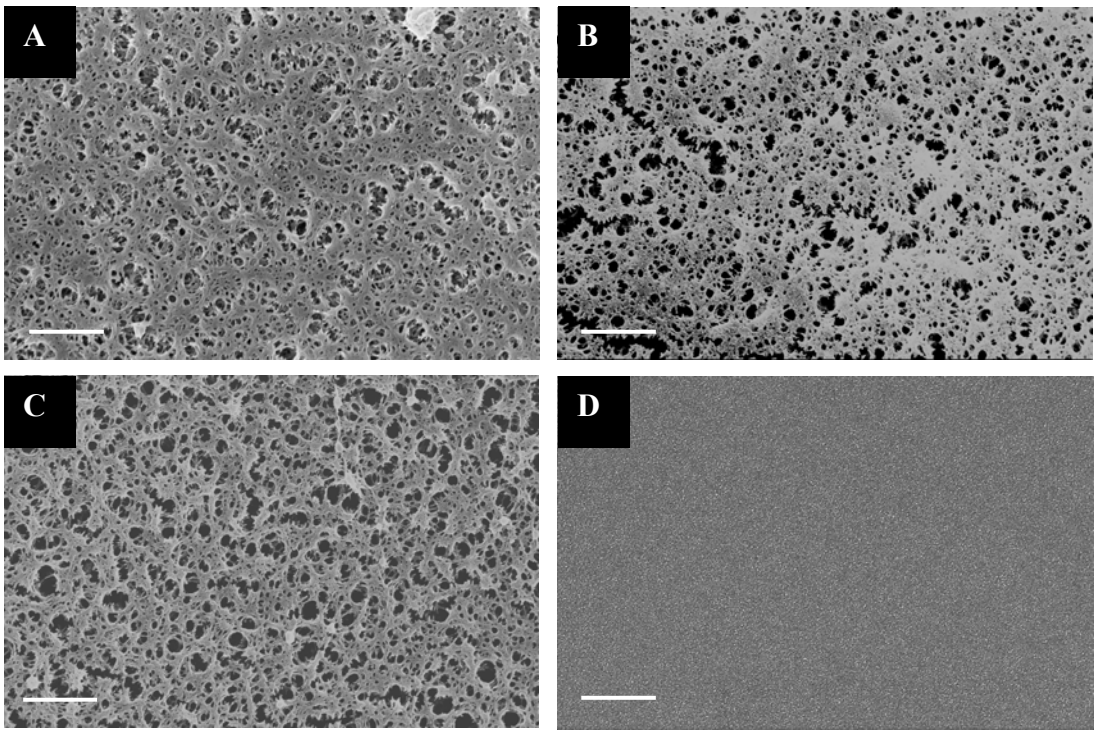

Figure 3.6: Surface morphology of (A) Si neural probe coated with 100 μg DEX-nitrocellulose before insertion, and (B) after insertion; (C) Si wafer coated with 100 μg DEX-nitrocellulose before insertion; (D) Uncoated oxidized Si surface as analyzed by SEM. Scale bar = 1 μm.

Coating Thickness

The thickness of Matrix 400 coatings before and after α-MSH was released was characterized. The coating thickness before drug release is 1.715 ± 0.158 μm, and the thickness after drug depletion is 1.434 ± 0.085 μm.

Impedance Measurement

To determine the effects of the coatings on the electrical properties of the electrodes, the electrical impedance of the 8 recording sites on the Michigan single shank acute probes was measured before and after coating at the biologically relevant frequency 1 kHz. There were 16 recording sites on the neural probe, every other recording site was selected for impedance measurement. As shown in Figure 3.7, the impedance magnitude of the recordings sites was significantly reduced after being coated with nitrocellulose-DEX at 1 kHz.

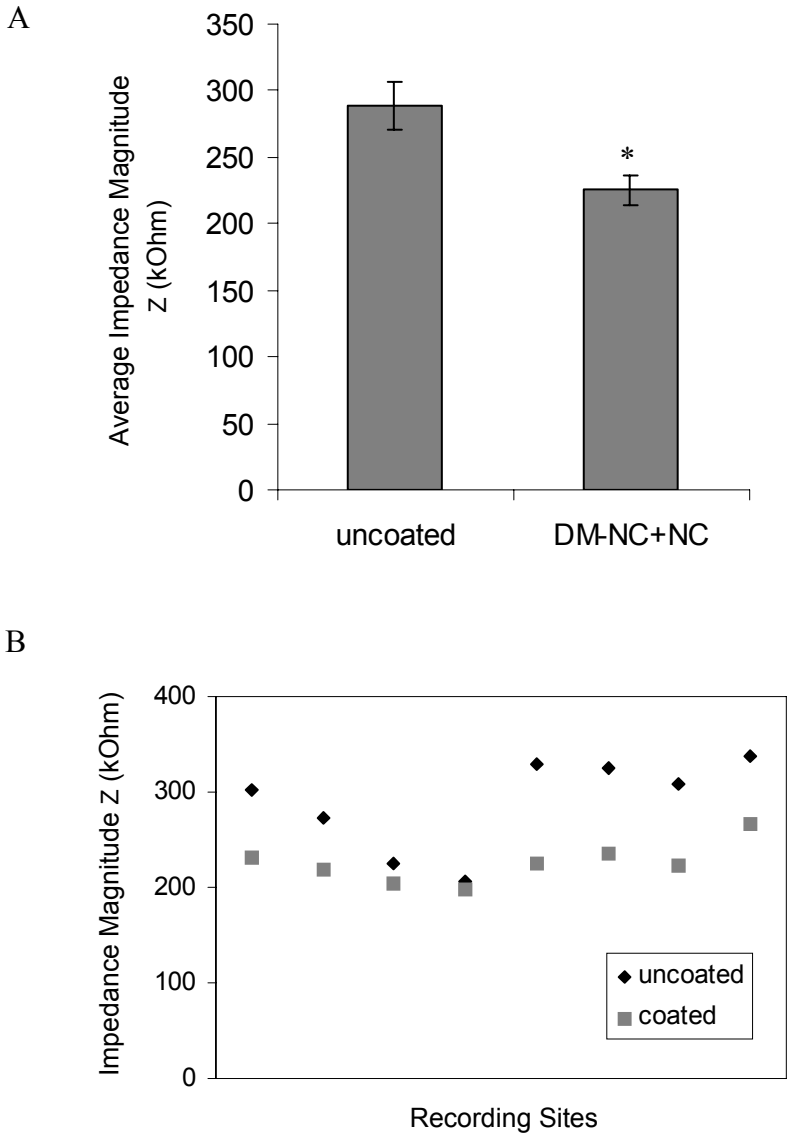

Figure 3.7: (A) Average impedance magnitude for the 8 recording sites before and after coating at 1 kHZ. The magnitude of impedance for coated electrode sites was statistically significantly lower (*P < 0.05) compared to the impedance of uncoated electrode sites (n = 8). **(B) Impedance magnitude for the 8 recording sites before coating (◆) and after coating (■).**

Impedance Spectroscopy

Impedance spectroscopy measures electrical impedance over a wide range of frequencies (10-10^5 Hz). As shown in Figure 3.8, for both uncoated and coated electrode sites, the electrical impedance magnitude decreased with the increase of frequency, indicating that the impedance of the electrode sites is mostly capacitive. Nitrocellulose-DEX coatings reduced the impedance magnitude of the recording sites at relatively low frequency range (< 4 kHz), and increased the impedance magnitude at high frequency range. Impedance spectroscopy further proved that at the biologically relevant frequency 1 kHz, the impedance magnitude for coated electrode sites were reduced.

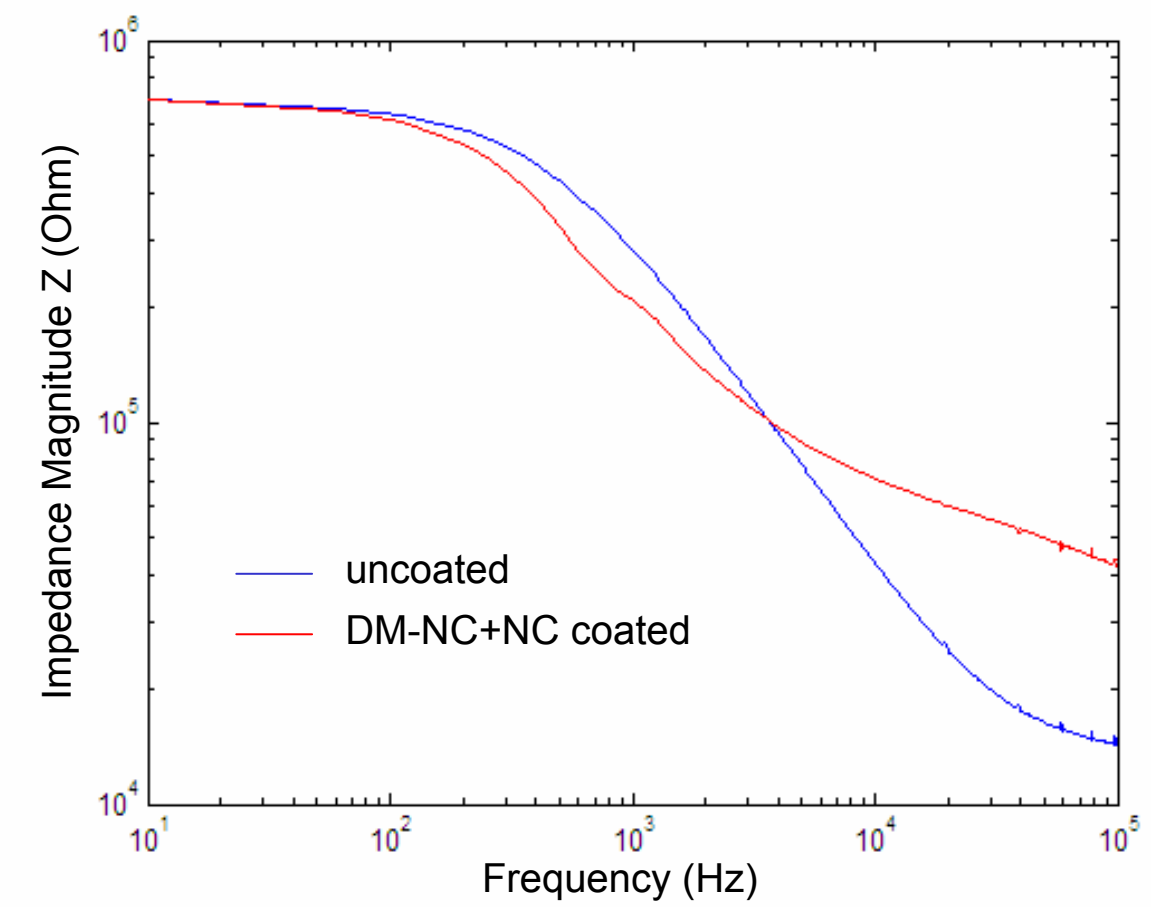

Figure 3.8: Impedance magnitude as a function of frequency for recording sites. Impedance spectroscopy proved the impedance drop at 1 kHz for coated electrode sites.

Discussion

Dexamethasone is known as a potent anti-inflammatory drug, and it has previously been shown to be capable of reducing inflammatory responses in the CNS (Holmin and Mathiesen, 1996; Spataro et al., 2005; Hermens and Verhaagen, 1998). DEX inhibits proliferation, iNOS synthesis and cytokine expression of microglia (Golde et al., 2003; Chao et al., 1992; Tanaka et al., 1997). DEX also directly inhibits astrocyte proliferation (Crossin et al., 1997). Administration of DEX to activated microglia-neuron cocultures protected neurons by down-regulating nitric oxide (NO) production (Golde et al., 2003). Therefore the development of neural probe coatings capable of sustained release of DEX holds promise for the long-term success of chronic neural probes.

In this study, we fabricated nitrocellulose coatings loaded with DEX. *In vitro* release study revealed sustained release over 16 days. It is not known how long the drug release is needed to obtain long-term stable neural recording. Ideally, continuous local drug release is expected to last over the time course of implantation, which may be many years. This is technically difficult to achieve. A number of studies on drug-eluting stents demonstrated that release of anti-inflammatory agents in the early stage of implantation inhibits the long-term tissue reaction (Huang et al., 2002; De Scheerder et al., 1996). Following brain injury, the first cells to respond and arrive are macrophages from the bloodstream and microglia migrating from the surrounding tissue (Fawcett and Asher, 1999, Kreutzberg, 1996). The activated microglia secrete proinflammatory cytokines such as IL-1β, TNFα, and IL-6, which subsequently activate adjacent microglia or other cell types, including astrocytes, via autocrine and paracrine passways, resulting in propagation and enhancement of the inflammatory response (Kyrkanides et al., 2001;

Hays, 1999; Bruccoleri et al., 1998; Takeuchi et al., 2001). Consequently, astrocytes express additional inflammatory mediators that further contribute to the inflammatory response and eventually lead to glial scar formation (Kyrkanides et al., 2001; Merrill and Benveniste, 1996; John et al., 2005; Hanisch, 2002). Both activated microglia and astrocytes are capable of releasing neurotoxic molecules such as radicals and NO (Lee et al., 1995; Kreutzberg, 1996). Therefore administration of anti-inflammatory agents in early stage of brain injury might be able to inhibit the expression of proinflammatory molecules that leads to progression of astroglosis, and reduce the production of neurotoxic molecules.

The evaporation method used in this study only allows for coating one side of the Si neural probe. A diffusion study was performed to assess the ability of DEX to diffuse to the uncoated side of the neural probes. In this *in vitro* diffusion model, Si wafers and 0.6% agarose gel were used as the substitutes for Si neural probes and brain tissue respectively. The results demonstrated that 1 h after release, the concentration of DEX in the PBS chamber on the uncoated side of the Si wafers was not significantly different from that in on the coated side, indicating that DEX can diffuse freely to the uncoated side of the Si wafers/neural probes. This is not surprising considering the small molecular weight of DEX. However, although 0.6% agarose gel closely resembles *in vivo* brain tissue with respect to several critical physical characteristics (Chen et al., 2004) and is commonly used to mimic the brain during drug trials, we have to be aware that there are no cell components in the agarose gel, therefore the drug diffusion rate in agarose gel may not really reflect that *in vivo*.

The bioactivity of released DEX was demonstrated by its ability to inhibit LPS-stimulated NO production in microglia. NO levels in cells treated with released DEX were not significantly different from that in cells treated with fresh DEX, indicating that the activity of released DEX was not reduced compared with fresh DEX.

To investigate the effects of these micron-scale coatings on the electrical propertiy of the electrodes, impedance measurement was conducted on Michigan single-shank neural recording probes. The Michigan probes are silicon-based electrodes with 16-channel recording electrode arrays made from gold. The impedance magnitude of the electrode sites before and after coating was measured at the biologically relevant frequency of 1 kHz. There was a significant reduction of impedance for the coated electrode sites, and consequently, improved the signal transport across the neural interface and helped to increase the detection sensitivity to neural activity (Cui et al., 2001; Cui et al., 2003; Robinson, 1968). Impedance spectroscopy showed decrease of impedance at relatively low frequency (< 4 kHz) range, and increase of impedance at higher frequency, suggesting that both resistance and capacitance of the coated electrodes were increased. At relatively low frequency, the increase of capacitor was the decisive factor, causing the decrease of impedance; while at higher frequency, the increase of resistance became the decisive factor, causing the increase of impedance. The increase of capacitance was related to the high dielectric constant of nitrocellulose.

Conclusions

In this study, a nitrocellulose-DEX coating for Si neural probe was fabricated. Anti-inflammatory agent dexamethasone can be released for over 16 days at 37°C. The

released dexamethasone was still bioactive. The nitrocellulose-DEX coated electrodes showed significant reduction of impedance compared with uncoated electrodes, indicating that the coating did not compromise the electrical performance of the electrodes and could be used for neuroprosthetic applications.

CHAPTER IV

IN VITRO EVALUATION OF ANTI-INFLAMMATORY EFFECTS AND CYTOTOXICITY OF A-MELANOCYTE STIMULATING HORMONE AND DEXAMETHASONE ON CORTICAL CELLS

Abstract

Dexamethasone (DEX) and α-melanocyte stimulating hormone (α-MSH) are potent anti-inflammatory agents that are promising to be used for controlling the tissue reaction to the implanted neural probes. The first objective of this study was to compare the anti-inflammatory potency of these two drugs *in vitro* based on their effects on glial cells including microglia and astrocytes. 1 μM DEX and α-MSH inhibited LPS-stimulated NO production in microglia by 91% and 30% respectively. DEX treatment significantly inhibited microglial and astrocyte proliferation, while α-MSH showed no effects on glial cell proliferation. These results suggest that DEX is a more potent anti-inflammatory agent than α-MSH.

While the release rate of DEX from polymer coatings can be measured *in vitro*, the precise dosage *in vivo* is hard to estimate. Therefore the second objective of this study was to further evaluate the anti-inflammatory effects and neurotoxicity of DEX at various dosages on cortical cells including microglia, astrocytes and neurons. 1, 10 and 100 μM DEX inhibited LPS-stimulated NO production in microglia by 91%, 98% and 90% respectively. In addition, DEX treatment at all three concentrations significantly reduced LPS-stimulated microglia proliferation. Quantitative real-time PCR analysis

demonstrated that 1 and 100 μM DEX significantly inhibited the expression of proinflammatory cytokines TNFα and IL-1β by microglia. When astrocytes were treated with 1, 10 or 100 μM DEX, the cell number was significantly reduced compared with control group. 1 and 10 μM DEX treatment significantly inhibited TGFβ1 and neurocan expression. When rat cortical neurons were incubated with 1, 10 or 100 μM DEX, DEX at all three concentrations did not significantly alter cell viability compared with control group, indicating that DEX was not neurotoxic. In all the experiments conducted in this study, the performance of DEX at different concentrations was not significantly different from one another. Collectively, these results suggest that the anti-inflammatory effects and safety of DEX are not affected even at 100 times more than its normal effective dosage.

Introduction

Long-term performance of chronically implanted neural microelectrodes is compromised by glial scar formation around the Si-microelectrodes and subsequent fibrotic encapsulation of the electrode. Glial scar is a consequence of inflammatory reaction to the implant associated injury to the CNS. One strategy to enhance the performance of implanted electrodes is to develop biocompatible electrode coatings that locally release anti-inflammatory drugs. Dexamethasone (DEX) and α-melanocyte stimulating hormone (α-MSH) are promising drug candidates to be incorporated into the electrode coatings for controlling the reactive tissue response to the implanted neural electrodes (see Chapter I). The first objective of this study was to evaluate the anti-inflammatory potency of these two drugs *in vitro* based on their effects on glial cells

including microglia and astrocytes. The initial response to CNS injury is mediated by microglia (Fawcett and Asher, 1999, Kreutzberg, 1996). The activated microglia proliferate and migrate to the injury site, release neurotoxic molecules such as free radicals and nitric oxide (NO). NO produced by the expression of inducible nitric oxide synthase (iNOS) is an important mediator of inflammation and neuronal cell death (Golde et al., 2003). Reactive microglia also produce proinflammatory cytokines including interleukin-1 (IL1), tumor necrosis factor-α (TNFα) and interleukin-6 (IL-6) (Kyrkanides et al., 2001; Hays, 1999; Fawcett and Asher, 1999; Bruccoleri et al., 1998; Takeuchi et al., 2001), which subsequently activate the astrocytes (Merrill and Benveniste, 1996; John et al., 2005). The reactive astrocytes undergo hypertrophy, proliferation, and upregulate trophic factors, cytokines, as well as extracellular matrix including chondroitin sulfate proteoglycans (CSPGs), important inhibitory molecules in glial scar (Fawcett and Asher, 1999; Polikov et al., 2005). The final structure of the glial scar is predominately astrocytic (Fawcett and Asher, 1999). The capacity of DEX and α-MSH to inhibit NO production in lipopolysaccharide (LPS)-stimulated microglia, and glial cell (microglia and astrocytes) proliferation was evaluated. The experiment results demonstrated that NO level in DEX treated microglial culture was significantly lower than α-MSH treated culture. DEX effectively inhibited microglia and astrocyte proliferation, while α-MSH showed no effect on microglia and astrocyte proliferation. These results suggested that DEX is a more powerful anti-inflammatory agent than α-MSH. Therefore DEX was selected as the anti-inflammatory agent for the following studies in this project.

While the release rate of DEX from polymer coatings can be measured *in vitro*, the precise dosage *in vivo* is hard to estimate. The initial drug release is usually higher

than normal target dosage due to the initial burst effect. Therefore second objective of this study was to further evaluate the anti-inflammatory effects and neurotoxicity of DEX at dosages higher than normal effective dosage on cortical cells including microglia, astrocytes and neurons. The anti-inflammatory effects of DEX on glial cells were widely studied. However, most studies use dosages equal or less than 1 μM. It has been previously reported that DEX effectively reduces the inflammatory tissue reaction around neural implants at a local concentration of 0.2 - 0.7 μM *in vivo* (Shain et al., 2003). *In vitro* studies have shown that DEX at 1 μM causes a significant decrease level of TGF-β1 mRNA in glial cells (Batuman et al., 1995), pronouncedly inhibits NO production and provides effective neuroprotection (Golde et al., 2003); DEX at 20 nM inhibits proliferation of microglial cells (Tanaka et al., 1997); DEX at 0.01 – 1 μM inhibits astrocyte proliferation. In this study, we explored the effects of DEX on cortical cells at 1, 10 and 100 μM. NO production, cell proliferation and expression of proinflammatory cytokines (TNFα and IL-1β) in microglial culture in the presence of DEX at different concentrations were examined. Astrocyte is a major cell component in glial scar. TGFβ1 is prominently detected in astrocytes following lesion *in vivo* (John et al., 2003; Unsicker and Strelau, 2000). It has been shown to be essential for wound healing and glial scar formation by enhancing the production of extracellular matrix components (Logan et al., 1994; John et al., 2003; Moon and Fawcett, 2001). CSPGs are important inhibitory extracellular matrix molecules in glial scar. Neurocan and phosphacan are two specific inhibitory CSPG molecules that are expressed by reactive astrocytes in the chronic glial scar (McKeon et al., 1999). Neurocan is expressed *in vitro* mostly by astrocytes, however, phosphacan is not made by astrocyte *in vitro* (Fawcett and Asher, 1999;

McKeon et al., 1999). Thus the effects of 1, 10 and 100 μM DEX on the expression of TGFβ1 and neurocan by astrocytes in primary cell mature were investigated. The ability of DEX at various dosages to inhibit astrocyte proliferation was examined as wells. To evaluate the neurotoxicity of variations in DEX dosing, rat cortical neurons were incubated with 1, 10 and 100 μM DEX and the cell viability was measured with a cell counting kit. Our results demonstrate that high dosages of DEX exhibited similar anti-inflammatory effects as DEX at normal dosage and didn't show neurotoxicity.

.

Materials and Methods

Isolation of Primary Cortical Microglia

All procedures involving animals were approved by the Institutional Animal Care and Use Committee (IACUC) of the Georgia Institute of Technology. Postnatal (day 0-1) Sprague-Dawley rats (Harlan) were anesthetized using isoflurane and rapidly decapitated. The cerebral cortices were isolated, separated from meninges, and minced in calcium- and magnesium-free Hanks' balanced salt solution (HBSS) (Invitrogen, Carlsbad, CA). The tissue was dissociated in 0.25% trypsin and 1mM EDTA (Invitrogen) for 20 min at 37°C. The trypsinization was stopped by adding Dulbecco's modified Eagle's medium with Ham's F12 (1:1) (DMEM/F12, Invitrogen) supplemented with 10% heat inactivated fetal bovine serum (FBS) (Invitrogen), and the tissue was triturated through a fire polished glass pipette. The dissociated cells were centrifuged at 1000 rpm for 3 minutes, and the supernatant was removed. The cells were resuspended in DMEM/F12 medium supplemented with 10% FBS, 2 mM L-glutamine, and 1% penicillin/streptomycin, and

plated in 75 cm^2 poly-L-lysine (0.1 mg/ml, Sigma) coated tissue culture flasks (Fisher) at a density of one brain per flask. Three days later, the culture medium was changed with DMEM/F12 medium supplemented with 20% FBS, 2 mM L-glutamine, and 1% penicillin/streptomycin to enrich for microglial cells. After 14 d, flasks were lightly shaken to release microglial cells into the media supernatant, and these floating microglia were subsequently used in the following study. The purity of microglia culture was 98 ± 1.3% as assessed by quantifying the number of Iba-1^+ cells versus the total number of cells (n = 6).

Isolation of Primary Cortical Astrocytes

Mixed cortical cells dissociated from postnatal (day 0-1) Sprague-Dawley rat cerebral hemispheres were obtained as described above. The cells were plated in tissue culture flasks (Fisher) at a density of one brain per flask in culture medium consisting of DMEM-F12 medium supplemented with 2 mM L-glutamine, 1% penicillin/streptomycin, and 10% heat inactivated FBS. Cultures were purified for astrocytes by vigorously shaking the flasks to remove nonadherent cells. Astrocytes were used between passages 4-12 to permit phenotypic maturation.

The purity of the astrocytic culture was assessed though glial fibrillary acidic protein (GFAP) immunostaining in conjunction with cell nuclei staining. Briefly, cells were fixed in Histochoice^{TM}MB (Electron Microscopy Sciences, PA) for 20 min, rinsed with PBS and blocked with 4% normal goat serum for 1h at room temperature. Primary antibody GFAP (Dako, 1:1000) was added at 4°C overnight. After rinsing, goat anti-mouse IgG1 Alexa 488 (Molecular Probes) was added for 1 h at room temperature. Cell nuclei were counterstained with 10 4'-6-Diamidino-2-phenylindole (DAPI). The purity of

astrocyte culture was 95.2 ± 2.6% as assessed by quantifying the number of Iba-1^{+} cells versus the total number of cells (n = 6).

Isolation of Primary Cortical Neurons

A time-pregnant Spague-Dawley rat (embryonic day 17) was anesthetized using halothane (Halocarbon, NJ) and decapitated. The uterus was removed and placed in HBSS solution. Each fetus was removed from the amniotic sac and quickly decapitated. The brains was removed and placed in HBSS. The cerebral cortices were isolated, separated from meninges, and minced in calcium- and magnesium-free HBSS. The tissue was dissociated in 0.25% trypsin and 1mM EDTA for 10 min at 37°C. Then the trypsin/EDTA was removed and 0.15 mg/mL DNase in HBSS was added. The tissue was triturated through a fire polished glass pipette. The dissociated cells were centrifuged at 1000 rpm for 3 minutes, and the supernatant was removed. The cells were resuspended in Neurobasal medium (Invitrogen) supplemented with 2% B27 Supplement (Invitrogen), 0.5 mM L-glutamine, and 1% penicillin/streptomycin.

The purity of the neuronal culture was assessed though NeuN immunostaining in conjunction with cell nuclei staining. Briefly, cells were fixed in Histochoice^{TM}MB (Electron Microscopy Sciences, PA) for 20 min, rinsed with PBS and blocked with 4% normal goat serum for 1h at room temperature. Primary antibody NeuN (Chemicon, 1:500) was added at 4°C overnight. After rinsing, goat anti-mouse IgG1 Alexa 488 (Molecular Probes) was added for 1 h at room temperature. Cell nuclei were counterstained with 10 4'-6-Diamidino-2-phenylindole (DAPI). The purity of astrocyte culture was 97.1 ± 0.6% as assessed by quantifying the number of Iba-1^{+} cells versus the total number of cells (n = 6).

DEX treatment

Primary rat cortical microglia were suspended in DMEM/F12 medium supplemented with 10% FBS, 2 mM L-glutamine, and 1% penicillin/streptomycin. For NO production (n = 3) and cell proliferation assays (n = 3), the cells were seeded in poly-L-lysine coated 96-well plates. For real-time PCR quantification of cytokine expression (n = 3), the cells were seeded in poly-L-lysine coated 6-well plates. The seeding density was 150,000 cells/cm^2. Twenty-four hours after seeding, DEX was added to the culture medium at a final concentration of 1, 10, or 100 μM for 48 h.

Primary rat cortical astrocytes were suspended in DMEM/F12 medium supplemented with 10% FBS, 2 mM L-glutamine, and 1% penicillin/streptomycin. For cell proliferation assay (n = 6), the cells were seeded in 24-well plates. For real-time PCR quantification of gene expression (n = 3), the cells were seeded in 6-well plates. After the cells approached confluency, they were treated with DEX at a final concentration of 1, 10, or 100 μM for 48 h.

Primary rat cortical neurons were seeded in poly-L-lysine coated 24-well plates at a density of 100,000 cells/cm^2 in Neurobasal medium supplemented with 2% B27 Supplement, 0.5 mM L-glutamine, and 1% penicillin/streptomycin. Twenty-four hours after seeding, the culture medium was changed with Neurobasal medium supplemented with 2% B27 Supplement Minus AO, 0.5 mM L-glutamine, and 1% penicillin/streptomycin. After 7 days in culture, DEX was added to the culture medium at a final concentration of 1, 10, or 100 μM for 48 h (n = 6).

Nitrite Assay

NO production in the microglial cultures was determined by measuring the accumulated levels of nitrite in the supernatant with Griess reagent (Promega). Briefly, 50 µl cell culture supernatant was incubated with 50 µl sulphanilamide and 50 µl N-1-napthylethylenediamine dihydrochloride (NED) for 10 min each at room temperature. The optical density was measured at 540 nm using a microplate reader (Bio-Tek instruments, VT).

Cell Viability

Cell viability was assessed using cell counting kit-8 (CCK-8, Dojindo). This colorimetric assay employs 2-(2-methoxy-4-nitrophenyl)-3-(4-nitrophenyl)-5-(2,4-disulfophenyl)-2H-tetrazolium (WST-8), which is reduced by dehydrogenases in metabolically active cells and the amount of the resulting colored formazan product is directly proportional to the number of living cells. Thus the number of viable cells can be estimated by spectrometry. 50 µl of the CCK-8 solution was added to the culture medium (500 µl) of each cell containing well. Culture plates were incubated in the humidified incubator at 37°C and in 5% CO_2 for 1 h. The absorbance was measured at 450 nm using a microplate reader.

Cell Survival

Cell survival was assessed using live/dead assay. Cells cultures were incubated with 2 µM calcein AM (Sigma) and 4 µM ethidium homodimer-1 (EthD-1) in 0.1M Dulbecco's phosphate-buffered saline (DPBS, Invitrogen) at 37°C for 30 min, followed by rinsing with DPBS three times. Cell survival was defined as the percentage of viable cells. Live cells were stained green by intracellularly converting Calcein AM to green fluorescent calcein with esterase activity. Dead cells were stained red by EthD-1, a red

DNA stain only permeable to cells with compromised cell membranes. The number of live and dead cells was counted to calculate the percentage of viable cells.

Real-Time Reverse Transcription Polymerase Chain Reaction (Real-Time RT-PCR)

Levels of TNFα, IL-1β, TGFβ1, and neurocan mRNA expression were analyzed via real-time RT-PCR using the iCycler system (Bio-Rad, Hercules, CA). Total cellular RNA was isolated from microglia or astrocytes using Trizol reagent (Invitrogen), according to the manufacturer's instructions. RNA was quantified by spectrophotometer at 206 nm, and 1 μg of total cellular RNA was used for first strand cDNA synthesis by iScrpit cDNA Synthesis Kit according to the manufacturer's protocol. Real-time PCR was performed on an iCycler thermal cycler (Bio-Rad) equipped with MyiQ Real Time PCR detection system. Each PCR reaction contained 1 μl of cDNA, 0.2 μM primers, and 12.5 μl iQ^{TM} SYBER Green Supermix reagent (Bio-Rad). Thermal cycling was initiated with a first denaturation step of 3 min at 95°C, followed by 35 cycles of 95°C for 30 sec (denaturing), 55°C or 57.9°C for 30 sec (annealing), and 72°C for 1 min (extension). The amplification fluorescence was read at the end of each extension period. Amplification specificity was checked using melting curve analysis. Standard curves for all primer amplifications were generated by plotting average cycle threshold (Ct) values against the logarithm starting quantity of target template molecules (series dilution of cDNA template), followed by a sum of least squares regression analysis. The gene expression in each sample was calculated as 2^(35-Ct). All mRNA expression levels were normalized to the content of house-keeping gene glyseraldehyde-3-phosphate dehydrogenase (GAPDH) as an internal standard for each treatment condition. The sequences of the primers used in this study are listed in Table 4.1. Primers for TNFα,

TGFβ1, and neurocan were designed via the Beacon Designer 2.1 software (Bio-Rad), primers for IL-1β (Wisse et al, 2004) and GAPDH (Raghavendra et al., 2003) were previously described.

Table 4.1: Primer sequence for real-time PCR.

GENE	FORWARD PRIMER	REVERSE PRIMER
TNFα	TGCCTCAGCCTCTTCTCATT	CGATCACCCCGAAGTTCAGT
IL-1β	TACAAGGAGAGACAAGCAACGACA	GATCCACACTCTCCAGCTGCA
TGFβ1	AGTGGCTGAACCAAGGAGAC	CATTATCTTTGCTGTCACAAGAGC
neurocan	TGTCCCCAATCCCACTCTCC	CTCGGGGTCTTCTGCTCCAA
GAPDH	CCCCCAATGTATCCGTTGTG	TAGCCCAGGATGCCCTTTAGT

Data Analysis

Data are represented as the average value ± the standard error of the mean (S.E.M). A general linear ANOVA model was used to compare mean values of the different conditions. Pairwise comparisons were conducted using Tukey 95% simultaneous confidence intervals, and $P < 0.05$ was used to indicate statistical significance.

Results

Effects of DEX and α-MSH on Microglia

Primary microglial culture was stimulated by LPS (1 ng/ml), DEX and α-MSH were added to the culture medium at a final concentration of 1 μM. As shown in Figure 4.1.1, LPS significantly increased NO production in microglia, 1μM DEX or α-MSH inhibited NO production by 91% and 30% respectively. The NO level in LPS + DEX treated microglial culture was not significantly different from control culture, however, the NO level in LPS + α-MSH treated culture was still significantly higher than control culture and DEX treated culture. This result suggested that DEX had a more potent inhibitory effect on NO production in LPS stimulated microglia.

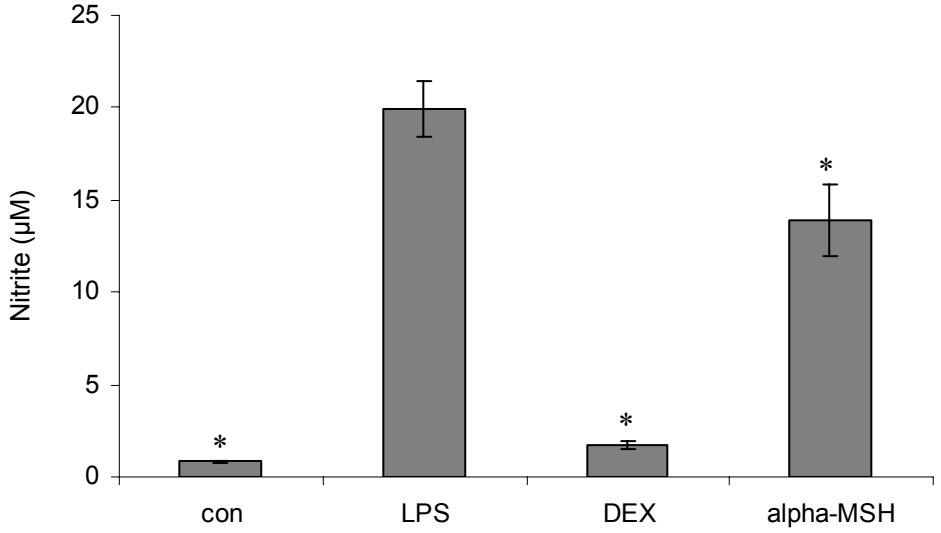

Figure 4.1.1: Effect of DEX and α-MSH on LPS-induced NO production in microglial culture. Microglia were treated with LPS, LPS + 1 μM DEX, or LPS + 1 μM α-MSH for 48 h, cells without LPS treatment served as negative control (con). *$P < 0.05$ compared with LPS-treated cultures (n = 3).

Microglia proliferation was assessed using cell counting kit-8. LPS treatment significantly stimulated microglia proliferation. 1μM DEX inhibited LPS-stimulated microglia proliferation to control level, while 1μM α-MSH had no effect on microglia proliferation.

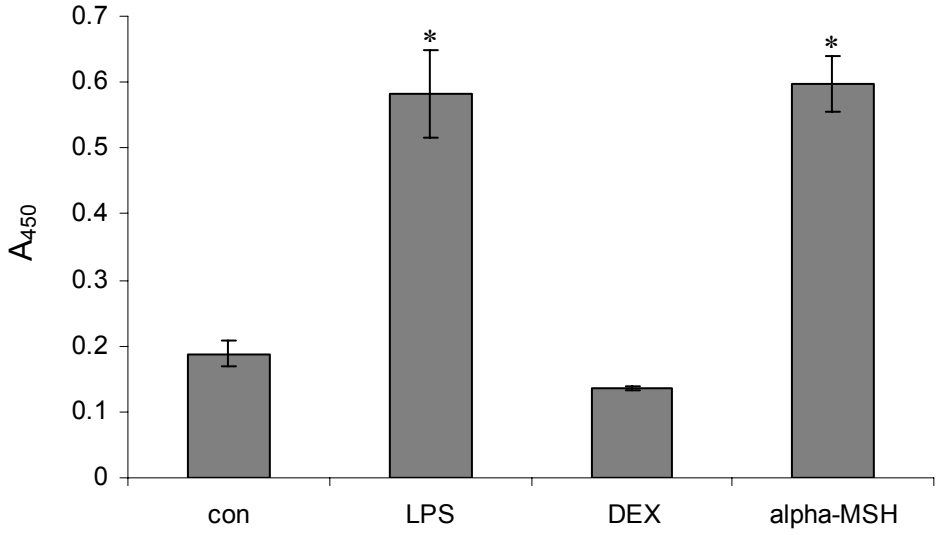

Figure 4.1.2: Effect of DEX and α-MSH on LPS-induced microglia proliferation. Microglia were treated with LPS, LPS + 1 μM DEX, or LPS + 1 μM α-MSH for 48 h, cells without LPS treatment served as negative control (con). **P* < 0.05 compared with LPS-treated cultures (n = 3).

Effects of DEX and α-MSH on Astrocyte Proliferation

Astrocyte proliferation was assessed using cell counting kit-8. DEX and α-MSH were added to the culture medium at a final concentration of 1 μM for 48 h. DEX treatment significantly reduced the number of living cells, while α-MSH didn't show any effects on the number of living cells compared to control culture (Figure 4.2). There were two possible causes for the decrease of viable cells in DEX treated cultures. One was that DEX inhibited astrocyte proliferation, the other was that DEX killed astrocytes. To elucidate the cause of decrease of viable cells in DEX treated culture, live/dead cell assay was performed to measure cell survival. The percentages of viable cells for control culture and DEX treated culture were 99.15% and 98.95% respectively, indicating that DEX was not toxic to astrocytes, and the decrease of viable cell number in DEX treated culture was caused by inhibition of cell proliferation.

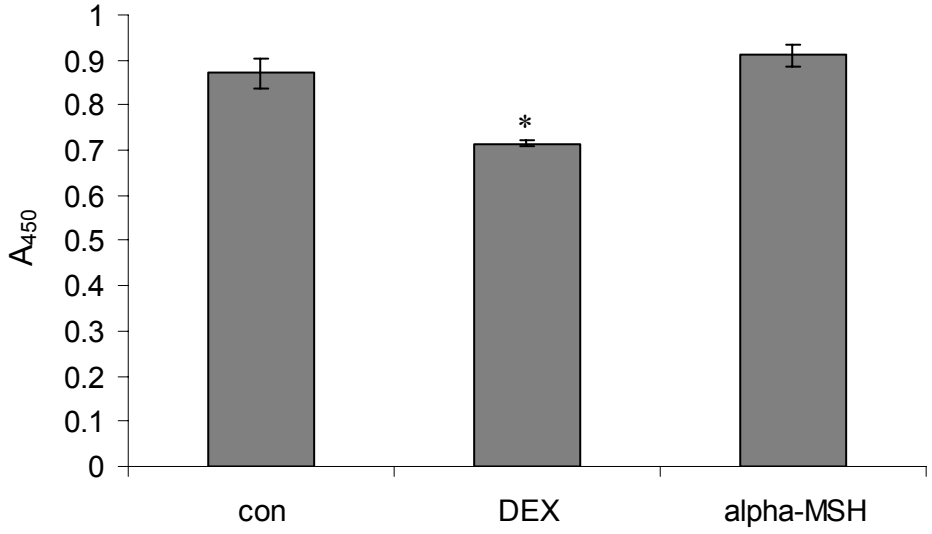

Figure 4.2: Effect of DEX and α-MSH on astrocyte viability. Astrocytes were treated with 1 μM DEX or α-MSH for 48 h, cells without any treatment served as control (con). *$P < 0.05$ compared with control cultures (n = 6).

Response of Microglia to DEX at Various Dosages

To evaluate the anti-inflammatory effects of high dosages of DEX, DEX was added to LPS-stimulated microglial culture at final concentrations of 1, 10 or 100 μM DEX. As shown in Figure 4.3.1, DEX at all three concentrations significantly inhibited LPS-stimulated NO production in microglial culture. NO levels in 1, 10 or 100 μM DEX treated microglial cultures were not significantly different from control culture (without LPS treatment). Figure 4.3.2 showed that 1, 10 or 100 μM DEX significantly inhibited LPS-induced microglia proliferation. The cell numbers in DEX treated cultures were not significantly different from control culture.

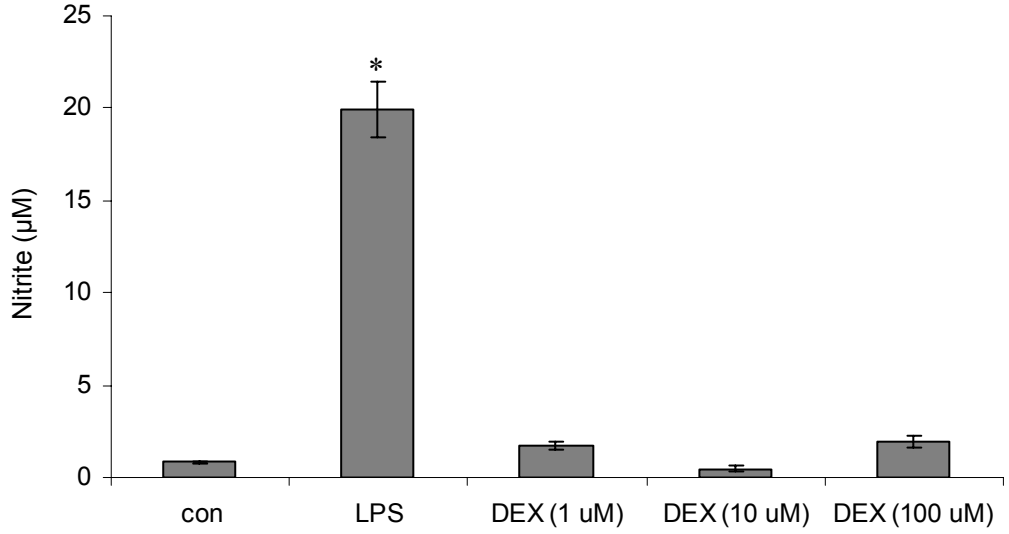

Figure 4.3.1: Effect of DEX dosages on LPS-induced NO production in microglial culture. Microglia were treated with 1, 10 or 100 μM DEX for 48 h, cells without LPS treatment served as negative control (con). **P* < 0.05 compared with control culture (n = 3).

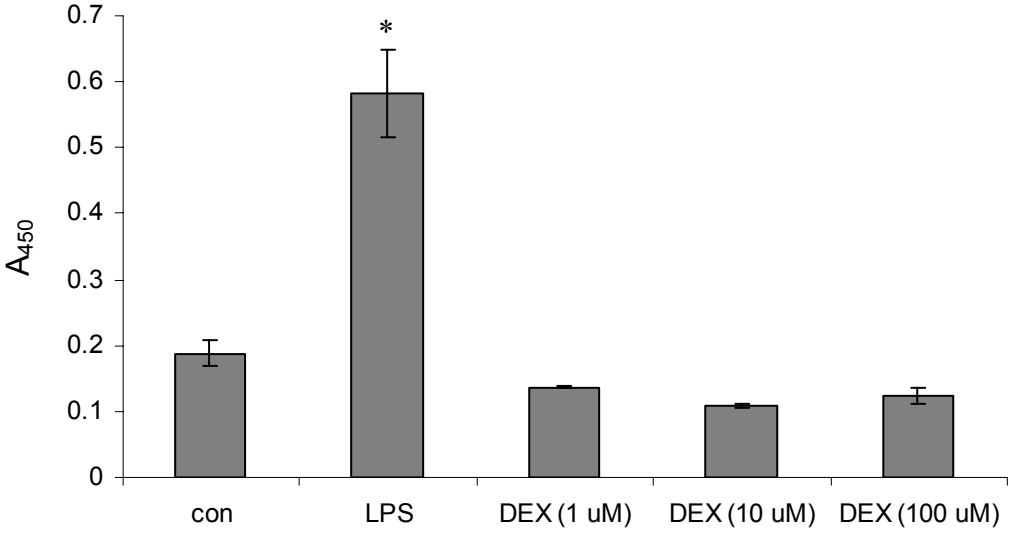

Figure 4.3.2: Effect of DEX dosages on LPS-induced microglia proliferation. Microglia were treated with 1, 10 or 100 μM DEX for 48 h, cells without LPS treatment served as negative control (con). **P* < 0.05 compared with control culture (n = 3).

Resting microglial cells show a highly ramified structure in the normal adult brain. In response to brain injury, microglia are activated and develop a round, amoeboid morphology (Stence et al., 2001; Jones et al., 1998, Bohatschek et al., 2001). *In vitro* purified primary microglia in culture have morphological and antigenic features resembling that of adult activated microglia (Slepko and Levi, 1996). Thus the purified primary microglial culture was used as a model of activated microglia to investigate the capacity of DEX at normal (1 μM) or high dosage (100 μM) to inhibit proinflammatory cytokines TNFα and IL-1β production using real-time RT-PCR. As demonstrated in Figure 4.3.3, 1 or 100 μM DEX treatment significantly reduced the mRNA levels of TNFα and IL-1β in microglial culture compared to control culture. For both TNFα and IL-1β, the mRNA levels in 1 and 100 μM DEX treated cultures were not significantly different.

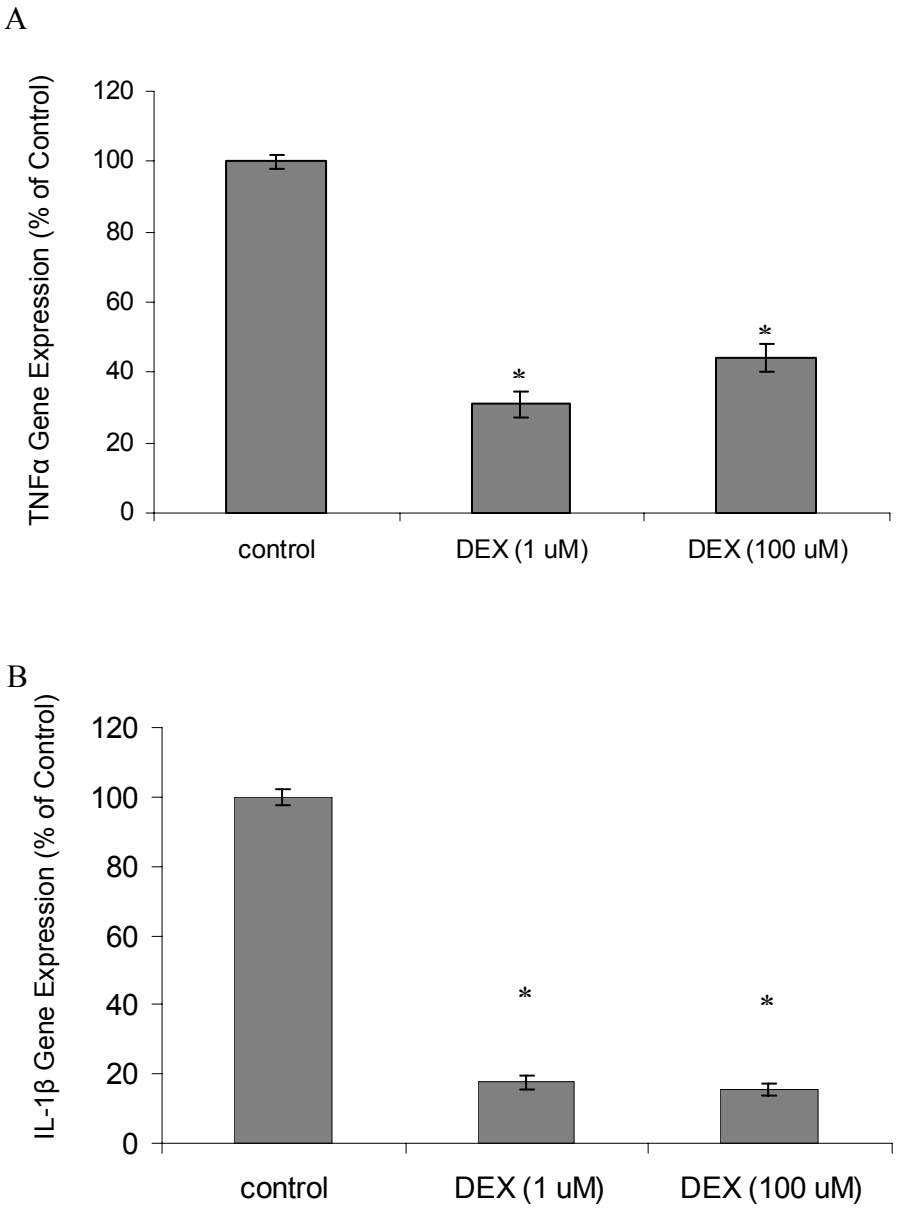

Figure 4.3.3: Effect of DEX dosages on gene expression of proinflammatory cytokines in microglial culture. (A) TNFα expression, and (B) IL-1β expression. Microglia were treated with 1 or 100 μM DEX for 48 h, cells without DEX treatment served as negative control. The level of gene expression was calculated after normalizing against GADPH in each group and is presented as relative mRNA expression units. **P* < 0.05 compared with control culture (n = 3).

Response of Astrocytes to DEX at Various Dosages

Purified primary astrocytes culture is more reactive than normal mature astrocytes as evidenced by high basal level of reactive gliosis related products and cell proliferation (McMillian et al., 1994; Wu and Schwartz, 1998). Thus the purified primary astrocyte culture was used as a model of reactive astrocytes to investigate the capacity of DEX at various dosages to inhibit astrocyte proliferation as well as the gene expression of TGFβ1 and neurocan. As demonstrated in Figure 4.4.1, 1, 10 or 100 μM DEX treatment significantly reduced the number of viable cells compared to control culture, while the cell number in DEX treated cultures were not significantly different. Live/dead cell assay showed that the percentages of viable cells for control culture, 1, 10, and 100 μM DEX treated cultures were 98.96%, 98.99%, 99.48%, and 99.15 respectively, indicating that all DEX at all three concentrations was not toxic to astrocytes, and the ability of DEX to inhibit astrocyte proliferation was not affected at high dosages.

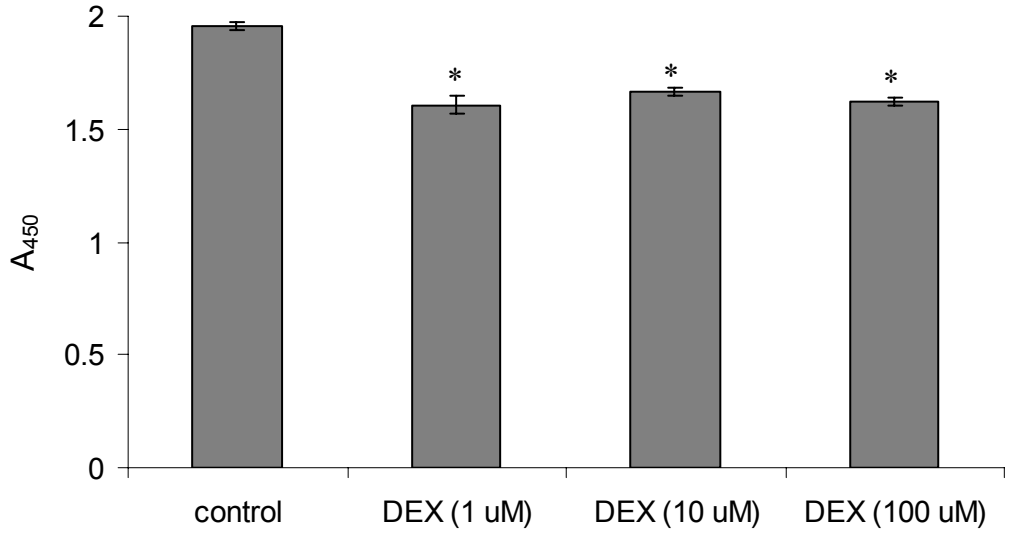

Figure 4.4.1: Effect of DEX dosages on astrocyte viability. Astrocytes were treated with 1, 10 or 100 μM DEX for 48 h, cells without DEX treatment served as control. *$P < 0.05$ compared with control culture (n = 6).

The capacity of DEX at normal (1 μM) or high dosage (100 μM) to inhibit TGFβ1 and neurocan expression was assessed using real-time RT-PCR. As demonstrated in Figure 4.4.2, 1 or 100 μM DEX treatment significantly reduced the mRNA levels of TGFβ1 and neurocan in DEX treated astrocyte culture compared to control culture. For both TGFβ1 and neurocan, the mRNA levels in 1 and 100 μM DEX treated cultures were not significantly different.

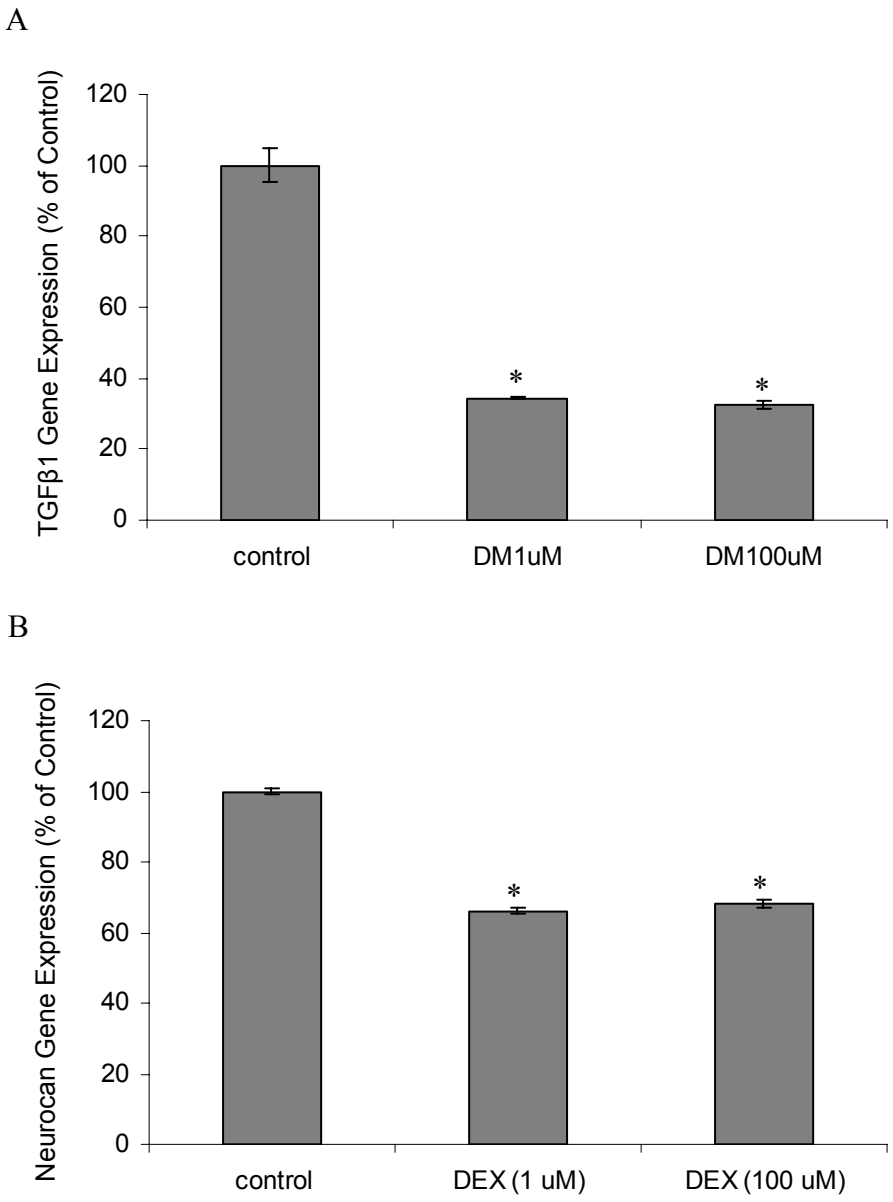

Figure 4.4.2: Effect of DEX dosages on gene expression of glial scar associated molecules in astrocyte culture. (A) TGFβ1 expression, (B) neurocan expression. Astrocytes were treated with 1 or 100 μM DEX for 48 h, cells without DEX treatment served as negative control. The level of gene expression was calculated after normalizing against GADPH in each group and is presented as relative mRNA expression units. *$P < 0.05$ compared with control culture (n = 3).

Response of Neurons to DEX at Various Dosages

The neurotoxicity of DEX at various dosages was evaluated using cell counting kit-8 to assess the number of viable cells. Purified rat cortical neurons were incubated with 1, 10 or 100 μM DEX for 48 h. Figure 4.5 demonstrated that DEX at all three concentrations did not significantly change the number of viable neurons, indicating that DEX is not neurotoxic even at 100 times of its normal effective dosage.

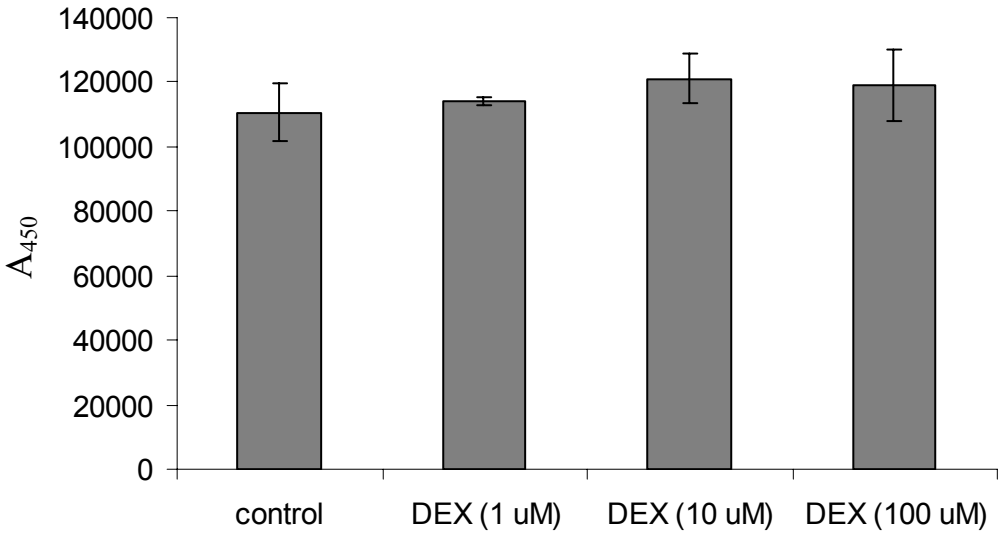

Figure 4.5: Effect of DEX dosages on neuron cell viability. Cortical neurocans were treated with 1, 10 or 100 μM DEX for 48 h, cells without DEX treatment served as control. **P* < 0.05 compared with control culture (n = 6).

Discussion

The first objective of this study was to compare the anti-inflammatory potency of α-MSH and DEX based on NO production in microglia and glial cell proliferation. Purified primary microglial culture originated from neonatal brains shows a round, amoeboid morphology resembling adult activated microglia (Stence et al., 2001; Jones et al., 1998, Bohatschek et al., 2001) and phagocytic activity. Thus they were suggested to be activated microglia (Slepko and Levi, 1996). However, unlike activated microglia *in vivo*, NO production in primary microglia culture is low and the cells are not in active proliferation. The bacterial endotoxin LPS has been widely used to establish an experimental model of glial activation *in vitro* (Sola et al., 2002; Golde et al., 2003; Mizuno et al., 2005). Thus in this study LPS was used to stimulate microglial culture to upregulate NO production and proliferate. It has been well documented that α-MSH inhibits the production of proinflammatory cytokines and NO by activated microglia via the modulation of NF-κB activation (Ichiyama et al., 1999; Manna and Aggarwal, 1998; Starowicz and Przewlcka, 2003, Lipton et al., 2000). However, to our knowledge, the effect of α-MSH on microglia proliferation hasn't been reported. This study showed that α-MSH does not impact LPS-stimulated microglia proliferation which, in contrast, was completely inhibited by DEX treatment. This is consistent with previous studies showing that DEX inhibits microglia proliferation (Tanaka et al., 1997; Ganter et al., 1994).

Both α-MSH and DEX were reported to have inhibitory effects on NO production (Galimberti et al., 1999; Lipton et al.; 1997, Lipton et al., 2000; Golde et al., 2003; Cui et al., 1994). It was suggested that DEX reduced NO production through regulation of iNOS expression by accelerating proteasome-dependent degradation (Golde et al., 2003).

This study showed that both α-MSH and DEX significantly inhibited LPS-stimulated NO production in microglia culture. However, NO level in α-MSH treated culture was still significantly higher than control culture, while DEX treatment completely abolished LPS-stimulated NO upregulation.

Purified primary astrocyte cultures derived from neonatal brains are highly reactive compared with astrocytes in normal adult brains even when the culture is matured for 4 weeks before use. The cells have high basal level of reactive gliosis related products and are highly proliferative (McMillian et al., 1994; Wu and Schwartz, 1998). Thus it was used as a model of reactive astrocytes to investigate the anti-inflammatory effects of α-MSH and DEX on astrocytes in this study. The results show that α-MSH does not impact astrocyte proliferation, while DEX significantly reduced astrocyte proliferation. It was previously reported that DEX inhibits astrocyte proliferation in primary culture through glucocorticoid receptor pathways (Crossin et al., 1997). Collectively, these results suggest that the anti-inflammatory effects of DEX is more powerful than α-MSH in that it has stronger inhibitory effects on LPS-stimulated NO production by microglia and it inhibits the cell proliferation of microglia and astrocytes.

The second objective of this study was to further evaluate the anti-inflammatory effects and neurotoxicity of DEX at dosages higher than normal effective dosage to assess the safe and effective dosage range. Previous studies suggest DEX at dosages dosages equal or less than 1 μM effectively exerts anti-inflammatory effects on glial cells, therefore the anti-inflammatory effects and cytoxicity of DEX at 1, 10 and 100 μM on cortical cells including microglia, astrocytes and neurons were evaluated. The results from microglial culture showed that the ability of DEX at all three concentrations to

inhibit LPS-stimulated NO production and cell proliferation in microglia was similar. In addition, 1 and 100 μM DEX significantly reduced the gene expression of proinflammatory cytokines TNFα and IL-1β in microglia, and the inhibitory effects of DEX at both concentrations were not significantly different. These results demonstrated that the anti-inflammatory effects of DEX on microglia were not affected at the concentration more than 100 times higher than normal effective dosage.

DEX at all three concentrations exhibited similar effects on inhibiting astrocyte proliferation. Cell survival study demonstrated that DEX at all three concentrations were not cytotoxic to astrocytes. A previous study showed that the inhibitory effects of DEX on astrocyte proliferation were dose dependent over the range of 0.1 to 10 nM, and then reached plateau over the range of 10 nM to 10 μM (Crossin et al., 1997), however, this study didn't investigate the effects of DEX at concentrations higher than 10 μM. Our results demonstrated that inhibitory effects of DEX on astrocyte proliferation DEX at 100 μM remained unchanged.

Astrocytes produce TGFβ1 as well as responding to it in response to CNS insult (John et al., 2003). Upregulation of TGFβ1 after brain injury was shown to be involved in the deposition of extracellular matrices that forms the glial-fibrotic scarring observed at the wound site (Smith and Strunz, 2005; Logan et al., 1994). Inhibition of TGFβ1 activity has been shown to prevent reactive astrocytes from organizing into a limiting glial membrane around the injury site, and reduced the deposition of laminin, fibronetin, and CSPGs in the glial scar (John et al., 2003; Logan and Berry, 1993; Griffith and McKeon, 1999). CSPGs are important inhibitory molecules in glial scar (Properzi and Fawcett, 2004; Fawcett and Asher, 1999). A number of studies have shown that TGFβ1 increased

neurocan production in primary astrocyte culture (Smith and Strunz, 2005; Asher et al., 2000). Neurocan is an important inhibitory CSPG that is produced mostly by astrocytes, and oligodendrocyte precursors. This study demonstrated that DEX significantly reduced the gene expression of TGFβ1 and neurocan in primary astrocyte culture. The experimental result of TGFβ1 gene expression is in accordance with previous studies showing that DEX caused a significant decrease in the basal and PMA-induced levels of TGFβ1 mRNA in glial cells (Batuman et al., 1995). It is noteworthy that DEX also reduced neurocan expression in astrocytes. Although the anti-inflammatory effects of glucocorticoid were widely studied in the CNS, these studies have been focused on the inhibitory effects of glucocorticoids on the production of proinflammatory molecules and glial cell proliferation. The effects of glucocorticoids on CSPG production in the CNS hasn't been addressed yet. Studies outside the nervous system have shown that glucocorticoids suppress proteoglycan production by human tenocytes and equine articular cartilage explants (Wong et al., 2005; Doyle et al., 2005). However, the mechanism was not discussed in these studies. The effects of DEX on CSPG production in astrocytes are unclear. The effects may be indirect via inhibition of TGFβ1 expression, as TGFβ1 knowingly promotes neurocan expression. It is also possible that DEX directly affects neurocan production through glucocorticoid receptor pathways. The inhibitory effects of DEX at 100 μM on TGFβ1 and neurocan expression were similar to its effects at 1 μM, suggesting that the anti-inflammatory effects of DEX on astrocytes were not affected at 100 μM.

The neurotoxicity study showed that DEX at all three concentrations were not cytotoxic to neurons. Collectively, these results demonstrate that DEX is safe and exerts effective anti-inflammatory effects over the range of 1 to 100 μM.

Conclusions

In this study, both DEX and α-MSH were shown to be able to inhibit NO production by activated microglia and were not neurotoxic, therefore both drugs have the potential to be used to as the anti-inflammatory agent to mitigate the inflammatory tissue response at the electrode-brain interface in *vivo*. However, DEX was shown to be a more potent anti-inflammatory agent than α-MSH, as it not only reduced NO production more effectively, but also inhibited microglia and astrocyte proliferation. In addition, this study demonstrates that DEX is safe and exerts effective anti-inflammatory effects over the range of 1 to 100 μM, suggesting that DEX is suitable to be used in drug delivery systems with initial burst release. This study suggests that local delivery of DEX may have the potential to reduce the inflammation at the electrode-brain interface and facilitate long-term recording from cortical neural prosthetics *in vivo*.

CHAPTER V

IN VIVO EVALUATION OF ANTI-INFLAMMATORY POTENTIAL OF DEXAMETHASONE-NITROCELLULOSE COATING IN A RODENT MODEL

Abstract

Glial scar formation around implanted silicon neural probes compromises their ability to facilitate long-term recordings. One approach to modulate the tissue reaction around implanted probes in the brain is to develop probe coatings which locally release anti-inflammatory drugs. In this study, we developed a nitrocellulose-based coating for the local delivery of the anti-inflammatory drug dexamethasone (DEX). Silicon neural probes with and without nitrocellulose-DEX coatings were implanted into rat brains, and inflammatory response was evaluated 1 week and 4 weeks post implantation. DEX coatings significantly reduced the reactivity of microglia and macrophages one week post implantation as evidenced by ED1 immunostaining. CS56 staining demonstrated that DEX treatment significantly reduced chondroitin sulfate proteoglycan (CSPG) expression one week post implantation. Both at one week and at four week time points, Glial fibrillary acidic protein (GFAP) staining for reactive astrocytes and neurofilament (NF) staining revealed that local DEX treatment significantly attenuated astroglial response and decreased neuronal reduction in the vicinity of the probes. Weak ED1, neurocan and NG2 positive signal was detected four weeks post implantation for both coated and uncoated probes, suggesting a stabilization of the inflammatory response over time in this

implant model. In conclusion, this study demonstrates that the nitrocellulose-DEX coating can effectively attenuate the inflammatory response to the implanted neural probes, and decrease neuronal reduction in the vicinity of the coated probes. Thus anti-inflammatory probe coatings may represent a promising approach to attenuate astroglial scar and decrease neural reduction around implanted neural probes.

Introduction

Functional recording from the nervous system using silicon micromachined neural probes potentially aids patients with movement disorders by enabling the processing and decoding of recorded neural signals into movement commands (Donoghue, 2002; Otto et al., 2003; Sanchez et al., 2004). However, the long-term performance of the implanted neural probes is compromised by the formation of glial scar around the Si-microelectrodes, which is a typical consequence of the inflammatory tissue reaction to implantation-induced injury in the CNS. The glial scar is inhibitory to neurons and forms a barrier between the electrode and neurons in the surrounding brain tissue (Schwartz, 2004; Shain et al., 2003; Edell et al., 1992).

When a neural probe is inserted into the brain, neurons and glial cells are killed or injured during insertion, blood vessels are disrupted and the blood-brain barrier (BBB) is damaged. The tissue injury and breakdown of BBB cause release of cytokines and neurotoxic free radicals, invasion of blood-borne macrophages, and edema (Fitch and Silver, 1997; Schwartz, 2004). The main cell types involved in tissue reaction to the brain injury are astrocytes, microglia/blood-borne macrophages, and oligodendricyte precursors (OPCs) (Fawcett and Asher, 1999; Norton, 1999; Hampton et al., 2004).

These cells express chondroitin sulfate proteoglycans (CSPGs), important inhibitory molecules in glial scar (Properzi and Fawcett, 2004; Fawcett and Asher, 1999). Astrocytes produce neurocan, phosphacan, and brevican; microglia/macrophages produce NG2; and OPCs produce neurocan, NG2, and versican (Properzi and Fawcett, 2004; Fawcett and Asher, 1999; Tang et al., 2003; Tatsumi et al., 2005; Hampton et al., 2004). It has recently been suggested that part of NG2 positive cells proliferating in the injury site differentiate into the glial scar astrocytes (Alonso et al., 2005; Tatsumi et al. 2005). The CSPGs and other glial scar associated inhibitory molecules create an inhibitory environment that blocks the regrowth of neural processes and may potentially cause the exclusion of neural cells by their presence. Although CSPG expression has been extensively studied in CNS injuries, its role in the tissue reactions to implanted neural electrodes has not been addressed.

The failure of the implanted neural probes over time can be attributed to the neuronal loss around the probe including both neuron cell body loss and neural process loss (Liu et al., 1999; Spataro et al., 2005; Schwartz, 2004). Therefore, to maintain long-term recording stability, reactive gliosis and other inflammatory processes around the electrode need to be minimized. One approach to modulating the inflammatory response around neural probes is to develop coatings to modify the neural probe surfaces to achieve better integration of the neural probes with brain tissue. Dexamethasone (DEX) is a synthetic glucocorticoid hormone that is used to treat many inflammatory responses. In CNS, systematic injection of DEX was shown to reduce tissue reaction around neural implants (Shain et al., 2003; Spataro et al., 2005). Addition of DEX to activated microglia-neuron cocultures protect neurons by down-regulating nitric oxide (NO)

production (Golde et al., 2003). However, systemic administration of DEX may cause serious side effects including myopathy and diabetes (Kaal and Vecht, 2004; Koehler, 1995; Twycross, 1994). Therefore local delivery of DEX is a promising strategy to minimize the side effects. In this study, a nitrocellulose-based coating that is capable of sustained local release of DEX from implanted neural probes was designed. Scar/inflammation related cellular and molecular responses to neural probes with and without DEX coatings were characterized.

Materials and Methods

In vivo implantation of DEX coated probes

All procedures involving animals were approved by the Institutional Animal Care and Use Committee (IACUC) of the Georgia Institute of Technology. Adult male Sprague Dawley rats weighing between 275-299 g were used in this study. The rat was pre-anesthetized with a mixture of 5% isoflurane and 1 L/min oxygen in a chamber, and maintained in anesthesia with 2-3% isoflurane and 0.3 L/min by a nose mask during surgery. The rat was immobilized in a stereotaxic frame by mounting the stereotaxic ear bars into the rat auditory meatus. The surgical area was shaved and disinfected with isopropyl alcohol and chlorohexaderm using a slight scrubbing motion before making the incision. Ophthalmic ointment will be applied to the eyes to prevent drying during surgery. Following a midline incision, the periosteum connective tissue adhering to the bone was scraped and removed till the cranial sutures were exposed. Two 3 mm holes were created +0.2 mm anterior, and 3 mm lateral to the bregma using a 3-mm trephine

attached to a dental drill. Physiological saline was applied to the skull to reduce the heat caused by drilling. The bone plug was removed carefully, and the dura was gently pierced and retracted with fine microforceps. Two neural probes were inserted into each brain manually, with one DEX-coated probe in one side of the brain and one uncoated probe in the other side of the brain. The two holes were covered with 1% agarose gel and dental acrylic, the skin was closed with suture, and then the animal was allowed to recover.

Tissue preparation and immunohistochemistry

At two distinct time points, one week and four weeks post surgery, the rats were anesthetized with ketamine (1 mL/kg), xylazine (0.17 mL/kg), and acepromazine (0.37 mL/kg), and perfused transcardially with 0.1 M PBS (pH7.4) followed by 4% paraformaldehyde in PBS. The brains were removed carefully so that the implanted neural probes remained intact. After post-fixation of the brains in 4% paraformaldehyde for 24 h, the neural probes were retrieved; the brains were cryoprotected in 30% sucrose in PBS solution until the brains sunk. The brains were frozen in Tissue Tek OCT embedding compound. Cryostat sections 30 μm in thickness were cut in the horizontal plane.

The floating sections were blocked with 4% normal goat serum for 1h at room temperature with 0.5% Triton X-100 (Sigma) and incubated overnight at 4°C with primary antibodies. Secondary antibody incubations were performed at room temperature for 1 h. All the sections were counterstained with the nuclear dye 4',6-diamidino-2-phenylindole (DAPI, Molecular Probes). Tissue sections were mounted on

glass microscope slides with Fluoromount-G (Southern Biotechnology Associates, Inc. Birmingham AL).

The following primary antibodies were used: rabbit polyclonal anti-glial fibrillary acidic protein (GFAP, Dako, 1:1000) to identify astrocytes, mouse monoclonal ED1 (Serotec, 1:1000) to identify reactive microglia and macrophages, rabbit polyclonal anti-Iba-1 to identify microglia/macrophages (Wako Chemicals, 1:500), mouse monoclonal anti-neurofilament 160 (NF160, Sigma, 1:500) to identify neuron cell body and processes, mouse monoclonal anti-NeuN (Chemicon, 1:500) to identify neuronal nuclei, monoclonal anti-chondroitin sulfate (CS56, Sigma, 1:100) to identify CSPGs, mouse monoclonal anti-neurocan (Chemicon, 1:1000) to identify neurocan, rabbit polyclonal anti-NG2 (Chemicon, 1:500) to identify NG2, rabbit polyclonal anti-fibrinogen (Dako, 1:500) to evaluate BBB leakage, and mouse monoclonal anti-RECA-1 to identify endothelial cells (Serotec, 1:500). The secondary antibodies were diluted 1: 200 in blocking medium. In general, goat anti-rabbit IgG Alexa 488 (Molecular Probes) was used for polyclonal primary antibodies, and goat anti-mouse IgG1 Alexa 594 (Molecular Probes) was used for monoclonal primary antibodies. The secondary antibody for CS56 was goat anti-mouse IgM Alexa 594 (Molecular Probes). Sections treated without primary antibodies were used to distinguish specific staining from nonspecific antibody binding.

Hematoxylin and eosin (H&E) staining was performed to evaluate the fibrous encapsulation around implanted neural probes. Slides of frozen sections were rinsed in water and hematoxyline for 2 min and then washed well in tap water. After rinsing the slides in 95% alcohol, the slides were stained with eosin for 10 sec and rinsed with tap

water, then dehydrated with alcohol, cleared with xylene, and mounted with polymount mounting media.

Quantitative image analysis

Fluorescent images were captured from a Zeiss fluorescence upright light microscope (Wetzlar, Germany) equipped with an Olympus digital camera. The fluorescent staining intensity was quantified using a custom-built Matlab-based image analysis program based on a method previously reported (Kim et al., 2004). This program generates 30 line intensity profiles starting from the probe-brain interface. The 30 line profiles were averaged while keeping track of distance from the probe to obtain the fluorescent intensity plots as a function of distance from the implanted probe surface (Figure 5.1.1). The staining intensity at both sides of the electrode will be quantified in the same way and averaged to get the intensity - distance profile for each image. To account for variations in staining intensity due to immunohistochemical methods, for each brain section, the fluorescent intensity in non-injured regions was defined as background intensity, and was normalized to 1. The fluorescent intensity along the line profiles was then quantified and plotted relative to the background intensity.

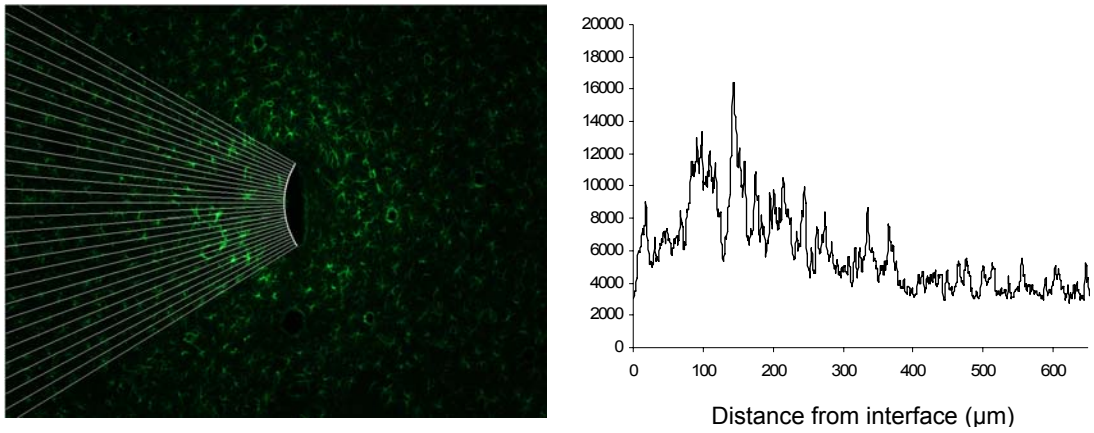

Figure 5.1.1: Method for quantitative analysis of immunostained brain sections. (A) 30 lines starting from the electrode-brain interface are generated. (B) The 20 fluorescent intensity – distance profiles obtained from each line in (A) are averaged to get the averaged intensity – distance profile.

For quantification of ED1 staining, the total area under the intensity-distance curve subtracted by the background area (the shaded area in Figure 5.1.2A) within a 100 μm radius from the surface of the inserted probe was used to calculate the total fluorescent intensity. The 100 μm radius was chosen because it was previously shown that there was a strong inverse correlation between ED1 and neurofilament immunoreactivity within100 μm of the neural probe interface at both 2 and 4 weeks (Biran et al., 2005).

For quantification of GFAP and CS56 staining, the total area under the intensity-distance curve subtracted by the background area (the shaded area in Figure 5.1.2A) within 250 μm from the interface was used to calculate the total fluorescent intensity. The 250 μm radius was chosen because it was reported that significant reductions in neurofilament immunoreactivity extended up to 230 μm from the interface (Biran et al., 2005). Reactive astrocytes produce inhibitory molecules such as CSPGs that are

inhibitory to neurons, and elevated GFAP expression extended over a distance greater than 400 μm from the interface. Thus the neurofilament loss over 100 μm may be correlated to reactive astrocytes and CSPGs produced by both reactive astrocytes and microglia.

Neurofilament (NF 160kDa) staining was used to assess neuronal reduction, the NF reduction was defined as the percentage of the NF reduction area (the shaded area in Fig. 7B) relative to the sum of NF reduction area and the remaining NF area within a 50 μm radius from the surface of the inserted probe. The 50 μm radius was chosen because neurons more than 50 μm away from the recording sites are difficult to discriminate for single unit isolation (Henze et al., 2000). At least 12 images from 4 rats along the probes were used to quantify each marker analyzed.

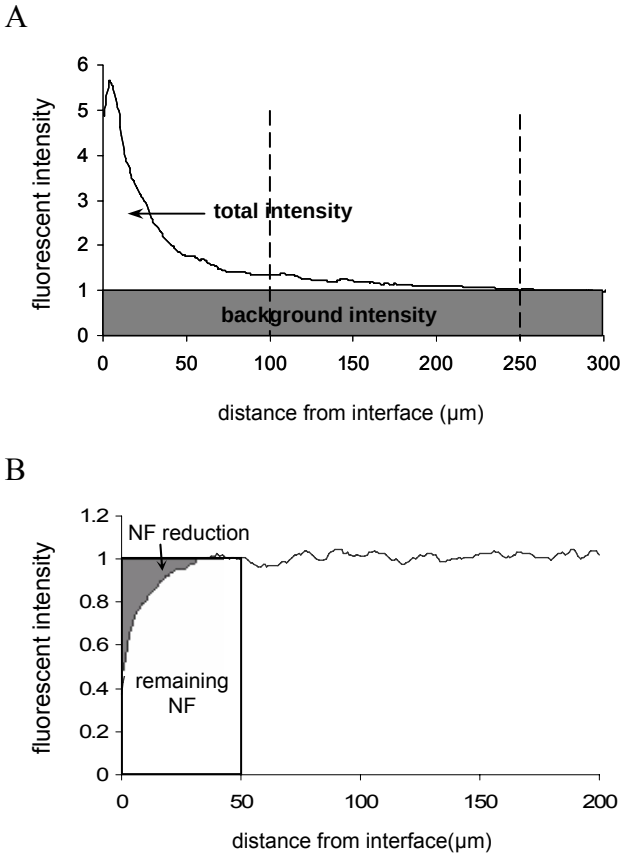

Figure 5.1.2: Diagram for quantification of (A) GFAP, ED1, and CS56 staining, the total area under the intensity-distance curve subtracted by the background (the shaded area) is defined as the total intensity, and (B) neurofilament staining, the percentage of the NF reduction area relative to the sum of the NF reduction area and the remaining NF area is defined as % of NF reduction.

For quantification of the number of astrocytes and neurons, fluorescent images of GFAP staining and NeuN staining were used to identify astrocytes and Neurons respectively. A custom-built Matlab-based image analysis program was used to automatically count the cell distribution as a function of distance at 50 μm intervals. As illustrated in Figure 5.1.3, each white dot represents an astrocyte. Due to the complexity of astrocyte structure, the program can not accurately identify all the astrocytes.

Therefore the cells that the program failed to count were added manually (indicated by red dots).

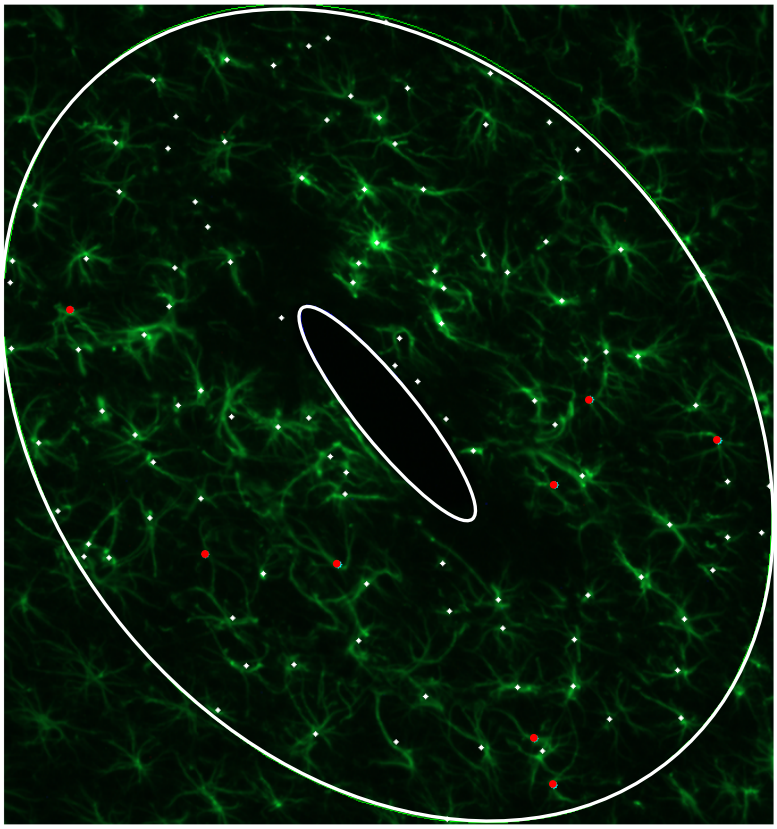

Figure 5.1.3: Sample fluorescent image GFAP immunostaining for quantification of astrocyte number. All the astrocytes within 200 µm distance from the probe-brain interface were counted by a custom-built Matlab-based image analysis program. Each white dot represents an astrocyte identified by the program, each red dot represents an astrocyte that the program failed to identify and added manually.

Animal number and Data Analysis

Four animals were used for each time point (n = 4). For 1 week time point, 6 brain sections at equal depth interval were selected for each staining spanning approximately

1.5 mm of the cerebral cortex. The number of brain sections for each staining is listed in Table 5.2. For 4 week time point, 3 brain sections were selected for each staining.

Data are represented as the average value ± the standard error of the mean (S.E.M). A general linear ANOVA model was used to compare mean values of the different conditions. Pairwise comparisons were conducted using Tukey 95% simultaneous confidence intervals, and $P < 0.05$ was used to indicate statistical significance.

Table 5.1: Summary of section number for each staining

Staining	Section Number					
CS56/NeuN	4	12	20	28	36	44
GFAP/NF	5	13	21	29	37	45
GFAP/ED1	6	14	22	30	38	46
H&E	7	15	23	31	39	47

Results

Assessing reactive microglia and macrophages around the probes

Immunostaining for ED1 around the probe site reveals reactive microglia/macrophages. One week post implantation, for both uncoated and DEX coated probes, the ED1 staining was concentrated around the probe-brain interface (Figure 5.2A

and B). The ED1 positive cells were small, and amoeboid in appearance. Both peak intensity and the reactive area for coated probes were reduced compared with uncoated probes at 1 week (Figure 5.2E). The total ED1 intensity for coated probes was significantly lower than uncoated probes (Figure 5.2F).

At the end of 4 weeks, the ED1 staining was significantly reduced compared with 1 week for uncoated probes (Figure 5.2A, C, and F). The difference of the total intensity between the uncoated probes and DEX coated probes at 4 weeks was not statistically significant (Figure 5.2A, D and F).

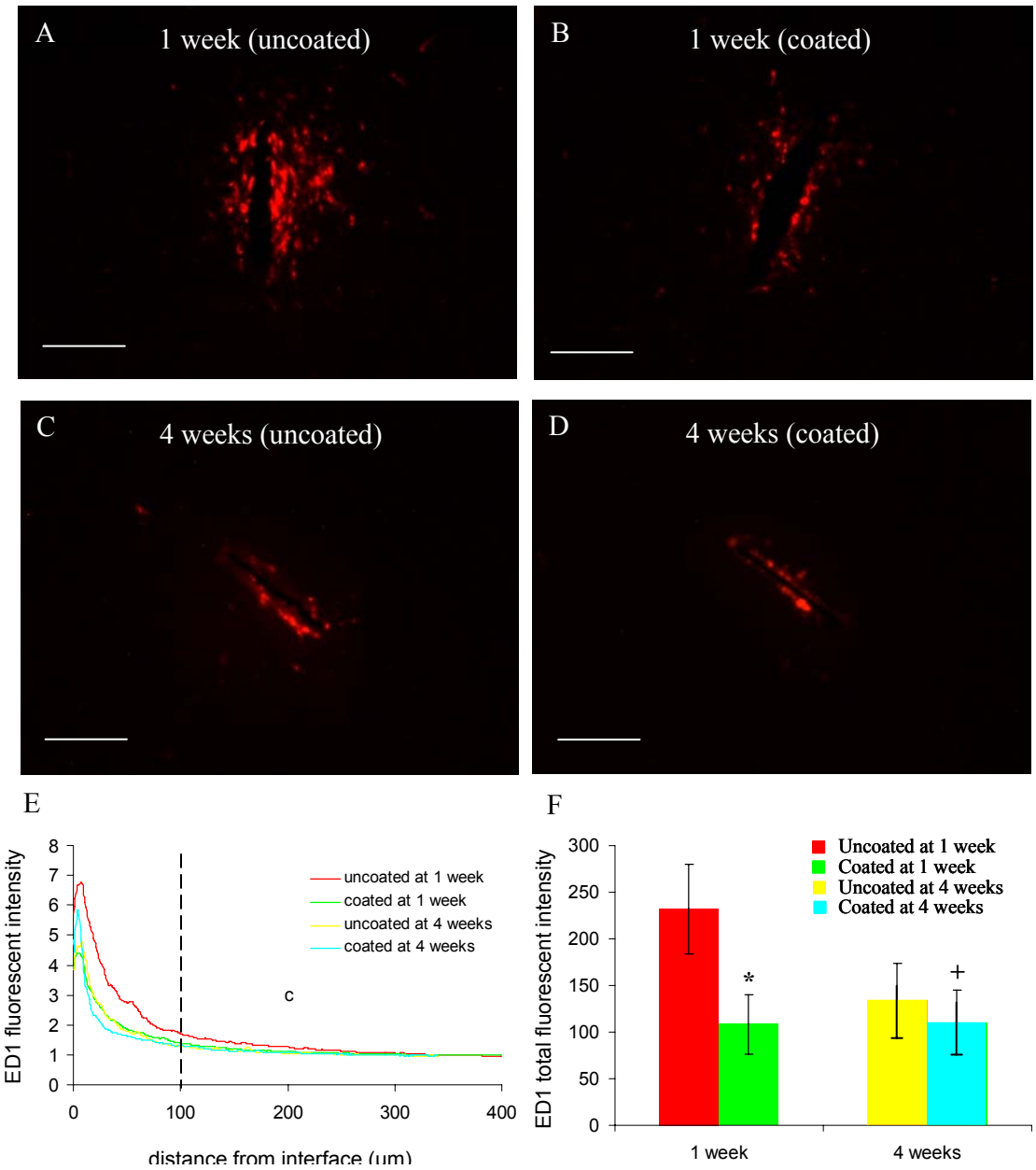

Figure 5.2: Quantitative fluorescent intensity analysis of ED1 staining. (A)-(D) Representative images of ED1 staining for reactive microglia/macrophages in the horizontal brain sections 1 week and 4 weeks post implantation for both uncoated and DEX coated probes. Scale bar = 100 μm. (E) ED1 fluorescent intensity profiles as a function of distance 1 week and 4 weeks post implantation. (F) Quantification of total ED1 fluorescent intensity 1 week and 4 weeks post implantation (n = 4). Statistical differences between uncoated and coated probes at the same time point are indicated by * ($P < 0.05$ compared with uncoated probes). Statistical difference of uncoated probes between 1 week and 4 weeks is indicated by + ($P < 0.05$ compared with uncoated probes at 1 week).

Characterizing reactive astrocytes in vicinity of implanted probes

GFAP staining was used to identify reactive astrocytes. One week post implantation, extensive GFAP elevation extending over a 400 μm radius around the uncoated probes could be observed. The GFAP intensity was relatively weak in the region within 40 μm from the probe-brain interface (Figure 5.3.1A and E), as there were few GFAP-positive cells/processes in this region. It is noteworthy that this region is correlated with intensive ED1 staining (Figure 5.2A and E). GFAP intensity started to increase from about 40 μm, peaked between 60 to 110 μm, and decreased rapidly after 200 μm (Figure 5.3.1E). Most astrocytes in the GFAP intensive area (40-200 μm) appeared hypertrophic (Figure 5.3.1A, inset), the processes of astrocyte were interwoven to form a dense meshwork. In contrast, GFAP positive astrocytes located further away were more stellate in appearance and the processes were less densely distributed.

The intensity distribution as a function of distance for coated probes showed similar pattern as the uncoated probe: weak GFAP staining around the probe-brain interface (40 μm), followed by an intensive region (40-165 μm), and a drop of GFAP intensity after 165 μm (Figure 5.3.1B and E). DEX treatment significantly reduced the total GFAP intensity (Figure 5.3.1F). Compared with uncoated probes, the astrocytes subjected to DEX treatment in the GFAP intensive area still remained stellate morphology, although they were hypertrophied compared to astrocytes in non-injured area (Figure 5.3.1B, inset). The astrocyte processes were less dense in this region compared to the same region for the uncoated probes (Figure 5.3.1A and B).

Four weeks post implantation, there was still a region of less intensive GFAP staining around the probe-brain interface (Figure 5.3.1C). GFAP intensity peaked

between 40 to 60 μm (compared with 60 to 110 μm at 1 week), and decreased rapidly after 120 μm (Figure 5.3.1E). The GFAP intensive region (20-120 μm) became more compact and closer to the probe-brain interface compared with 1 week (40-200 μm). Most astrocytes in the GFAP intensive area were hypertrophied compared with normal astrocytes (Figure 5.3.1C, inset); the astrocyte processes were interwoven to form a dense meshwork. Compared with uncoated probes, astrocytes in the same region around DEX coated probes were less hypertrophied and the processes were less densely distributed (Figure 5.3.1D, inset). The total GFAP intensity was significantly higher for uncoated probes compared with DEX coated probes (Figure 5.3.1F).

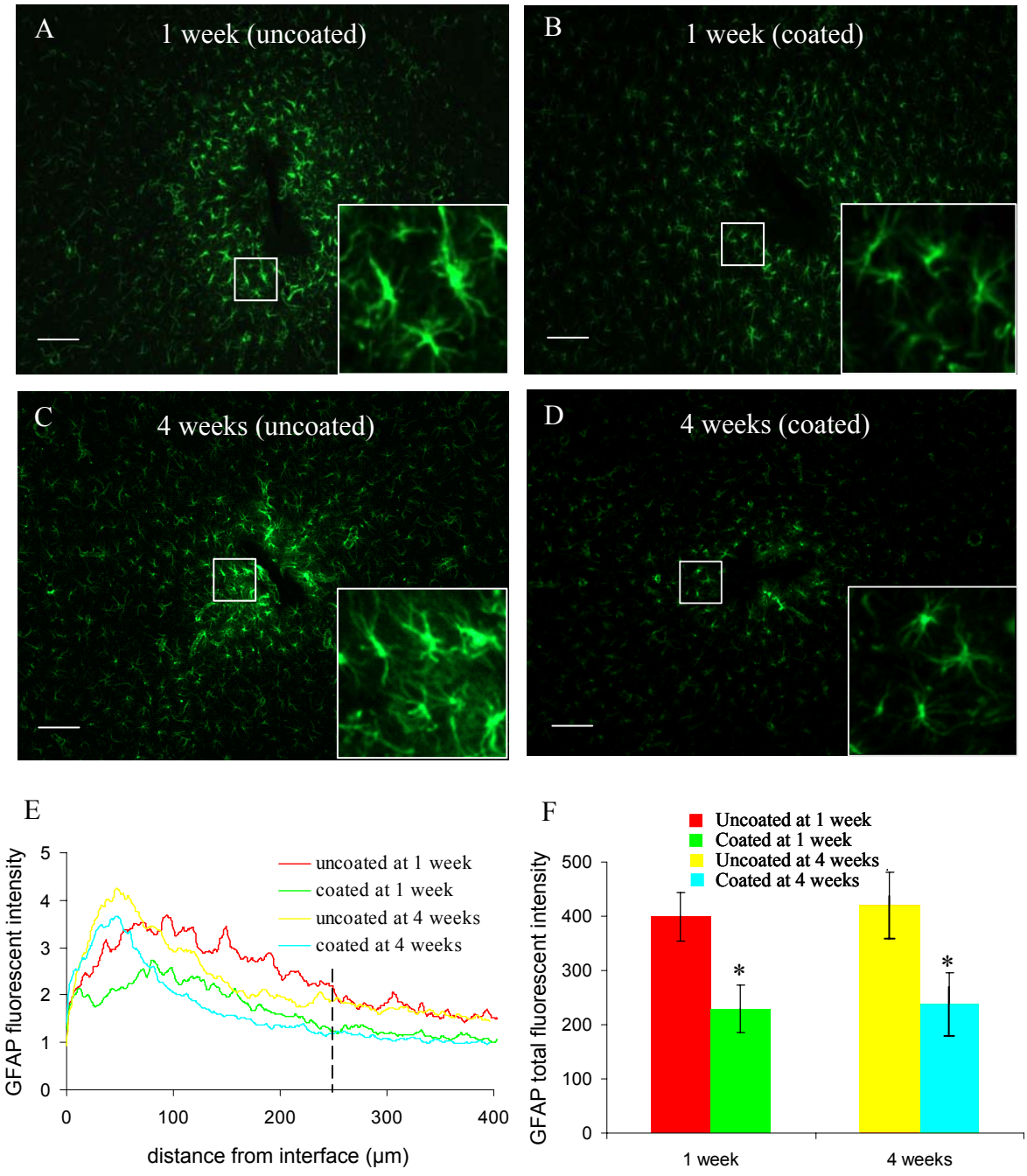

Figure 5.3.1: Quantitative fluorescent intensity analysis of GFAP staining. (A)-(D) Representative images of GFAP staining for reactive microglia/macrophages in the horizontal brain sections 1 week and 4 weeks post implantation for both uncoated and DEX coated probes. Scale bar = 100 μm. (E) GFAP fluorescent intensity profiles as a function of distance 1 week and 4 weeks post implantation. (F) Quantification of total GFAP fluorescent intensity 1 week and 4 weeks post implantation (n = 4). Statistical differences between uncoated and coated probes at the same time point are indicated by * ($P < 0.05$ compared with uncoated probes).

The histogram of astrocyte cell density distribution (Figure 5.3.2) showed that 1 week post implantation, the number of astrocytes for both uncoated and coated probes was reduced within a 50 μm radius from the interface compared with uninjured area. This is consistent with the intensity distribution profile (Figure 5.3.1E). The number of astrocytes was mildly increased between 50 to 250 μm, and started to approach normal cell distribution beyond 250 μm. There was not significant difference between the uncoated groups and coated groups.

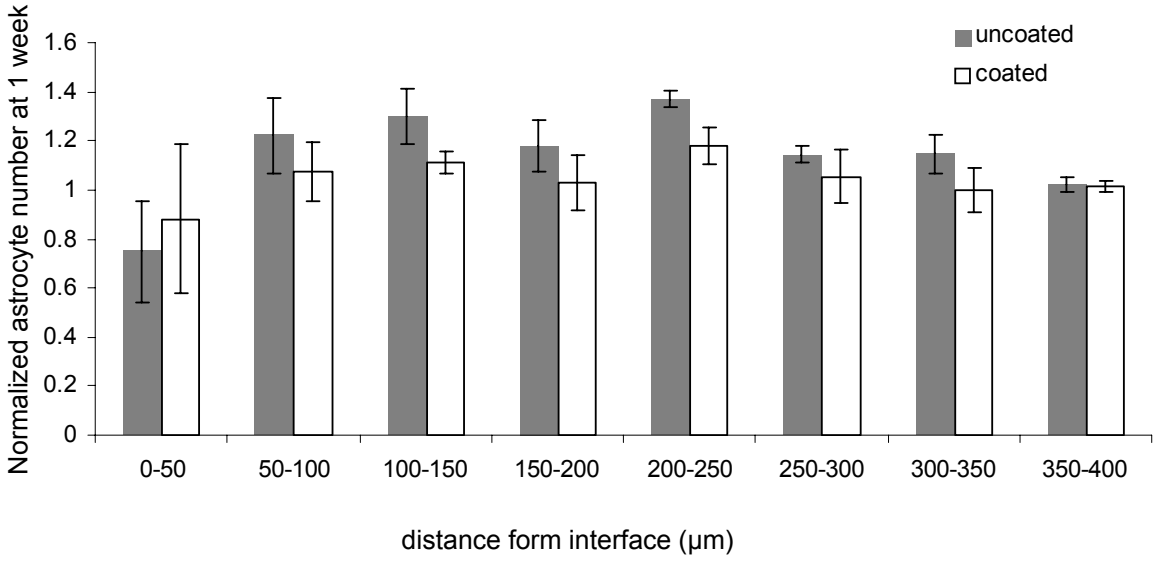

Figure 5.3.2: Histogram of astrocyte distribution around implanted neural probes. Values were normalized to the average number of $NeuN^+$ neurons of the uninjured area. (n = 4)

Presence of chondroitin sulfate proteoglycans

CS56 staining was used to identify the presence of chondroitin sulfate proteoglycans around the probe**.** Similar to ED1 localization, the intensive CS56 staining was concentrated around the probe-brain interface 1 week post implantation (Figure 5.4A

and B). For uncoated probes, the intensive staining area extended about 44 μm from the electrode-brain interface, followed by a extensive but much less intensive area (44-135 μm), beyond which the CS56 intensity started to approach background intensity (Figure 5.4E). It is noteworthy that the CS56 intensive region is correlated with the weakly GFAP stained region, and ED1 intensive region (Figure 5.2A and E, and Figure 5.3.1A and E). In the less intensive CS56 staining region, individual cells with a hypertrophied stellate morphology can be identified (Figure 5.4A), double staining with GFAP showed that these cells are hypertrophic reactive astrocytes (data not shown).

In comparison with uncoated probes, CS56 staining was significantly reduced for DEX coated probes. The total intensity for coated probes was significantly lower than uncoated probes (Figure 5.4F). Regardless of the great reduction of CS56 staining for the coated probes, the pattern of CS56 distribution was similar to that of the uncoated probes: intensive CS56 staining in the vicinity of the electrode-brain interface (27 μm), followed by a less intensive region with cells positive for both CS56 and GFAP staining (Figure 5.4E).

Four weeks post implantation, the CS56 staining was significantly reduced for uncoated probes compared with one week (Figure 5.4A and C). The intensity around the probe-brain interface was only slightly higher than background intensity (Figure 5.4E). There was no significant difference in the total CS56 intensity between the uncoated and coated probes (Figure 5.4F).

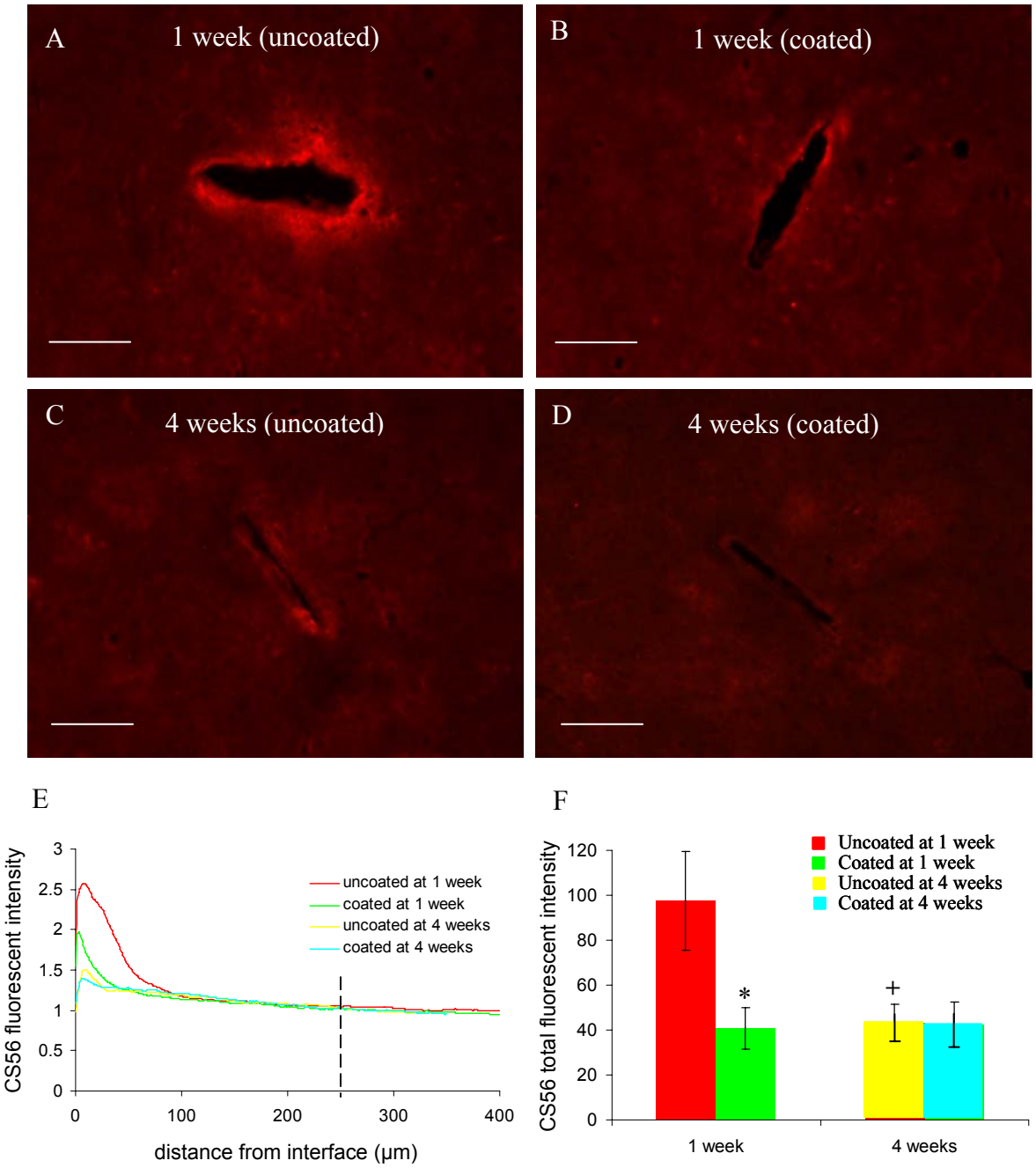

Figure 5.4: Quantitative fluorescent intensity analysis of CS56 staining. (A)-(D) Representative images of CS56 staining for reactive microglia/macrophages in the horizontal brain sections 1 week and 4 weeks post implantation for both uncoated and DEX coated probes. Scale bar = 100 μm. (E) CS56 fluorescent intensity profiles as a function of distance 1 week and 4 weeks post implantation. (F) Quantification of total CS56 fluorescent intensity 1 week and 4 weeks post implantation (n = 4). Statistical differences between uncoated and coated probes at the same time point are indicated by * ($P < 0.05$ compared with uncoated probes). Statistical difference of uncoated probes between 1 week and 4 weeks is indicated by + ($P < 0.05$ compared with uncoated probes at 1 week).

Examining the presence of specific CSPGs Neurocan and NG2

Immunostaining for neurocan and NG2 was carried out to investigate the specific nature of proteoglycan expression level with time. At the end of 1 week, elevated neurocan staining was observed around the probe-brain interface (Figure 5.5A). Double staining with NG2 antibody (marker for OPCs) showed upregulation of NG2 intensity around the probe-brain interface as well (Figure 5.5C). Neurocan and NG2 staining distribution partly overlapped. While positive neurocan staining was only observed around the probe-brain interface, NG2 staining was distributed all over the whole brain sections in the form of NG2 positive cells except around the probe-brain interface where no individual cells could be identified (Figure 5.5A and C). Four weeks post implantation, both neurocan and NG2 staining were considerably reduced compared with 1 week (Figure 5.5B and D).

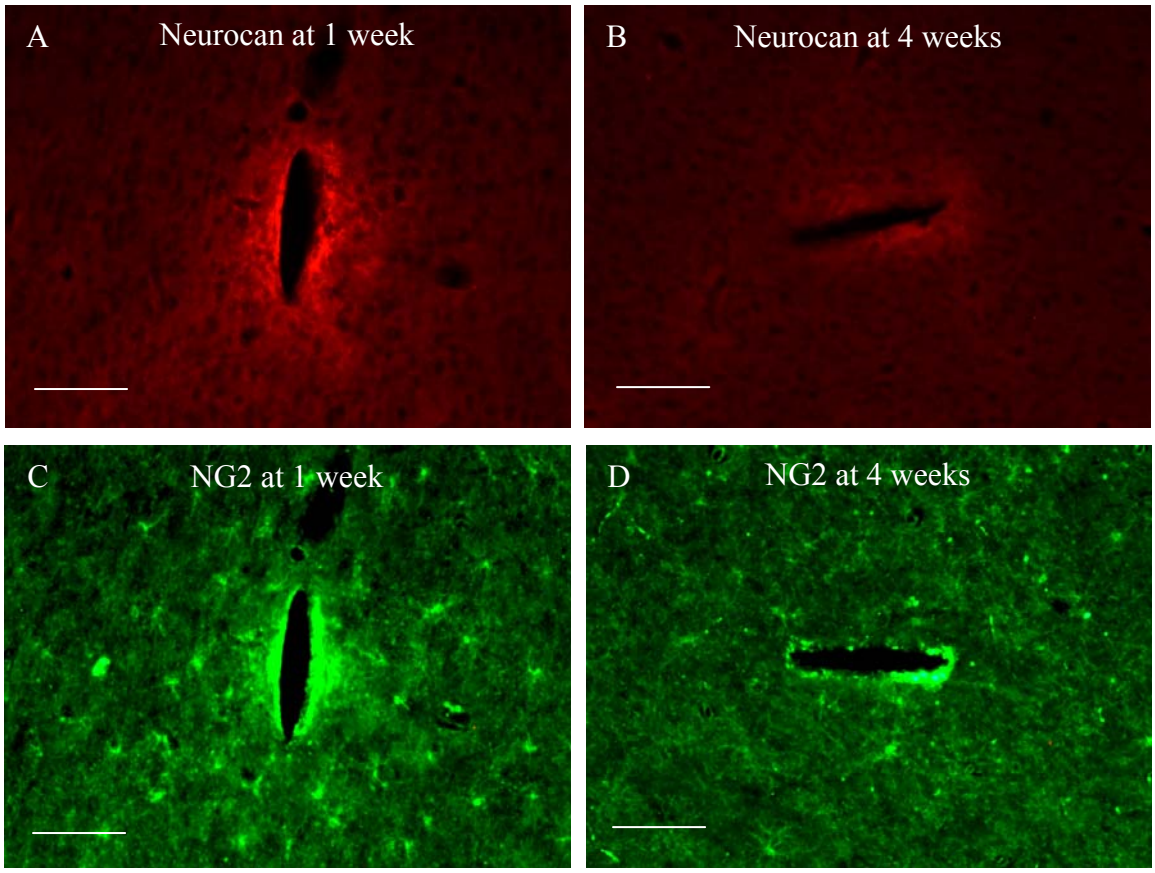

Figure 5.5: Representative fluorescent images of horizontal brain sections immunostained for Neurocan and NG2 1 week and 4 weeks post implantation. Scale bar = 100 μm.

Evaluating Fibrous Encapsulation around the Probes

H&E staining was used to investigate the fibrous encapsulation around the implanted neural probes. Figure 5.6 showed that there was no seemingly fibrous encapsulation around the implanted neural probes at all conditions. However, a thin rim of tissue (about 20 μm in thickness) at the probe-brain interface showed structural change as indicated by nuclei aggregation and alignment along the implanted probes.

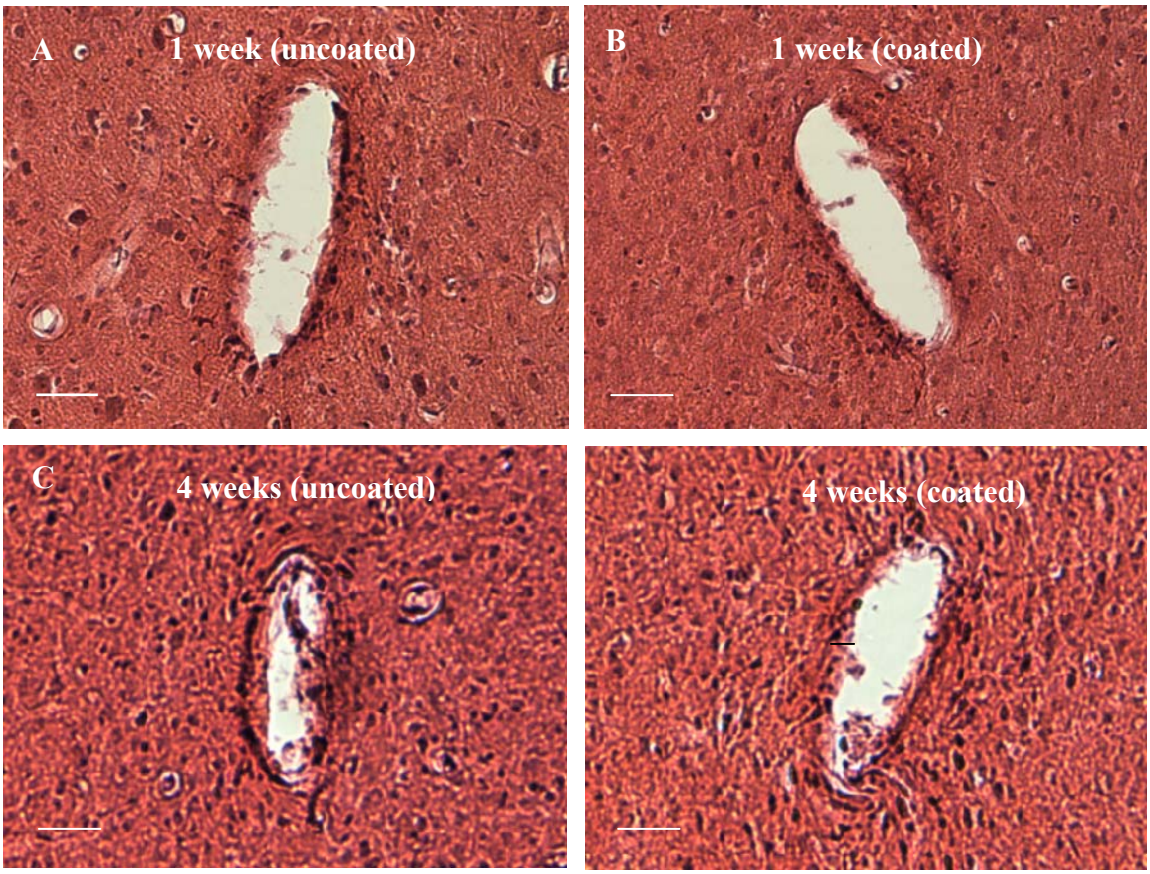

Figure 5.6: Light micrograph of horizontal brain sections stained with H&E for evaluation of fibrous encapsulation around the implanted neural probes at 1 week (A-B) and 4 weeks (C-D) for uncoated (A, C) and coated probes (B, D). Scale bar = 50 μm.

Characterizing Neuronal Presence around the Probes

Neurofilament staining stains for neuron cell body and neural processes. NF staining showed a region with reduced NF intensity around the probe-brain interface 1 week post implantation (Figure 5.7.1A). NF reduction for uncoated probes was significantly higher than coated probes (Figure 5.7.1E and F). At the end of 4 weeks, NF reduction around the uncoated probes did not significantly increase compared with 1 week (Figure 5.7.1C, D, and E). The NF reduction for uncoated probes was significantly higher than coated probes at 4 weeks (Figure 5.7.1F). It is noteworthy that the NF reduction region overlapped the ED1, CS56 positive area with weak GFAP staining, and extended to the GFAP intensive area.

The numbers of neurons within a 50 μm radius of the neural probes were reduced 65% and 50% respectively for uncoated and coated probes (Figure 5.7.2). However, there was no significant difference between the neuronal reduction around uncoated and coated probes.

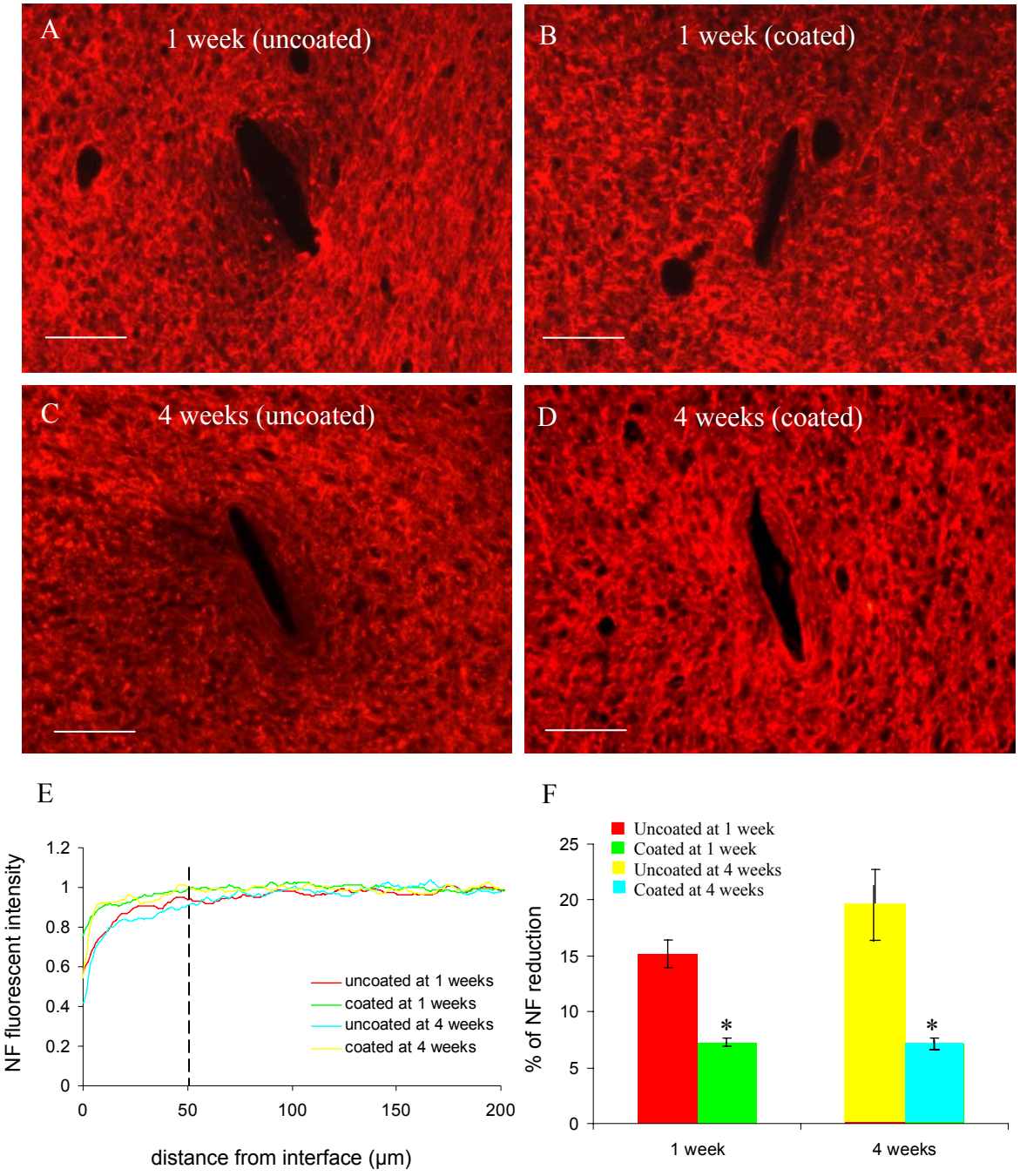

Figure 5.7.1: Quantitative fluorescent intensity analysis of NF staining. (A)-(D) Representative images of NF staining for neurons in the horizontal brain sections 1 week and 4 weeks post implantation for both uncoated and DEX coated probes. Scale bar = 100 μm. (E) NF fluorescent intensity profiles as a function of distance 1 week and 4 weeks post implantation. (F) Quantification of % of NF reduction 1 week and 4 weeks post implantation (n = 4). Statistical differences between uncoated and coated probes at the same time point are indicated by * ($P < 0.05$ compared with uncoated probes).

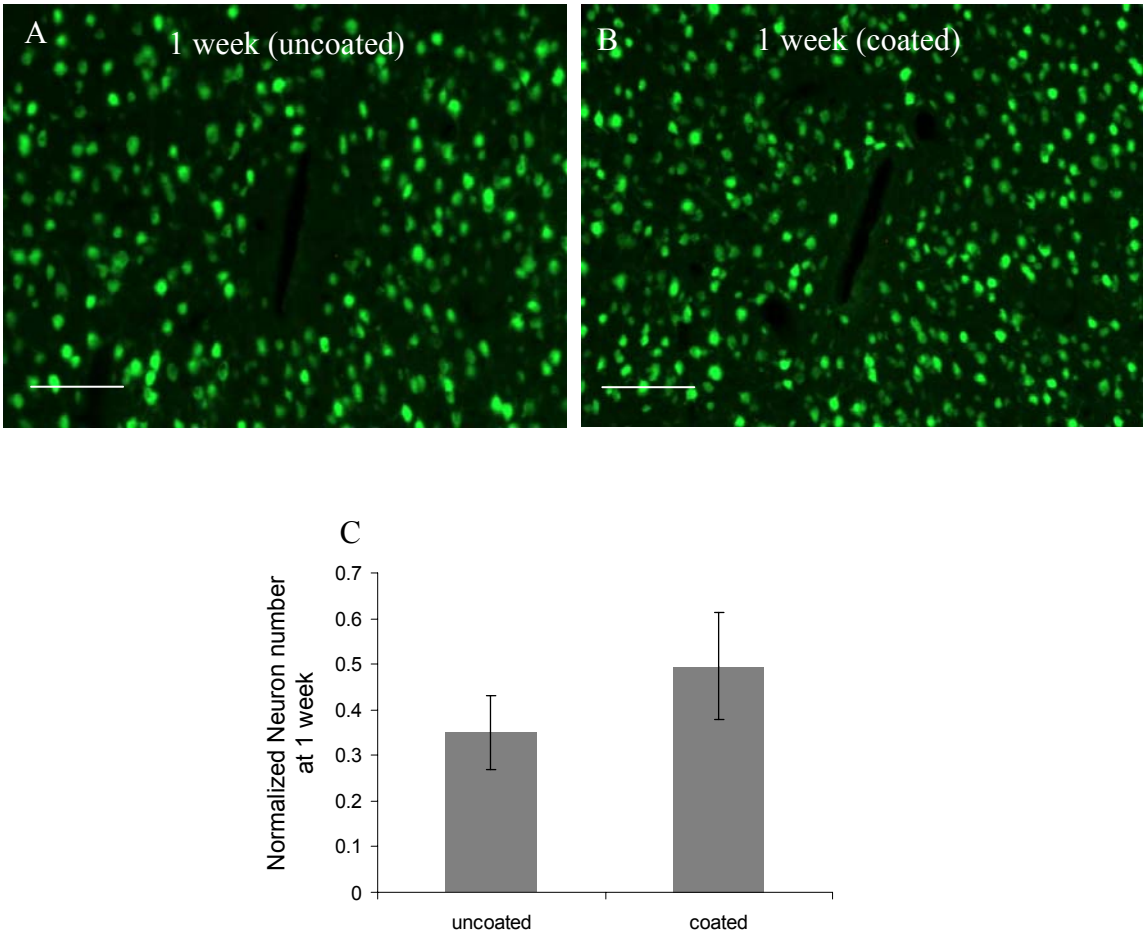

Figure 5.7.2: Neuronal cell body density around implanted neural probes. (A)-(B) Representative images of NeuN staining for neurons in the horizontal brain sections 1 week post implantation for uncoated and DEX coated probes. Scale bar = 100 μm. (C) Number of neurons within 50 μm from the probe interface (n = 4). Values were normalized to the average number of NeuN+ neurons of the uninjured area.

Characterizing Tissue Response along the Depth in the Cerebral Cortex

Tissue response along the depth of the cerebral cortex was evaluated by quantification of ED1, GFAP, CS56 and NF staining. The selection of brain sections for each staining was listed in Table 5.2. Briefly, 6 sections at the level of cerebral cortex at equal depth interval (240 μm) from top to bottom were selected for each staining spanning approximately 1.5 mm of the cortex. As shown in Figure 5.8, normalized tissue immunoreactivity to all four antibodies did not change along the depth of cerebral cortex, suggesting that glial and neuronal response to the implanted neural probes was not depth-dependent.

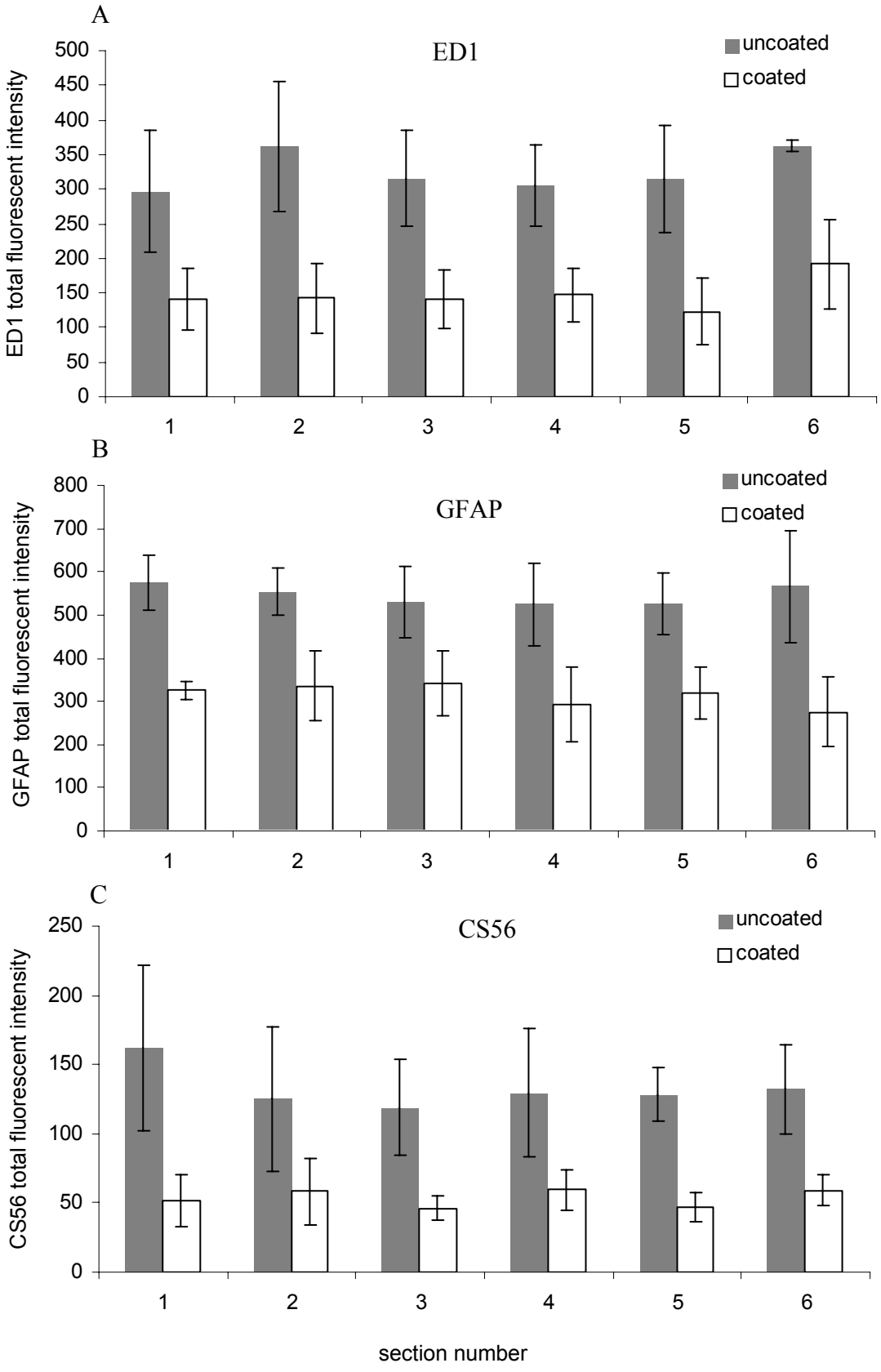
A
ED1
uncoated
coated
ED1 total fluorescent intensity
500
450
400
350
300
250
200
150
100
50
0
1
2
3
4
5
6
B
GFAP
uncoated
coated
GFAP total fluorescent intensity
800
700
600
500
400
300
200
100
0
1
2
3
4
5
6
C
CS56
uncoated
coated
CS56 total fluorescent intensity
250
200
150
100
50
0
1
2
3
4
5
6
section number

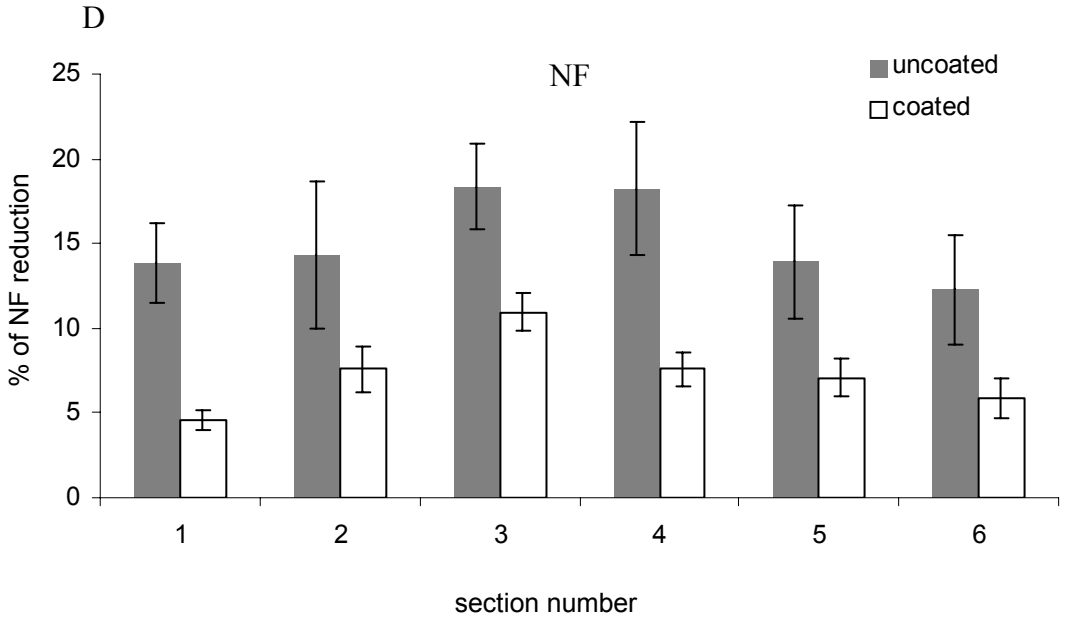

Figure 5.8: Quantitative fluorescent intensity analysis of tissue response along the depth of cerebral cortex. (A)-(C) Quantification of total ED1, GFAP and CS56 fluorescent intensity 1 week post implantation from brain sections of increasing depth (n = 4). (F) Quantification of % of NF reduction 1 week post implantation from brain sections of increasing depth (n = 4). Section 1 to 6 at the level of cerebral cortex at equal depth interval (240 μm) from top to bottom were selected for each staining spanning approximately 1.5 mm of the cerebral cortex.

Assessing Blood-brain Barrier Breakdown and Repair

BBB leakage was assessed by immunostaining of the plasma protein fibrinogen (Fb). The brain sections were double stained with RECA-1 antibody for endothelial cells to identify blood vessels. As shown in Figure 5.9.1, there was severe BBB leakage 1 day post implantation as indicated by strong Fb staining (Figure 5.9.1B), and the vasculature lost the normal morphology as indicated by RECA-1 staining (Figure 5.9.1A). 3 days post implantation, the vasculature almost restored the normal morphology (Figure 5.9.1D), there was still Fb leakage, however, the area of positive Fb staining was considerabely reduced (Figure 5.9.1E). Overlapping RECA-1 and Fb staining for both day 1 (Figure 5.9.1C) and day 3 (Figure 5.9.1F) showed that Fb staining overlapped RECA-1 staining at both time points, indicating that Fb protein was co-localized with leaked blood vessels.

One week post implantation, Fb staining was further reduced for both uncoated and DEX coated probes (Figure 5.9.2A and B). There was very little overlapping of Fb staining and RECA-1 staining for both uncoated and coated probes, indicating that the BBB leakage is almost restored. There was some scattered Fb staining that distributed all over the brain sections for both uncoated and coated probes in a random pattern, and was not co-localized with RECA-1 staining. The scattered Fb staining seemed to be background staining. It could also be Fb released from blood vessels before BBB was restored since it was not co-localized with RECA-1 staining, and therefore can not be used to indicate leaked blood vessels. Four weeks after implantation, there was no overlapping of Fb staining and RECA-1 staining for both uncoated and coated probes (Figure 5.9.2C and D), indicating that the BBB breakdown was restored.

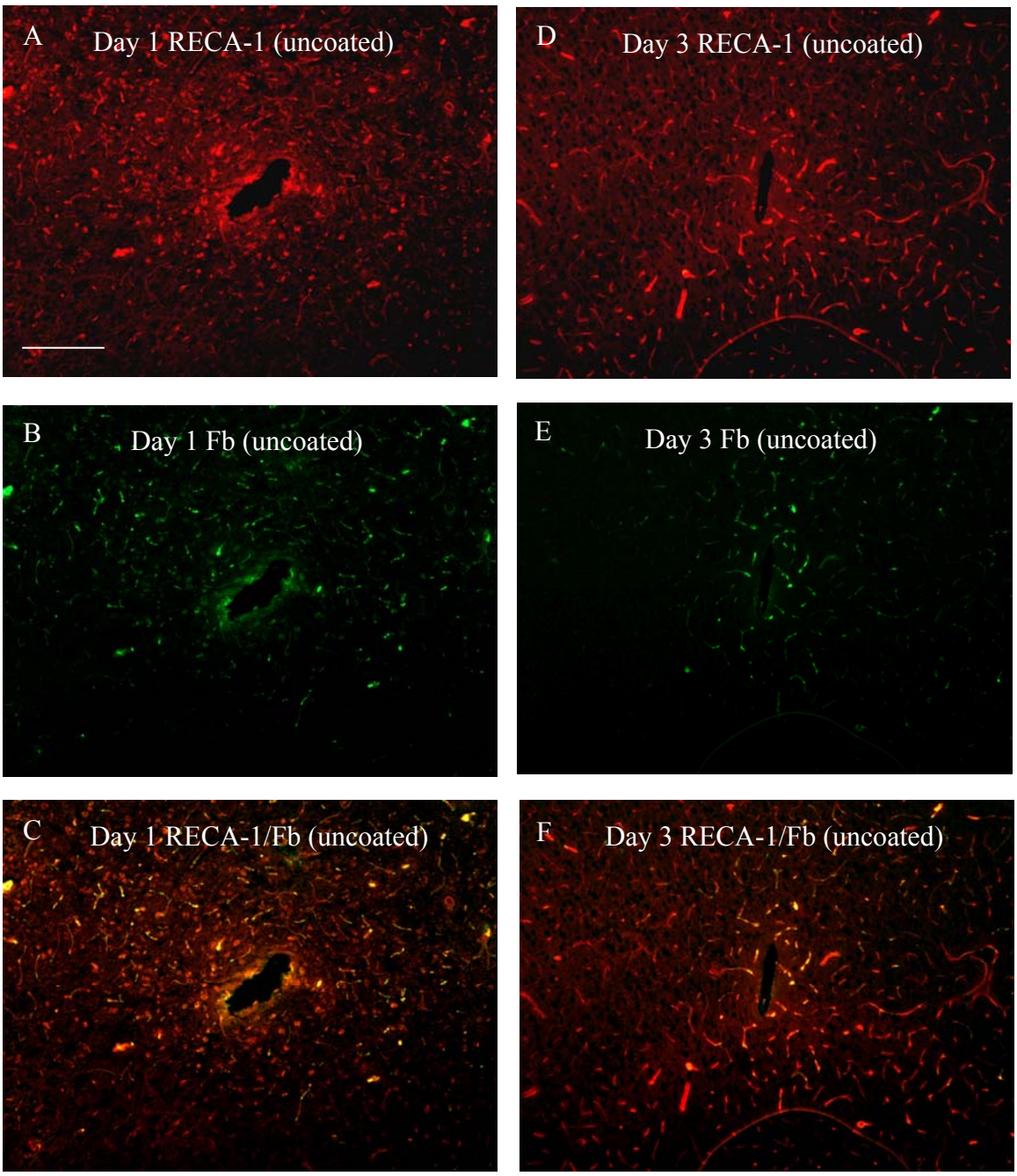

Figure 5.9.1: Representative fluorescent images of horizontal brain sections double stained with RECA-1 and Fibrinogen. (A, D) RECA-1 staining, (B, E) Fb staining, (C, F) Overlays of RECA-1and Fb staining (A-C) 1 day and (D-F) 3 days post implantation. Scale bar = 200 μm.

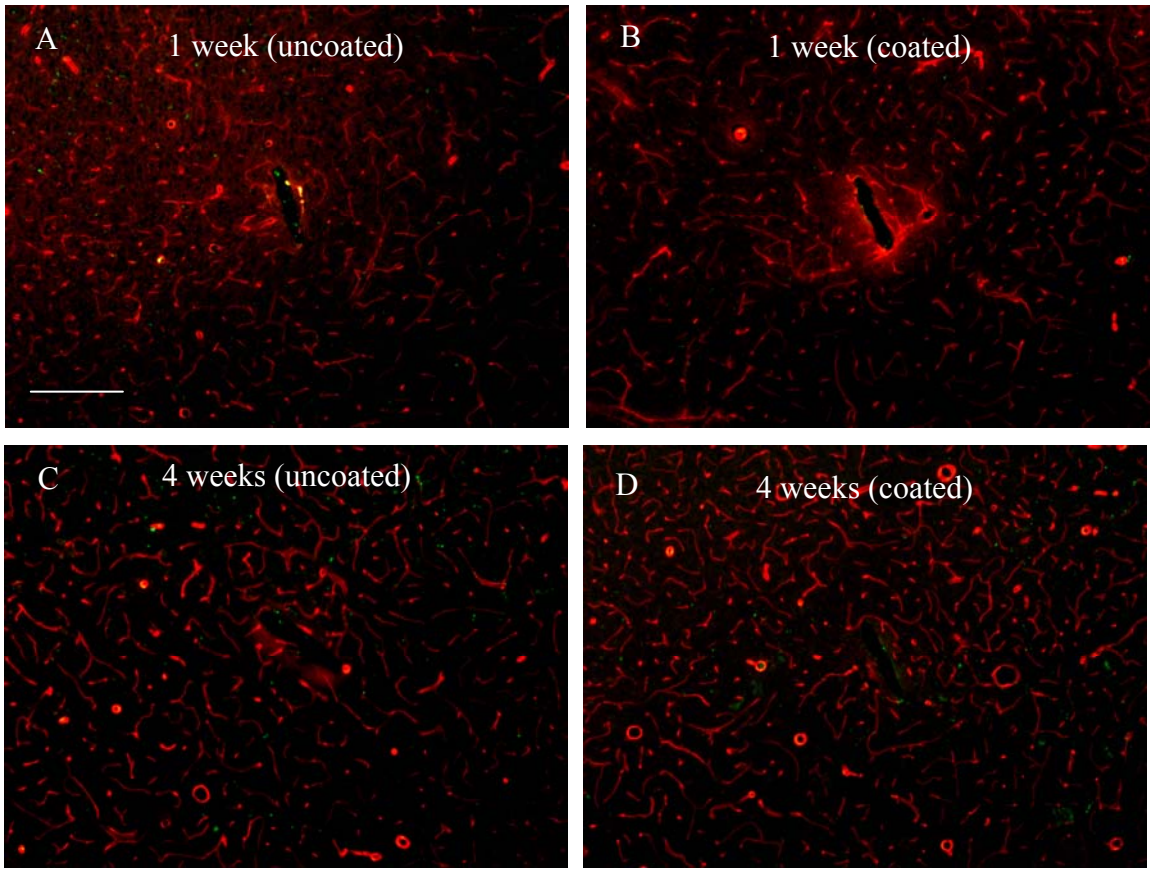

Figure 5.9.2: Representative fluorescent images of horizontal brain sections double stained with RECA-1 and Fibrinogen for (A, C) uncoated and (B, D) coated probes at (A, B) 1 week and (C, D) weeks. Scale bar = 200 µm.

Discussion

To maintain long term functional recording from the silicon neural probes, the neural elements of recording interest need to be preserved in the vicinity of the implanted electrodes. This study demonstrates that local release of DEX from neural probe coatings can attenuate the cellular inflammatory responses to implanted neural probes, suppress the expression of inhibitory molecules (CSPGs), and significantly decrease neuronal reduction around the neural probes.

In this study, the cellular and molecular responses to the implanted silicon neural probes was investigated to give us an insight into the cellular and molecular environment local DEX delivery helps create around the probe-brain interface. The glial cell types involved in glial scar formation include astrocytes, microglia/blood-borne macrophages, and OPCs. Microglia/macrophages and OPCs respond very rapidly to brain injuries (Fawcett and Asher, 1999; Hampton et al., 2004, Kato and Walz, 2000). Following injury to the adult CNS, a large number of microglia/macrophages and OPCs were recruited to the injury site. The activated microglia become more macrophage-like with an amoeboid morphology, and they proliferate and migrate to injury sites (Fawcett and Asher, 1999). The activated microglia/blood-borne macrophages release neurotoxic molecules such as free radicals, nitric oxide (NO), as well as proinflammatory cytokines including interleukin-1 (IL-1), tumor necrosis factor-α (TNF-α) and interleukin-6 (IL-6) (Kyrkanides et al., 2001; Hays, 1999; Bruccoleri et al., 1998; Takeuchi et al., 2001), which subsequently activate the astrocytes (Merrill and Benveniste, 1996; John et al., 2005). The activation of astrocytes is also mediated by blood-borne factors including growth factors and hormone, albumin, thrombin, angiotensin II and cAMP (Logan and

Berry, 2002) The reactive astrocytes undergo hypertrophy, proliferation, and upregulate trophic factors, cytokines, as well as extracellular matrix (Fawcett and Asher, 1999; Polikov et al., 2005).

Chondroitin sulfate proteoglycans are important inhibitory molecules in the glial scar (Fawcett and Asher, 1999). Upregulated CSPGs have differential sulfation patterns (Properzi et al., 2003; Properzi and Fawcett, 2005) and differential sulfation patterns affect neurite outgrowth (Gilbert et al., 2005). Following chondroitinase treatment, glycosaminoglycan removal enhanced neurite outgrowth, suggesting an inhibitory role for CSPGs (Bradbury et al., 2002). Neurocan and NG2 are identified as two important proteoglycans that inhibit neurons (Alonso, 2005; Tang et al., 2003, Jones et al., 2002, Asher et al., 2000). Immunostaining for neurocan and NG2 1 week and 4 weeks post implantation was carried out to investigate the individual proteoglycan expression level with time. One week post implantation, the immunostainings for glial cells (astrocytes, microglia, and OPCs) as well as inhibitory molecules (CSPGs including neurocan and NG2) reached peak. It is noteworthy that for all the inhibitory molecules the intensive staining was concentrated around the probe-brain interface, and appeared to be inversely correlated with NF staining intensity. Interestingly, GFAP staining was weak in this region. Similar observation has been previously reported (Fitch and Silver, 1997), and the authors suggested that the CSPGs in the area lacking GFAP-positive cells may be produced by astrocytes that subsequently died, migrated away from the injury site, or lost their GFAP immunoreactivity. The authors also suggested that microglia/macrophages may be another possible source of inhibitory CSPGs. Since neurocan staining was

correlated with NG2 staining, it is possible that OPCs also contributed to neurocan upregulation.

In the intensive NG2 staining area, it is difficult to identify individual NG2 positive cells. In the normal tissue of CNS, NG2 is found almost exclusively on the surfaces of OPCs (Ughrin, 2003; Levine, 2001). Therefore the intensive NG2 staining might be a marker of the proliferated and aggregated OPCs. However, since NG2 can be shed from the cell surface and secreted into extracellular matrix, there is the possibility that the intensive NG2 staining was not only a cell marker, but also the marker for NG2 proteoglycan in extracellular matrix secreted by OPCs as well as other types of cells. Double staining with ED1 antibody showed that the intensity distribution of NG2 staining was also correlated to ED1 staining (data not shown), therefore reactive microglia/macrophages might be another cell source for upregulation of NG2.

Four weeks post implantation, the intensity of ED1 staining was reduced compared with 1 week. CS56, neurocan and NG2 staining intensity was almost back to normal levels. Several studies have shown that CSPGs decreased with time. Levine reported that in a rat brain injury model NG2 immunoreactivity dramatically increased beginning at 4-5 days post lesion (dpl), and continued to increase over the next 3 days so that by 7 dpl, there was a dense plague of immunoreactivity surrounding the lesion site. Between 10-15 dpl, NG2 immunoreactivity began to decline, the intensity of NG2 immunoreactivity continued to decline over the next 2-5 weeks. At 30 dpl, the plaque of anti-NG2 immunoreactivity had disappeared. Camand et al reported that in a mouse spinal cord injury model, CS56 immunoreactivity reached peak 8 days postinjury. One month post lesion, this CS56 immunolabelling was practically abolished. Morel et al

reported in a mouse cerebellum injury model that CS56 immunostaining was rapidly and strongly upregulated 8 days after the lesion. It remained for at least one month, although the thickness of the labeled band was smaller than 8 days. By 6 month after the lesion, CS56 immunoreactivity had disappeared. Taken together, the time course of CSPGs change depends on the injury model, and in all three studies CSPGs eventually disappeared. We speculate that the time course of CSPG expression and depletion is dependent on the degree of injury. In our study, the tissue injury is relatively small, considering the small size of the neural probe (33 to 200 μm in width, and 15 μm in thickness), which might explain why the upregulation of CSPG immunostaining almost disappeared at the end of 4 weeks. This result is also consistent with the observation that ED1 immunoreactivity was significantly reduced at 4 weeks, as reactive microglia/macrophages also contribute to CSPG expression. The significant reduction of reactive microglia/macrophages and CSPGs at 4 weeks suggests that the inflammatory responses may start to stabilize at 4 weeks in our injury model.

Local release of DEX significantly attenuated the inflammatory responses at 1 week, and reduced neural loss both at 1 week and 4 weeks as evidenced by NF staining. NeuN staining showed that the number of neurons within 50 μm radius from the coated probes was higher than uncoated probes, however, the difference is not statistically significant. It might be that the sample size is not big enough. The NF and NeuN staining results suggest that DEX is more protective for neurite loss rather than cell body loss. Thus DEX alone may not be sufficient to keep enough neurons close to the electrode sites. If this is the case, we need deliver neurotrophic factors together with DEX to further improve neuronal survival and attract neurons to migrate to the electrode sites.

DEX is known as a potent anti-inflammatory drug, and it has previously been shown to be capable of reducing inflammatory responses in the CNS (Holmins and Mathiesen, 1996; Spataro et al., 2005; Hermens and Verhaagen, 1998). Its anti-inflammatory effects have usually been attributed to its effects on microglia/macrophages, which knowingly express high levels of glucocorticoid receptors (Tanaka et al., 1997). DEX has been show to inhibit iNOS synthesis and cytokine production by microglia, as well as microglia proliferation (Golde et al., 2003; Chao et al., 1992; Tanaka et al., 1997). A recently study showed that DEX inhibited proliferation of NG2 positive cells, which may differentiate into astrocytes in injured brain (Alonso, 2005). As these NG2 positive cells do not express the glucocorticoid receptors, the authors suggested that DEX may have indirect effects on these cells via modification of glutamate release and/or interaction with microglia.

Astrocyte activation is featured by upregulation of GFAP expression and glosis-associated molecules, hypertrophy, and some astrocytes undergo cell division (Fawcett and Asher, 1999; Chen and Swanson, 2003, Polikov et al., 2005). This study demonstrated that DEX reduced the astrocytic reaction to the implanted neural probes as evidenced by reduction of GFAP staining intensity and less hypertrophied cell morphology. We have demonstrated (in Chapter IV) that DEX significantly inhibited astrocyte proliferation *in vitro*. However, local release of DEX did not significantly reduce the density of astrocyte around the implanted neural probe. One possible explanation is that the reactive astrocytes in our injury model were not in active proliferation. This assumption is consistent with the observation that the number of astrocytes in the reactive zone was only mildly increased compared with that in uninjured

region. The origins of the reactive astrocytes in injured brain have been unclear. The possible sources could be resident astrocytes, astrocytes migrating from undamaged parenchyma, and glial precursors (Alonso, 2005; McGraw et al., 2001; Ridet et al., 1997; Norton, 1999). A number of studies showed that regardless of the high concentration of astrocytes along the glial scar, the proliferation of astrocytes in the injured area was always found to be modest and hardly match the high concentration of astrocytes in this area (Alonso, 2005; Norton, 1999, Janeczko, 1993). Therefore it was suggested astrocyte proliferation only partly contributes to the increase of astrocytes in the injured brain. In addition, our *in vitro* study showed that the inhibition of DEX on astrocyte proliferation was mild. This might explain why the astrocyte density around the DEX coated probes was not significantly reduced compared with uncoated probes. The histogram of astrocyte density distribution as a function of 50 μm distance bins from 0 to 400 μm from the probe-brain interface showed a reduction of astrocyte density in the first 50 μm distance bin at 1 week, which is consistent with the GFAP intensity profile. The loss of astrocytes at the interface could be attributed to the mechanical trauma caused by implantation. It is interesting that beyond 50 μm, while the cell densities was only mildly increased for uncoated probes, the intensity distribution profile showed a drastic increase of intensity. This inconsistency between cell density and GFAP staining intensity suggests that the upregulation of GFAP intensity was more from upregulation of GFAP expression as well as cell hypertrophy than from increase of cell number. Indeed, we observed that reactive astrocytes around uncoated probes showed more hypertrophied morphology and denser processes, indicating upregulation of GFAP expression.

This study demonstrated that DEX coatings on Si probes not only reduced the cellular inflammatory response, but also reduced the expression of chondroitin sulfate proteoglycans, the important inhibitory molecules in glial scar. There was no significant difference between the uncoated probes and DEX coated probes for ED1 and CS56 staining at 4 weeks, this could be either due to drug depletion, or due to the stabilization of the inflammatory response. However, DEX treatment significantly reduced neuronal reduction both at 1 week and 4 weeks after implantation, which suggests that reducing inflammation immediately after implantation may have long term beneficial consequences. Reactive glial cells may contribute to neuronal reduction through the secretion of neurotoxic molecules including glutamate, pro-inflammatory cytokines, prostaglandins, NO and free radical species; as well as inhibitory molecules such as CSPGs. Therefore inhibition of glial cell activation may reduce the expression of these molecules, which result in less neuronal damage.

Insertion of neural probes into the brain inevitably ruptures blood vessels, which leads to an infiltration of pro-inflammatory cells and molecules into the brain parenchyma, and initiates a cascade of inflammatory responses to the implanted probes (Schwartz, 2004; Polikov et al., 2005; Spataro et al., 2005). Several studies suggested that astrocytes are involved in the BBB formation and repair by inducing endothelial cells to form specialized junctional complexes (Brightman, 1991; Neuhaus et al., 1991, Bush et al., 1999). In a transgenic mouse model which selectively ablates dividing, reactive, transgene-expressing astrocytes, BBB was found to fail to re-form (Bush et al., 1999; Faulkner et al., 2004). Since DEX was shown to reduce the reactivity of astrocytes, the effects of DEX on BBB repair was investigated in this study. Fibrinogen immunostaining

revealed severe BBB leakage 1 day post implantation, which was markedly reduced at 3 days. By 7 days, the leaked BBB was almost restored for both uncoated and coated probes. Complete sealing of BBB for both uncoated and coated probes was observed at the end of 4 weeks. The time course of BBB breakdown and repair in our study is in agreement with other BBB breakdown studies in brain or spinal cord injuries (Spataro et al., 2005; Jaeger and Blight, 1997; Prior et al., 2004; Faulkner et al., 2004). As discussed earlier, local release of DEX didn't change the astrocyte density in the vicinity of the neural probes in our study, thus the interaction between astrocytes and endothelial cells may not be compromised in our injury model.

In this study, we evaluated tissue response along the depth of the implanted neural probes. We found that glial and neuronal response to the implanted neural probes was not depth-dependent. This result is consistent with the observation from other research group (Leung et al., 2006). We also found that the reduction of tissue reaction and decrease of neural loss by DEX treatment did not change along the implantation tract, which is not surprising since tissue reactivity was not depth-dependent. Therefore we expect small variability of recording capability for each electrode site along the probe shank.

This tissue response in this study was mostly analyzed by fluorescent staining. The advantages of this technique include 1) specific tissue, cell type and molecules can be identified; 2) it can provide the information of spatial distribution of reactive glial cell, glial scar associated molecules, and neurons; 3) it is sensitive compared with traditional staining; 4) it is more practical and less time-consuming compared with alternative methods such as real-time PCR or protein purification; and 5) this technique is widely used in evaluation of glial scar and neuronal loss following tissue injury or implantation

in the CNS, therefore this technique allows us to compare our results with related studies in this field. To reduce the variance of staining intensity caused by cell density, the intensity for each staining was normalized to background intensity for each section. In addition, both uncoated and coated conditions were in the same sections, if one section had higher/lower background staining intensity, intensity on both sides of the section would be relatively higher/lower accordingly, so it won't change the result that which side had higher intensity due to tissue reaction. We also performed cell counting as a supplement to intensity quantification analysis. The disadvantages of this technique are 1) fluorescent intensity is affected by many factors, including staining procedure, exposure time when taking the pictures, and cell density; 2) fluorescent intensity may not be proportional to the degree of activation. For example, if the GFAP intensity is reduced 50%, it doesn't mean that the GFAP expression was reduced 50%. We can not tell how much GFAP expression is reduced exactly. If GFAP fluorescent intensity is significantly reduced, we can tell that GFAP expression is significantly reduced, but we can not tell the degree of GFAP reduction. To reduce the effects of these factors on fluorescent intensity, for each type of staining, the sections were stained simultaneously, and the same exposure time was used for all sections. Then the fluorescent intensity was normalized to background intensity to reduce the effect of cell density.

Conclusions

This study demonstrates that local delivery of DEX can reduce the cellulular and molecular inflammatory responses to the implanted neural probes, as well as significantly decrease neural reduction in the immediate vicinity of the probes in a 4 week period

study. This might be a promising strategy to improve the long-term recording stability of silicon neural probes. The levels of reactive microgla/macrophages and CSPGs around uncoated probes were significantly reduced at 4 weeks compared with 1 week, suggesting that they may not play an important role in chronic inflammatory response. In contrast, astrocyte reactivity did not decrease with time. Therefore the role of astrocyte in chronic inflammatory response and glial scar development needs to be investigated in the future. If future study shows that astrocytes do not contribute to further neuronal loss and increase of electrode impedance in the long term (months to years), then local delivery of DEX in early stage may be sufficient for mitigating the inflammatory tissue reaction. Otherwise it is important to investigate if early DEX treatment is sufficient to reduce astrocyte reactivity in the long term. If not, then alternative strategy needs to be explored to enable continuous drug delivery throughout the course of electrode implantation.

CHAPTER VI

CLOSING

Summary

Stable single-unit recordings from the nervous system using microelectrode arrays can have significant implications for the treatment of a wide variety of sensory and movement disorders. However, the long-term performance of the implanted neural electrodes is compromised by the formation of glial scar around these devices, which is a typical consequence of the inflammatory tissue reaction to implantation-induced injury in the CNS. The glial scar is inhibitory to neurons and forms a barrier between the electrode and neurons in the surrounding brain tissue (Cui et al, 2003; Schwartz, 2004; Turner et al; 1999). Therefore, to maintain long-term recording stability, reactive gliosis and other inflammatory processes around the electrode need to be minimized.

This work has succeeded in the development of neural electrode coatings that are capable of sustained release of anti-inflammatory agents while not adversely affecting the electrical performance of the electrodes. The effects of coating methods, initial drug loadings on release kinetics were investigated to optimize the coatings. The physical properties of the coatings and the bioactivity of released anti-inflammatory agents were characterized. The effect of the coatings on the electrical property of the electrodes was tested. Two anti-inflammatory agents were screened by evaluating their anti-inflammatory potency *in vitro*. Finally, neural electrodes coated with the anti-inflammatory coatings were implanted into rat brains to assess the anti-inflammatory

potential of the coatings *in vivo*. This work represents a promising approach to attenuate astroglial scar around the implanted silicon neural electrodes, and may provide a promising strategy to improve the long-term recording stability of silicon neural electrodes.

Conclusions

Development and characterization of coatings capable of releasing α-MSH

This work developed and characterized nitrocellulose-based coatings for Si-substrates/electrodes. Anti-inflammatory neuropeptide α-MSH was incorporated in this system and slow, sustained release over 21 days was achieved *in vitro*. α-MSH released on day 21 was still bioactive and successfully inhibited NO production. Both coating methods and initial drug loading directly affected the release rate. Matrix loading method showed a lower initial burst compared with reservoir delivery method, suggesting that Matrix method has a more stable release rate. Higher initial loading increased the release rate as well as the mass released. Therefore high initial loading enables fast, high dosage release, while low initial loading allows for slow, low dosage release. In addition, impedance measurement showed that the α-MSH loaded nitrocellulose coatings reduced the magnitude of electrode impedance at the biologically relevant frequency of 1 kHz, and consequently, improved the signal transport across the neural interface and helped to increase the detection sensitivity to neural activity.

Development and characterization of coatings capable of releasing dexamethasone

This work developed and characterized a nitrocellulose-based coating for the sustained local delivery of the anti-inflammatory drug dexamethasone (DEX), a synthetic glucocorticoid that effectively reduces inflammation in the CNS. *In vitro* DEX release was observed over 16 days, with a relatively high release in the first three days and a slow, stable release thereafter. The released DEX remained bioactive. Impedance spectroscopy showed that the dexamethasone-loaded nitrocellulose coatings significantly reduced the magnitude of electrode impedance at the biologically relevant frequency of 1 kHz through an increase of capacitance. Coating stability test demonstrated that the coatings remained intact during the insertion procedure.

***In vitro* evaluation of the anti-inflammatory agents**

This work examined the anti-inflammatory potency of DEX and α-MSH. Both anti-inflammatory agents were shown to be able to inhibit NO production by activated microglia and were not neurotoxic. However, DEX was shown to be more powerful than α-MSH, as it not only reduced NO production more effectively, but also inhibited microglia and astrocyte proliferation. This work further evaluated the anti-inflammatory effects and neurotoxicity of DEX at various dosages on cortical cells including microglia, astrocytes and neurons. 1, 10 and 100 μM DEX showed similar inhibitory effects on LPS-stimulated NO production and proliferation in microglia culture. In addition, DEX at all three concentrations inhibited astrocyte proliferation and didn't show neurotoxicity. 1 and 100 μM DEX significantly inhibited the cytokine production by microglia and astrocytes. These results suggest that the anti-inflammatory effects and safety of DEX are not affected even at 100 times of its normal treatment dosage.

***In vivo* evaluation of nitrocellulose-DEX coatings**

This work assessed the anti-inflammatory potent of nitrocellulose-DEX coatings *in vivo*. Silicon neural probes with and without nitrocellulose-DEX coatings were implanted into rat brains, and inflammatory response was evaluated 1 week and 4 weeks post implantation. DEX coatings significantly reduced the reactivity of microglia and macrophages one week post implantation as evidenced by ED1 immunostaining. CS56 staining demonstrated that DEX treatment significantly reduced chondroitin sulfate proteoglycan (CSPG) expression one week post implantation. Both at one week and at four week time points, Glial fibrillary acidic protein (GFAP) staining for reactive astrocytes and neurofilament (NF) staining revealed that local DEX treatment significantly attenuated astroglial response and reduced neural reduction in the vicinity of the probes. Weak ED1, neurocan and NG2 positive signal was detected four weeks post implantation for both coated and uncoated probes, suggesting that they may not play an important role in chronic inflammatory response. In contrast, astrocyte reactivity did not decrease with time. Therefore the role of astrocyte in chronic inflammatory response and glial scar development needs to be investigated in the future. If future study shows that astrocytes do not contribute to further neuronal loss and increase of electrode impedance in the long term (months to years), then local delivery of DEX in early stage may be sufficient for mitigating the inflammatory tissue reaction. Otherwise it is important to investigate if early DEX treatment is sufficient to reduce astrocyte reactivity in the long term. If not, then alternative strategy needs to be explored to enable continuous drug delivery throughout the course of electrode implantation. Collectively, this study demonstrated that the nitrocellulose-DEX coating can effectively attenuate the

inflammatory tissue response to the implanted neural probes, and reduce neural reduction in the vicinity of the coated probes in a 4 week period. This may represent a promising approach to attenuate astroglial scar and reduce neural reduction around implanted neural probes.

Directions for Future Work

Quantification of DEX Release *in Vivo*

This research studied the release profile of DEX *in vitro*, however, the duration and spatial distribution of DEX released *in vivo* is difficult to estimate. This may be accomplished by using radiolabel DEX such as [^{3}H]-DEX for quantification of DEX release *in vivo*. In detail, neural probes coated with nitrocellulose-[^{3}H]-DEX will be implanted into rat brains as described in Chapter V, the spatial distribution of DEX will be assessed at different time points (1 day, 3 days, 1 week and 4 weeks) by measuring the radioactivity using a scintillation counter and autoradiography. At each time point, the rats will be decapitated and the brains are frozen immediately. For quantification of [^{3}H]-DEX radioactivity, sagittal sections parallel to the probe shaft will be cut and homogenized, the tissue radioactivity will be determined by a scintillation counter. For visualization of DEX distribution, horizontal sections perpendicular to the probe shaft will be cut and used for autoradiography. A mathematical model will be developed to predict the time and spatial distribution of DEX released *in vivo*. By comparing the drug release profile *in vivo* with the results from histological analysis and chronic recording, this mathematical model will help optimize initial drug loading and release duration.

Chronic Neural Recording

The ultimate goal of this research is to achieve long-term recording stability of silicon neural probes. This research has demonstrated significant decrease of inflammatory responses and neural reduction around the nitrocellulose-DEX coated neural probes, it would be valuable to correlate this improvement in tissue response with the long-term recording performance of the silicon neural probes. The failure of chronic recording can be attributed to two factors: the isolation of neurons from the electrode sites and increase of electrode impedance. Both factors are caused by the glial scar formation around the implanted neural probes. Neuron isolation form the electrodes may cause poor recording quality such as low signal-to-noise ratio (SNR) or unresolvable action potentials (noise). The change of following parameters over time will be used to evaluate the functional recording stability of the neural probes.

1) *Number of active electrodes:* An electrode is considered to be active if it could record resolvable action potentials (Rousche and Normann, 1998). The total number of active electrode sites as a function of time will be assessed.

2) *Single unit stability:* Recording sites containing single units will be used to calculate the ratio "# of units/recording sites" over time.

3) *Stability index:* To evaluate the stability of the electrode-tissue interface for the implanted neural probes. A template for each neural unit is obtained by averaging all of the neural spikes in that unit. If there is no significant change in template amplitude and shape, this indicates that there is no significant change of the interface between the neural electrode and the neural tissue (Liu et al, 1999).

4) *Signal-to-noise ratio:* SNR will be calculated by dividing the peak-to-peak amplitude of template waveform (V_{PP}) by twice the standard deviation (Stdev) of raw data from which template was generated (Nordhausen et al., 1996).

$$SNR=Vpp / 2 \times Stdev \quad [1]$$

5) *Recording longevity:* The recording longevity of a neural electrode is defined as the largest number of consecutive days during which resolvable action potentials can be recorded by the electrode (Liu et al, 1999).

6) *Electrode impedance*

These parameters will be correlated with histological analysis to investigate the relationship between tissue reaction and functional electrode performance.

Delivery of Neurotrophic Factors

This research demonstrated that local delivery of DEX decreased neural reduction around the neural probes. However, it remains unknown if this improvement is sufficient for obtaining stable neural recordings. A chronic recording study demonstrated that many electrode sites with low impedance stopped detecting neural activity over time (Cui et al, 2003). The authors suggested that this was caused by migration of neurons away from the electrode sites. If we observe the same phenomena in our chronic recording study, then DEX alone may not be sufficient to keep neurons close to the electrode sites. If this is the case, we will deliver neurotrophic factors together with DEX to further improve neuronal survival and attract neurons to migrate to the electrode sites.

Brain derived neurotrophic factor (BDNF) is a potent neurotrophic agent promoting survival of CNS neurons. Neurotrophic factors play an important role in developing and adult nervous system (Davies, 1996; Lindsay, 1996). The chemotactic

guidance of various migrating neurons is potentially mediated by the neurotrophin BDNF. BDNF has been shown to be upregulated in response to injuries to the spinal cord (Friedman et al, 1994; Dougherty et al, 2000), retinal neurons (Caleo et al, 2000), and in cortical neurons in Alzheimer's patients (Durany et al, 2000). Furthermore, local delivery BDNF has been demonstrated to stimulate neurite growth and permit functional recovery after spinal cord injury (Jain et al, 2006; Tobias et al, 2005). In addition to its neurotrophic effects, recently studies have shown that BDNF have anti-inflammatory and anti-oxidant effects (Joosten and Houweling, 2004; Jain et al, 2006). Therefore BDNF is an excellent candidate to promote neuronal survival and migration at the site of implant, and attenuate inflammatory tissue responses.

Alternative Animal Models

The results of this research were all done in rats. Rodent model is well characterized and widely used for preliminary variable screening and optimization. This research has demonstrated that local delivery of DEX had anti-inflammatory and neuroprotective effects in rat model. The efficacy of the anti-inflammatory coatings needs to be further evaluated in higher animals that are genetically more close to human beings such as primates. Functional recording studies showed that it is easier to obtain consistent high-yield recordings in the rodent than higher animals such as cats and monkeys (Witte et al, 1999; Rousche et al, 1998, Maynard et al, 1996). This may be related to the differences in the reaction to implantation or to the differences in cortical folding between the rodent (lissencephalic) and primate (gyrencephalic) (Schwartz, 2004). If our functional recording study in rat model shows stable chronic recording for

uncoated control silicon neural probes, we will switch the animal model to cats or primates.

New Electrode Designs

This research demonstrates that local delivery of DEX from electrode coatings is capable of mitigating the inflammatory tissue response, as well as reducing neural loss around the implanted neural electrodes in a 4-week period study. However, the disadvantage of this strategy is the problem of drug depletion. While we can modify the coating design to slow the process of drug depletion, the drug will eventually be depleted. It remains unknown if the inflammatory response will come back after the drug is depleted. If future long term study demonstrates that continuous drug treatment is necessary for suppressing the inflammatory response throughout the course of electrode implantation, then coating strategy will not be applicable. In this case, new electrode designs need to be developed.

One promising strategy is the microfluidic drug delivery system as discussed in Chapter I. In current designs microfluidic channels are not connected to outer devices, thus drug can not be refilled into the channels after drug depletion. In the future, new designs can be developed so that the microfluidic channels can be connected to an outer drug reservoir for drug refilling. Another potential problem for this delivery system is that the outlet ports where the drug is released from the microchannels could be clogged by tissue infiltration. However, we may turn this disadvantage into advantage by releasing neurotrophic factors to induce neuronal ingrowth to the electrodes.

APPENDIX A

A SIMPLE ULTRAVIOLET SPECTROSCOPY METHOD FOR THE DETERMINIATION OF ALPHA-MELANOCYTE STIMULATING HORMONE CONCENTRATION

Introduction

Alpha-melanocyte stimulating hormone (α-MSH) is a powerful drug candidate due to its pleiotropic effects on inflammation and energy homeostatis, and has potential therapeutic applications for the treatment of inflammatory diseases (Etemad-Moghadam et al., 2002; Starowicz and Przewlocka, 2003). Thus a fast and reliable method of measuring α-MSH concentration is highly desirable to support the development of local delivery systems for α-MSH. The standard method for determination of α-MSH concentration is high-performance liquid chromatography (HPLC). The aim of this study was to develop an alternative analytical method to the more time consuming HPLC method.

α-MSH is a peptide with a molecular weight of 1,665 daltons. As there is no common method for peptide quantification, we first explored the possibility of using protein quantification methods. One of the most common methods of measuring protein concentrations involves determination of the absorption of protein solution between 260 to 280 nm (Murphy and Kies, 1960, Wolf, 1983). However, this method is insensitive to protein concentrations less than 50 μg/ml (Wolf, 1983). The normal therapeutic level for α-MSH is less than 2 μg/ml, thus it is highly desirable that the sensitivity of the

quantification method is less than 2 μg/ml. Bradford assay is a sensitive colormetric technique that is commonly used for determination of protein concentration in solution (Bradford, 1976; Sapan et al, 1999). However, the detection limit of protein molecular weight for this method is 3,000 to 5,000 daltons, which is higher than that of α-MSH. Waddell's method uses the difference between 215 and 225 nm (Waddell, 1956). The sensitivity of this method was reported to be dependent on the protein tested, and the near linear range did not generally extend beyond the range of 1.5 – 45 μg/ml (Wolf, 1983). In this study, we explored the possibility of using the Waddell's method to quantify α-MSH concentration.

Materials and Methods

Preparation of an α-MSH Standard Curve

A stock solution containing 1 mg/ml of α-MSH (Sigma) was prepared by dissolving 1 mg of α-MSH in 1 ml 0.1 M Dulbecco's phosphate-buffered saline (DPBS, Invitrogen). The stock solution was diluted in 0.1 M DPBS to a concentration of 512 μg/ml. 15 serial 2-fold dilution was performed with 0.1 M DPBS to generate the α-MSH standard curve (512, 256, 128, 64, 32, 16, 8, 4, 2, 1, 0.5, 0.25, 0.125, 0.0625, 0.03125, 0.01563 μg/ml).

Ultraviolet Spectrophotometric Measurement

100 μl α-MSH at each concentration was added into the wells of a 96-well UV plate (Greiner Bio-one) in triplicate. The absorbance was measured at 215 and 225 μm with a microplate reader (Bio-Tek instruments, VT). The absorbance at 225 μm was

subtracted from that at 215 μm. The subtracted absorbance was plotted against the concentrations to generate the α-MSH standard curve.

Results and Discussions

215 and 225 nm absorbances of α-MSH were measured over the concentration range of 0.01563 to 512 μg/ml. Linear relationship of the subtracted absorbance relative to concentration was observed over the concentration range of 0.25 to 128 μg/ml (Figure A.1). However, when we fit the subtracted absorbance back to the standard curve to calculate the measured α-MSH concentration, the percentage differences between the measured concentrations and actual concentrations were less than 10% only at concentrations of 1, 32, 64 and 128 μg/ml (Table A.1*a*).

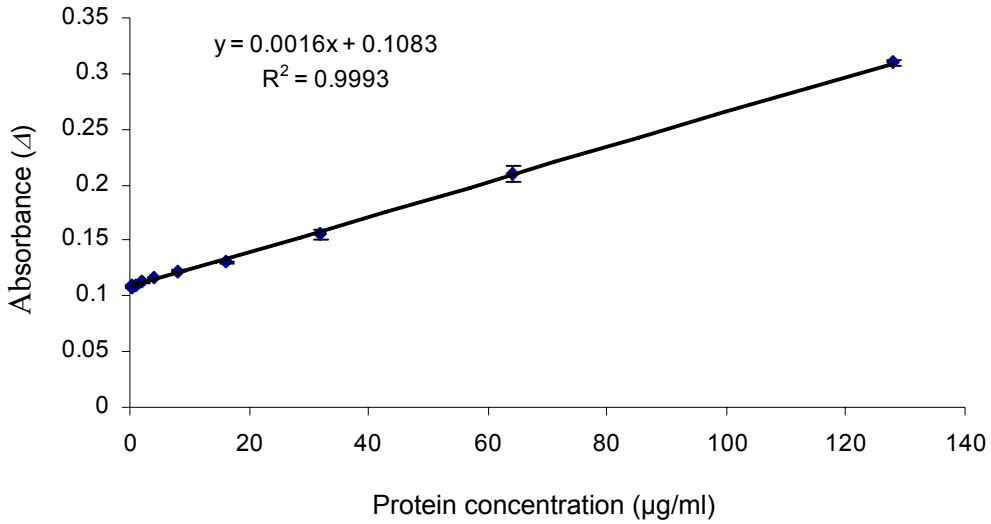

Figure A.1: α-MSH standard curve over a concentration range of 0.25 to 128 μg/ml. Absorbance *Δ*, is the difference between the absorbance at 215 and 225 nm (subtracted absorbance).

Table A.1: 215 nm-225 nm readings and measured α-MSH concentration calculated from the generated standard curves.

α-MSH concentration (μg/ml)	225 nm-215 nm reading	[a] measured concentration (0.25-128μg/ml)	[b] measured concentration (0.25-4 μg/ml)	[c] measured concentration (16-128 μg/ml)
0.25	0.10833	0.021 [d](92%)	0.242 (3%)	
0.5	0.109	0.438 (12.5%)	0.545 (9%)	
1	0.11	1.063 (6.3%)	1 (0%)	
2	0.11233	2.521 (26%)	2.061 (3%)	
4	0.11667	5.229 (30.7%)	4.03 (0.8%)	
8	0.12267	8.979 (12.2%)		
16	0.13033	13.771 (13.9%)		15.771 (1.4%)
32	0.15567	29.6 (7.5%)		31.604 (1.2%)
64	0.21	63.563 (0.7%)		65.563 (2.4%)
128	0.31	126.063 (1.5%)		128.063 (0.05%)

[a] α-MSH calculated based on the standard curve generated over the range of 0.25-128μg/ml.
[b] α-MSH calculated based on the standard curve generated over the range of 0.25-4 μg/ml.
[c] α-MSH calculated based on the standard curve generated over the range of 16-128μg/ml.
[d] Percentage difference between actual concentration and measured concentration.

To solve this problem, we generated a standard curves over a lower concentration range from 0.25 to 4 μg/ml (Figure A.2), as shown in Table A.1*b*, for the five concentration points in this range, the percentage differences between the calculated concentrations and actual concentrations were all less than 10%. In addition, four of them showed 3% or less differences between the measured concentrations and the actual concentrations. For our drug delivery application, 10% estimation error for concentration is reasonably accurate. Thus we generated a standard curve with acceptable accuracy over the range from 0.25 to 4 μg/ml. The detection limit was as low as 0.25 μg/ml. For α-MSH solution at a concentration higher than this range, we can use the full range (0.25 to 128 μg/ml) standard curve to estimate the concentration first, and then dilute the solution to a concentration within the this range to be measured. Next, we explored the

feasibility of generating a standard curve over a higher concentration range to reduce the need for dilution.

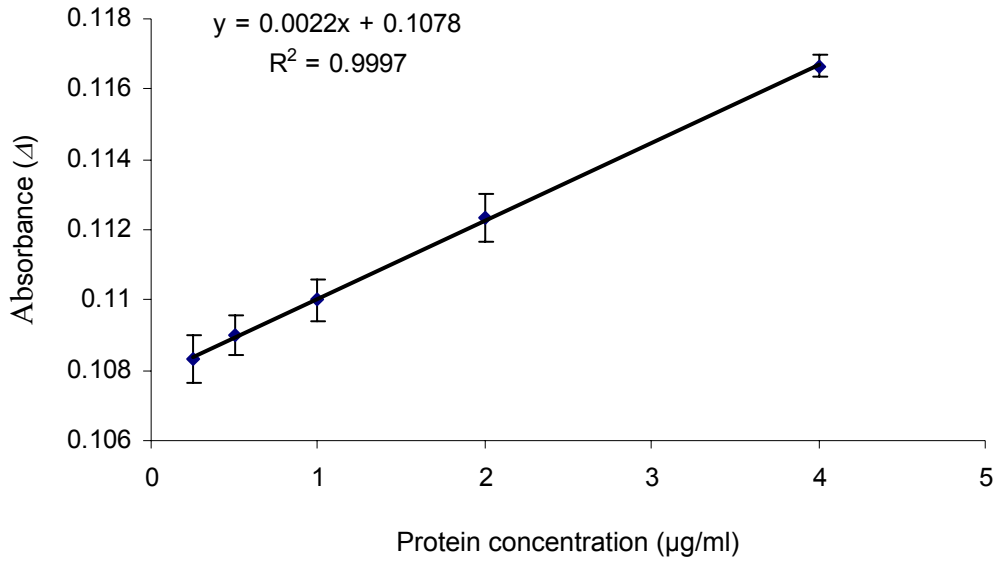

Figure A.2: α-MSH standard curve over a concentration range of 0.25 to 4 µg/ml. Absorbance *Δ*, is the difference between the absorbance at 215 and 225 nm (subtracted absorbance).

Figure A.3 showed a standard curve generated over the range from 16 to 128 µg/ml. as shown in Table A.1*c*, for all the concentration points in this range, the differences between the calculated concentrations and actual concentrations were less than 3%.

Collectively, we generated two standard curves over the ranges from 0.25 to 4 µg/ml, and 16 to 128 µg/ml respectively with Wadell's method for quantification of α-MSH. This method is simple, reasonably accurate, and highly sensitive. To our knowledge, this is the first report of using Wadell's method for peptide quantification.

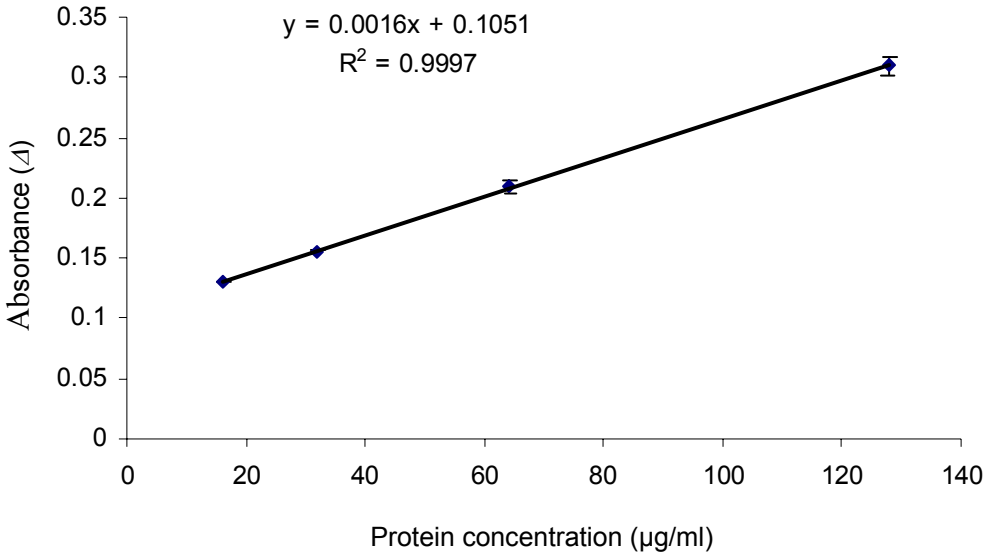

Figure A.3: α-MSH standard curve over a concentration range of 16 to 128 µg/ml. Absorbance Δ, is the difference between the absorbance at 215 and 225 nm (subtracted absorbance).

APPENDIX B

DETAILED GENERAL PROCEDURES

Real-Time RT-PCR Methodology

Outline:

I. Total RNA isolation

II. First strand cDNA synthesis

III. Amplification of target Sequence

IV. Generation of standard curves

V. Melting curve analysis

VI. Real-time PCR

Detailed Procedures

I. Total RNA isolation

A. Materials

TRIZOL Reagent (Invitrogen)

Chloroform

Isopropyl Alcohol

75% Ethanol (in DEPC-treated RNase/DNase Free Water)

DEPC-treated RNase/DNase Free Water

RNase/DNase Free Microcentifuge Tubes

B. Procedure

1. Add 1 ml of TRIZOL Reagent to 6-well plate well.
2. Pass through the pipet a few times to ensure lysis.
3. Place the lysate in a 1.5 ml conical tube and incubate for 5 min at room temperature.
4. Add 200 µl of chloroform to each sample, cap, and shake for 15 sec.
5. Incubate at room temperature for 3 min.
6. Centrifuge samples at 10K for 15 min at room temperature.
7. Remove colorless phase, and place into new tubes.
8. Add 0.5 ml of isopropanol to the colorless phase and mix well.
9. Incubate at room temperature for 10 min.
10. Centrifuge at 10K for 10 min at room temperature.
11. Remove supernatant and discard. Wash with 1 ml 75% ethanol, mix and centrifuge at 10K for 5 min.
12. Remove ethanol, brief dry the RNA pellet and dissolve the RNA in 11 µl RNase/DNase free water and incubate for 10 min at 55°C.

II. First strand cDNA synthesis

Reverse transcription of the first strand cDNA is carried out with the iScript™ cDNA synthesis kit (Bio-Rad). The following procedure is based on the manufacturer's protocol.

1. Prepare the following reaction mixture in each tube:

Components	Volume per reaction
5x iScript reaction mix	4 µl
iScript reverse transcriptase	1 µl
Nuclease-free water	x µl
RNA template (1 µg total RNA)	x µl
Total volume	20 µl

2. Reaction protocol

   Incubate the reaction mixture:

   5 min at 25°C

   30 min at 42°C

   5 min at 85°C

   Hold at 4°C (optional)

III. Amplification of target Sequence

This step is necessary to produce the standard curve to determine the starting quantity of unkown RNA. The reaction is carried out with the Taq recombinant DNA polymerase (Invitrogen). The following procedure is modified from the manufacturer's protocol.

1. Add the following components to a nuclease-free 0.5 ml microcentrifuge tube sitting on ice:

Components	Volume	Final concentraton
10x PCR buffer minus Mg	5 µl	1x
10 mM dNTP mixture	1 µl	0.2 mM each
50 mM $MgCl_2$	1.5 µl	1.5 mM
Forward primer (10 µM)	0.5 µl	0.1 µM
Reverse primer (10 µM)	0.5 µl	0.1 µM
Template DNA	1 µl	n/a
Taq DNA polymerase (5U/µl)	0.1 µl	0.5 U
Nuclease-free water	40.4 µl	n/a
Total volume	50 µl	

2. Incubate the tubes in a thermal cycler at 95°C for 3 min to completely denature the template.
3. Perform 35 cycles of PCR amplification as follows:

Denature	95°C for 30 s
Anneal	55°C for 30 s
Extend	72°C for 1 min

4. Incubate an additional 7 min at 72°C and maintain the reaction at 4°C.

IV. Generation of standard curves

1. Collect the amplified product from step III and determine its concentration by UV spectroscopic reading at 260 nm (A_{260}).
2. Dilute the amplified cDNA in nuclease-free water to a final concentration of 50 nM.

3. Make a series of serial dilutions ranging from 0.1 nM to 0.0001 pM to generate the standard curve.

V. Melting curve analysis

This step is a necessary step to determine the optimal annealing temperatures for the primers of genes of interest. The reaction is carried out with the iQ™ SYBR Green Supermix (Bio-Rad). The following procedure is modified from the manufacturer's protocol.

1. Prepare eight identical real-time PCR reactions for each gene.

Components	Volume	Final concentraton
iQ SYBR Green Supermix	12.5 µl	1x
Forward primer (100 µM)	0.05 µl	0.2 µM
Reverse primer (100 µM)	0.05 µl	0.2 µM
Template DNA	1 µl	n/a
Nuclease-free water	11.4 µl	n/a
Total volume	25 µl	

2. Perform a Two Step Amp + Melt Curve Analysis using the Bio-Rad MyiQ Cycler program. The annealing temperatures for the 8 reactions are 55°C, 56.1°C, 57.9°C, 60.5°C, 64.3°C, 67.1°C, 68.9°C and 70°C respectively.
    a. Incubate the tubes in a thermal cycler at 95°C for 3 min to completely denature the template.
    b. Perform 35 cycles of PCR amplification as follows:

Denature 95°C for 15 s

Anneal 55°C/ +15°C for 30 s

Extend 72°C for 30 s

c. Melting curve analysis was performed immediately after the amplification step under the following conditions:

Denature 95°C for 1 min

Anneal 55°C for 1 min

100 cycles of 0.4°C increments from 55°C to 95°C (10 s each)

3. Visualize Melt Curve to determine the primer binding efficiency and the optimum annealing temperature.

VI. Real-time PCR

1. Prepare real-time PCR reactions for unknown RNA in triplicate and standard RNA in replicate for each gene.

Components	Volume	Final concentraton
iQ SYBR Green Supermix	12.5 µl	1x
Forward primer (100 µM)	0.05 µl	0.2 µM
Reverse primer (100 µM)	0.05 µl	0.2 µM
Template DNA	1 µl	n/a
Nuclease-free water	11.4 µl	n/a
Total volume	25 µl	

2. Perform a Two Step Amp + Melt Curve Analysis using the Bio-Rad MyiQ Cycler program.

    a. Incubate the tubes in a thermal cycler at 95°C for 3 min to completely denature the template.

    b. Perform 35 cycles of PCR amplification as follows:

        Denature 95°C for 30 s

        Anneal optimal annealing temperature for each gene for 30 s

        Extend 72°C for 1 min

    c. Melting curve analysis is performed immediately to confirm that there were no primer dimmers in the PCR reaction under the following conditions:

        73°C for 3 min

        55°C for 1 min

        100 cycles of 0.4°C increments from 55°C to 95°C (10 s each)

3. The starting quantity of unknown RNA was decided with MyiQ™ Single-Color Real-Time PCR detection system.

Immunohistochemistry – Fluorescent Microscopy

Materials:

1x phosphate buffered saline (PBS, Roche)

Triton X-100 (Sigma)

Normal goat serum (Invitrogen)

Procedure:

1. Prepare washing solution: 0.5% triton in 1 x PBS:

   1 L of 1 x PBS + 5 ml of Triton X-100

2. Prepare blocking solution (blocking solution will minimize non-specific binding of antibodies):

   Blocking solution = 4% goat serum in washing solution

3. Prepare primary antibody:

   Primary antibodies are mixed with blocking solution to dilute.

4. Prepare secondary antibody:

   The secondary antibodies used in this research are goat anti-mouse IgG1 Alexa 594 (red), and goat anti-Rabbit IgG (H+L) Alexa 488 (green).

   The secondary antibodies are diluted in blocking solution (1:200).

5. Prepare nuclear dye 4',6-diamidino-2-phenylindole (DAPI, Molecular Probes) solution (cell nuclei marker):

   10 μM DAPI in 1 x PBS

6. Transfer floating tissue sections into the blocking solution for 1 h at room temperature.

7. Remove the blocking solution and add primary antibody without washing procedure. Incubate at 4°C overnight.
8. Wash the tissue sections with washing solution 3 times (10 min each time) on a orbital shaker.
9. Incubated the tissue sections with secondary antibody for 1 h at room temperature in dark.
10. Repeat step 9.
11. Incubate the tissue sections with DAPI solution for 10 – 15 min at room temperature in dark.
12. Wash with 1 x PBS twice.
13. The tissue sections are carefully mounted on glass microscope slides with Fluoromount-G (Southern Biotechnology Associates, Inc. Birmingham AL).

Hemotoxyline and Eosin (H&E) Staining

Reagents for H&E staining:

Xylene

Xylene substitute

Acid Ethanol (1 ml HCl in 200 ml 70% ethanol)

Scott's Solution (2% Magnesium Sulphate, 0.2% Sodium Bicarbonate in water)

Hematoxylin (Poly Scientific)

Eosin (Poly Scientific)

Cytoseal 60 Mounting Medium (Richard-Allan Scientific)

Procedure:

1. Place slides containing frozen sections in a slide holder.
2. Wash slides with water for 2 min
3. Hematoxylin staining:

Hematoxylin	10 sec
Water	1 min
Acid alcohol	1 sec
Water	1 min
95% alcohol	1 min

4. Eosin staining and dehydration:

Eosin	30 sec
95% alcohol	1 min
100% alcohol	1 min

100% alcohol	2 min
100% alcohol	2 min
Xylene substitute	2 min
Xylene substitute	2 min
Xylene	

5. Coverslip slides using Cytoseal 60 Mounting Medium.

REFERENCES

Alonso G., 2005. NG2 proteoglycan-expressing cells of the adult rat brain: possible involvement in the formation of glial scar astrocytes following stab wound. Glia. 49, 318-338.

Asher R.A., Morgenstern D.A., Fidler P.S., Adcock K.H., Oohira A., Braistead J.E., Levine J.M., Margolis R.U., Rogers J.H., Fawcett J.W., 2000. Neurocan is upregulated in injured brain and in cytokine-treated astrocytes. J. Neurosci. 20, 2427-2438.

Batuman O.A., Ferrero A., Cupp C., Jimenez S.A., Khalili K., 1995. Differential regulation of transforming growth factor beta-1 gene expression by glucocorticoids in human T and glial cells. J Immunol. 155(9), 4397-4405.

Biran R., Martin D.C., Tresco P.A., 2005. Neuronal cell loss accompanies the brain tissue response to chronically implanted silicon microelectrode arrays. Exp Neurol. 195, 115-126.

Bjornsson C.S.; Lo C.T.; Smith K.L.; Retterer S.; Isaacson M.; Tuner J.N.; Shain W. *Neural interfaces workshop*, 2003, Washington D.C., USA.

Bohatschek M., Kloss C.U., Kalla R., Raivich G., 2001. In vitro model of microglial deramification: ramified microglia transform into amoeboid phagocytes following addition of brain cell membranes to microglia-astrocyte cocultures. J Neurosci Res. 64(5), 508-522.

Bradbury E.J., Moon L.D., Popat R.J., King V.R., Bennett G.S., Patel P.N., Fawcett J.W., McMahon S.B., 2002. Chondroitinase ABC promotes functional recovery after spinal cord injury. Nature. 416, 636-640.

Bradford M.M., 1976. A rapid and sensitive method for the quantitation of microgram quantities of protein utilizing the principle of protein-dye binding. Anal Biochem. 72:248-254.

Brightman M., 1991. Implication of astroglia in the blood-brain barrier. Ann N Y Acad Sci. 633, 343-347.

Bruccoleri A., Brown H., Harry G.J., 1998. Cellular localization and temporal elevation of tumor necrosis factor-alpha, interleukin-1 alpha, and transforming growth factor-beta 1 mRNA in hippocampal injury response induced by trimethyltin. J. Neurochem. 71, 1577-1587.

Bush T.G., Puvanachandra N., Horner C.H., Polito A., Ostenfeld T., Svendsen C.N., Mucke L., Johnson M.H., Sofroniew M.V. 1999. Leukocyte infiltration, neuronal degeneration, and neurite outgrowth after ablation of scar-forming, reactive astrocytes in adult transgenic mice.Neuron. 23(2), 297-308.

Caleo M., Menna E., Chierzi S., Cenni M.C., Maffei L., 2000. Brain-derived neurotrophic factor is an anterograde survival factor in the rat visual system. Curr Biol. 10(19), 1155-1161.

Camand E, Morel MP, Faissner A, Sotelo C, Dusart I., 2004. Long-term changes in the molecular composition of the glial scar and progressive increase of serotoninergic fibre sprouting after hemisection of the mouse spinal cord. Eur J Neurosci. 20(5), 1161-1176.

Campbell P.K., Jones K.E., Huber R.J., Horch K.W., Normann R.A., Silicon-Based A., 1991. 3-Dimensional neural interface—manufacturing processes for an intracortical electrode array. IEEE Trans Biomed Eng. 38, 758–768.

Chao C.C., Hu S., Close K., Choi C.S., Molitor T.W., Novick W.J., Peterson P.K., 1992. Cytokine release from microglia: differential inhibition by pentoxifylline and dexamethasone. J. Infect. Dis. 166, 847-53.

Chen J.K., Wise K.D., Hetke J.F., Bledsoe S.C., 1997. A multichannel neural probe for selective chemical delivery at the cellular level. IEEE Trans Biomed Eng. 44, 760–769.

Chen Y., Swanson R.A., 2003. Astrocytes and brain injury. J Cereb Blood Flow Metab. 23(2), 137-149.

Chen Z.J., Gillies G.T., Broaddus W.C., Prabhu S.S., Fillmore H., Mitchell R.M., Corwin F.D., Fatouros P.P., 2004. A realistic brain tissue phantom for intraparenchymal infusion studies. J Neurosurg. 101(2), 314-322.

Crossin K.L., Tai M.H., Krushel L.A., Mauro V.P., Edelman G.M., 1997. Glucocorticoid receptor pathways are involved in the inhibition of astrocyte proliferation. Proc. Natl. Acad. Sci. 94(6), 2687-2692.

Cui X., Lee V.A., Raphael Y., Wiler J.A., Hetke J.F., Anderson D.J., Martin D.C., 2001. Surface modification of neural recording electrodes with conducting polymer/biomolecule blends, J Biomed. Mater. Res. 56(2), 261-272.

Cui X., Martin D.C., 2003. Electrochemical deposition and characterization of poly(3,4-ethylenedioxythiophene) on neural microelectrode arrays, Sensors and Acturators B. 89, 92-102.

Cui X., Wiler J., Dzaman M., Altschuler R.A., Martin D.C., 2003. In vivo studies of polypyrrole/peptide coated neural probes. Biomaterials. 24 (5), 777-787.

Cypes S.H., Saltzman W.M., Giannelis E.P., 2003. Organosilicate-polymer drug delivery systems: controlled release and enhanced mechanical properties. J Control Release. 90(2), 163-169.

Davies A.M., 1996. The neurotrophic hypothesis: where does it stand? Philos Trans R Soc Lond B Biol Sci. 351(1338), 389-394.

De Scheerder I., Wang K., Wilczek K., van Dorpe J., Verbeken E., Desmet W., Schacht E., Piessens J., 1996. Local methylprednisolone inhibition of foreign body response to coated intracoronary stents. Coron Artery Dis. 7(2), 161-166.

Delgado R., Carlin A., Airaghi L., Demitri M.T., Meda L., Galimberti D., Baron P., Lipton J.M., Catanina A., 1998. Melanocortin peptides inhibit production of proinflammatory cytokines and nitric oxide by activatied microglia, J Leukoc. Biol. 63 (6), 740-745.

Donoghue, J.P., 2002. Connecting cortex to machines: recent advances in brain interfaces. Nat. Neurosci. 5, Suppl: 1085-1088.

Dougherty K.D., Dreyfus C.F., Black I.B., 2000. Brain-derived neurotrophic factor in astrocytes, oligodendrocytes, and microglia/macrophages after spinal cord injury. Neurobiol Dis. 7(6 Pt B), 574-585.

Doyle A.J., Stewart A.A., Constable P.D., Eurell J.A., Freeman D.E., Griffon DJ., 2005. Effects of sodium hyaluronate and methylprednisolone acetate on proteoglycan synthesis in equine articular cartilage explants. Am J Vet Res. 66(1), 48-53.

Drake K.L., Wise K.D., Farraye J., Anderson D.J., Bement S.L. 1988. Performance of planar multisite microprobes in recording extracellular single-unit intracortical activity. IEEE Trans Biomed Eng. 35, 719–732.

Durany N., Michel T., Kurt J., Cruz-Sanchez F.F., Cervas-Navarro J., Riederer P., 2000. Brain-derived neurotrophic factor and neurotrophin-3 levels in Alzheimer's disease brains.
Int J Dev Neurosci. 18(8):807-813.

Edell, D.J., Toi, V.V., McNeil, V.M., Clark, L.D., 1992. Factors influencing the biocompatibility of insertable silicon microshafts in cerebral cortex. IEEE Trans. Biomed. Eng. 39, 635-643.

Etemad-Moghadam B., Chen H., Yin P., Aziz N., Hedley M.L., 2002. Inhibition of NF-kappaB activity by plasmid expressed alphaMSH peptide. J Neuroimmunol. 125(1-2), 23-29.

Faulkner J.R., Herrmann J.E., Woo M.J., Tansey K.E., Doan N.B., Sofroniew M.V., 2004. Reactive astrocytes protect tissue and preserve function after spinal cord injury. J Neurosci. 24(9), 2143-2155.

Fawcett, J.W., Asher R.A., 1999. The glial scar and central nervous system repair. Brain Res. Bull. 49, 377-391.

Fitch M.T., Silver J., 1997. Activated macrophages and the blood-brain barrier: inflammation after CNS injury leads to increase in putative inhibitory molecules. Exp. Neurol. 148, 587-603.

Fournier E., Passirani C., Montero-Menei C.N., Benoit J.P., 2003. Biocompatibility of implantable synthetic polymeric drug carriers: focus on brain biocompatibility, Biomaterials. 24, 3311-3331.

Friedman B., Kleinfeld D., Ip N.Y., Verge V.M., Moulton R., Boland P., Zlotchenko E., Lindsay R.M., Liu L., 1995. BDNF and NT-4/5 exert neurotrophic influences on injured adult spinal motor neurons. J Neurosci. 15(2), 1044-1056.

Galimberti D., Baron P., Meda L., Prat E., Scarpini E., Delgado R., Catania A., Lipton J.M., Scarlato G., 1999. α-MSH peptides inhibit production of nitric oxide and tumor necrosis factor-α by microglial cells activated with β-amyloid and interferon γ, Biochem. Biophys. Res. Commun. 263 (1), 251-256.

Ganter S., Northoff H., Mannel D., Gebicke-Harter P.J., 1992. Growth control of cultured microglia. J Neurosci Res. 33(2), 218-230.

Gilbert R.J., McKeon R.J., Darr A., Calabro A., Hascall V.C., Bellamkonda R.V., 2005. CS-4,6 is differentially upregulated in glial scar and is a potent inhibitor of neurite extension. Mol. Cell Neurosci. 29, 545-558.

Giulian D., Baker T.J., 1986. Characterization of ameboid microglia isolated from developing mammalian brain. J. Neurosci. 6, 2163-2178.

Golde S., Coles A., Lindquist J.A., Compston A., 2003. Decreased iNOS synthesis mediates dexamethasone-induced protection of neurons from inflammatory injury *in vitro*. Eur. J. Neurosci. 18, 2527-2537.

Hampton D.W., Rhodes K.E., Zhao C., Franklin R.J.M., Fawcett J.W., 2004. The responses of oligodendrocyte precursor cells, astrocytes and microglia to a cortical stab injury, in the brain. Neurosci. 127, 813-820.

Handman E., Jarvis H.M., 1985. Nitrocellulose-based assays for the detection of glycolipids and other antigens: mechanism of binding to nitrocellulose, J Immunol. Methods. 83, 113-123.

Harlow E. and Lane D., Antibodies: A Laboratory Manual, Cold Spring Harbor, NY: Cold Spring Harbor laboratories, 1988.

Hays S.J., 1998. Therapeutic approaches to the treatment of neuroinflammatory diseases. Curr. Pharm. Des. 4, 335-348.

Henze D.A, Borhegyi Z., Csicsvari J., Mamiya A., Harris K.D., Buzsaki G., 2000. Intracellular features predicted by extracellular recordings in the hippocampus *in vivo*. J. Neurophysiol. 84, 390-400.

Hermens W.T., Verhaagen J., 1998. Suppression of inflammation by dexamethasone prolongs adenoviral vector-mediated transgene expression in the facial nucleus of the rat. Brain. Res. Bull. 47, 133-140.

Hetke J.F., Anderson D.J., 2002. Silicon microelectrodes for extracellular recording. In Handbook of Neuroprosthetic Methods, ed. WE Finn, PG LoPresti, 7:163–91. Boca Raton, FL: CRC

Holmin S., Mathiesen T., 1996. dexamethasone and colchicine reduce inflammation and delayed oedema following experimental brain contusion. Acta. Neurochir. 138, 418-424.

Houle J.D., Johnson J.E., 1989. Nerve growth factor (NGF)-treated nitrocellulose enhances and directs the regeneration of adult rat dorsal root axons through intraspinal neural tissue transplants, Neurosci. Lett. 103(1), 17-23.

Houle J.D., Ziegler M.K.,1994. Bridging a complete transection lesion of adult rat spinal cord with growth factor-treated nitrocellulose implants, J Neural Transplant. Plast. 5(2), 115-124.

Huang Y., Wang L., Verweire I., Qiang B., Liu X., Verbeken E., Schacht E., De Scheerder I., 2002. Optimization of local methylprednisolone delivery to inhibit inflammatory reaction and neointimal hyperplasia of coated coronary stents. J Invasive Cardiol. 14(9), 505-513.

Ichiyama T., Lipton J.M., 1999. Autocrine α-melanocyte-stimulating hormone inhibits NF-κB activation in human glioma. J Neurosci. Res. 58, 684-689.

Jaeger C.B., Blight A.R., 1997. Spinal cord compression injury in guinea pigs: structural changes of endothelium and its perivascular cell associations after blood-brain barrier breakdown and repair. Exp Neurol. 144(2), 381-399.

Jain A., Kim Y.T., McKeon R.J., Bellamkonda R.V., 2006. In situ gelling hydrogels for conformal repair of spinal cord defects, and local delivery of BDNF after spinal cord injury. Biomaterials. 27(3), 497-504.

Janeczko K., 1993 Co-expression of GFAP and vimentin in astrocytes proliferating in response to injury in the mouse cerebral hemisphere. A combined autoradiographic and double immunocytochemical study. Int J Dev Neurosci. 11(2), 139-147.

John G.R., Lee S.C., Brosnan C.F., 2003. Cytokines: powerful regulators of glial cell activation. Neuroscientist. 9(1), 10-22.

John G.R., Lee S.C., Song X., Rivieccio M., Brosnan C.F., 2005. IL-1-regulated responses in astrocytes: relevance to injury and recovery. Glia. 49, 161-176.

Jones K.E., Campbell P.K., Normann R.A., 1992. A glass/silicon composite intracortical electrode array. Ann. Biomed. Eng. 20, 423–437

Jones L.L., Kreutzberg G.W., Raivich G., 1998. Transforming growth factor beta's 1, 2 and 3 inhibit proliferation of ramified microglia on an astrocyte monolayer. Brain Res. 795(1-2), 301-306.

Jones L.L., Yamaguchi Y., Stallcup W.B., Tuszynski M.H., 2002. NG2 is a major chondroitin sulfate proteoglycan produced after spinal cord injury and is expressed by macrophages and oligodendrocyte progenitors. J. Neurosci. 22, 2792-2803.

Joosten E.A., Houweling D.A., 2004Local acute application of BDNF in the lesioned spinal cord anti-inflammatory and anti-oxidant effects. Neuroreport. 15(7):1163-1166.

Kaal E.C., Vecht C.J. 2004. The management of brain edema in brain tumors. Curr. Opin. Oncol. 16, 593-600.

Kato H., Walz W. 2000. The initiation of the microglial responses. Brain Pathol. 10, 137-143.

Kewley D.T., Hills M.D., Borkholder D.A., Opris I.E., Maluf N.I., Storment C.W., et al. 1997. Plasma-etched neural probes. Sens Actuators A-Phys. 58,27–35.

Kim J.M., Son D., Lee P., Lee K.J., Kim H., Kim S.Y., 2003. Ethyl acetate soluble fraction of cnidium officinale MAKINO inhibits neuronal cell death by reduction of excessive nitrite oxide production in lipopolysaccharide-treated rat hippocampal slice cultures and microglia cells, J. Pharmacol. Sci. 92, 74-78.

Kim D.H., Martin D.C., 2006. Sustained release of dexamethasone from hydrophilic matrices using PLGA nanoparticles for neural drug delivery. Biomaterials. 27(15):3031-3037.

Kipke D.R., Vetter R.J., Williams J.C., Hetke J.F., 2003. Silicon-substrate intracortical microelectrode arrays for long-term recording of neuronal spike activity in cerebral cortex. IEEE Trans. Neural. Syst. Rehabil. Eng.. 11, 151-155.

Koehler P.J. 1995. Use of corticosteroids in neuro-oncology. Anticancer Drugs. 6, 19-33.

Kralik J.D., Dimitrov D.F., Krupa D.J., Katz D.B., Cohen D., Nicolelis M.A.L., 2001. Techniques for long-term multisite neuronal ensemble recordings in behaving animals. Methods. 25:121–50.

Kyrkanides S., O'Banion M.K., Whiteley P.E., Daeschner J.C., Olschowka J.A., 2001. Enhanced glial activation and expression of specific CNS inflammation-related molecules in aged versus young rats following cortical stab injury. J. Neuroimmunol. 119, 269-277.

Lagenaur C., Lemmon V., 1987. An L1-like molecule, the 8D9 antigen, is a potent substrate for neurite extension, Proc. Natl. Acad. Sci. 84(21), 7753-7757.

Lee S.C., Dickson D.W., Brosnan C.F., 1995. Interleukin-1, nitric oxide and reactive astrocytes. Brain Behav Immun. 9(4), 345-54.

Leung B.K., Williamson T.P., Chen X.K., Pollock A.L., Tresco P.A, Brain tissue reaction surrounding planar silicon penetrating microelectrode arrays varies as a function of depth in the rat cerebral cortex. *Society for Neuroscience Annual Meeting*, 2006, Atlanta, USA.

Levine J.M, Reynolds R., Fawcett J.W. 2001. The oligodendrocyte precursor cell in health and disease. Trends Neurosci. 24, 39-47.

Liberto C.M., Albrecht P.J., Herx L.M., Yong V.W., Levison S.W., 2004. Pro-regenerative properties of cytokine-activated astrocytes, J Neurochem. 89 (5), 1092-1100.

Lindsay R.M., 1996. Role of neurotrophins and trk receptors in the development and maintenance of sensory neurons: an overview. Philos Trans R Soc Lond B Biol Sci. 351(1338), 365-373.

Lipton J.M., Catania A.P., 1997. Anti-inflammatory actions of the neuro-immunomodulator α-MSH. Immunol. Today. 18(3), 140-145.

Lipton J.M., Zhao H., Ichiyama T., Barsh G.S., Catanina A., 1999. Mechanisms of anti-inflammatory action of α-MSH peptides. In vivo and in vitro evidence, Ann. N. Y. Acad. Sci. 20, 173-182.

Liu X., McCreery D.B., Carter R.R., Bullara L.A., Yuen T.G., Agnew W.F., 1999. Stability of the interface between neural tissue and chronically implanted intracortical microelectrodes. IEEE Trans. Rehabil. Eng. 7, 315-326.

Logan A., Berry M., 1993. Transforming growth factor-beta 1 and basic fibroblast growth factor in the injured CNS. Trends Pharmacol Sci. 14(9), 337-342.

Logan A., Berry M., Gonzalez A.M., Frautschy S.A., Sporn M.B., Baird A., 1994. Effects of transforming growth factor beta 1 on scar production in the injured central nervous system of the rat. Eur J Neurosci. 6(3), 355-363.

Logan A., Berry M., 2002. Cellular and molecular determinants of glial scar formation. In: Alzheimer C., Molecular and cellular biology of neuroprotection in the CNS. Kluwer Academic, pp. 115-137.

Ludwig K.A., Uram J.D., Yang .J, Martin D.C., Kipke D.R., 2006. Chronic neural recordings using silicon microelectrode arrays electrochemically deposited with a poly(3,4-ethylenedioxythiophene) (PEDOT) film. J. Neural. Eng. 3(1), 59-70.

Luger T.A., Schwarz T., Kalden H., Scholzen T., Schwarz A., Brzoska T., 1999. Role of epidermal cell-derived alpha-melanocyte stimulating hormone in ultraviolet light mediated local immunosuppression. Ann N Y Acad Sci. 885, 209-216.

Manna S.K., Aggarwal B.B., 1998. Alpha-melanocyte-stimulating hormone inhibits the nuclear transcription factor NF-kappa B activation induced by various inflammatory agents. J Immunol. 161(6), 2873-2880.

McGraw J.,. Hiebert G.W, Steeves J.D., 2001. Modulating astrogliosis after neruotrauma, J Neurosci. Res. 63 (2), 109-115.

McKeon R.J., Jurynec M.J.,Buck C.R., 1999. The chondroitin sulfate proteoglycans neurocan and phosphacan are expressed by reactive astrocytes in the chronic CNS glial scar. J Neurosci. 19(24), 10778-10788.

McMillian M.K., Thai L., Hong J.S., O'Callaghan J.P., Pennypacker K.R., 1994. Brain injury in a dish: a model for reactive gliosis. Trends Neurosci. 17(4), 138-142.

Meilander N.J., Yu X., Ziats N.P., Bellamkonda R.V., 2001. Lipid-based microtubular drug delivery vehicles. J Control Release. 71(1), 141-52.

Merrill J.E., Benveniste E.N., 1996. Cytokines in inflammatory brain lesions: helpful and harmful. Glia. 19, 331-338.

Mizuno T., Kuno R., Nitta A., Nabeshima T., Zhang G., Kawanokuchi J., Wang J., Jin S., Takeuchi H., Suzumura A., 2005 Protective effects of nicergoline against neuronal cell death induced by activated microglia and astrocytes. Brain Res. 1066(1-2), 78-85.

Moon L.D., Fawcett J.W., 2001. Reduction in CNS scar formation without concomitant increase in axon regeneration following treatment of adult rat brain with a combination of antibodies to TGFbeta1 and beta2. Eur J Neurosci. 14(10), 1667-1677.

Morel MP, Dusart I, Sotelo C., 2002. Sprouting of adult Purkinje cell axons in lesioned mouse cerebellum: "non-permissive" versus "permissive" environment. J Neurocytol. 31(8-9), 633-647.

Moxon K.A., Leiser S.C., Gerhardt G.A., Barbee K.A., Chapin J.K., 2004. Ceramic-based multisite electrode arrays for chronic single-neuron recording. IEEE Trans Biomed Eng. 51, 647–656.

Murphy J.B., Kies M.W., 1960. Notes on spectrophotometric determination of proteins in dilute solutions. Biochim. Biophy. Acta. 45, 382-384.

Neuhaus J., Risau W., Wolburg H., 1991. Induction of blood-brain barrier characteristics in bovine brain endothelial cells by rat astroglial cells in transfilter coculture. Ann N Y Acad Sci. 633, 578-580.

Nicolelis M.A., Ghazanfar A.A., Faggin B.M., Votaw S., Oliveira L.M., 1997. Reconstructing the engram: simultaneous, multisite, many single neuron recordings. Neuron. 18(4), 529-537.

Nicolelis M.A.L., Stambaugh C.R., Brisben A., Laubach M., 1999. Methods for simultaneous multisite neural ensemble recordings in behaving primates. In Methods for Neural Ensemble Recordings, ed. MAL Nicolelis, 7:121–56. Boca Raton, FL: CRC

Nicolelis M.A., Dimitrov D., Camena J.M., Crist R., Lehew G., et al. 2003. Chronic, multisite, multielectrode recordings in macaque monkeys. Proc. Natl. Acad. Sci. USA 100, 11041–11046

Nordhausen C.T., Maynard E.M., Normann R.A., 1996. Single unit recording capabilities of a 100 microelectrode array. Brain Res. 726(1-2), 129-140.

Norton W.T., 1999. Cell reactions following acute brain injury: a review. Neurochem. Res. 24, 213-218.

Oktar B.K., Alican I., 2002. Modulation of the peripheral and central inflammatory responses by alpha-melanocyte stimulating hormone. Curr Protein Pept Sci. 3(6), 623-628.

O'Neill L.A., Kaltschmidt C., 1997. NF-kappa B: a crucial transcription factor for glial and neuronal cell function. Trends Neurosci. 20(6),252-258.

Otto, K.J., Vetter, R.J., Marzullo T.C., Kipke D.R., 2003. Brain-machine interfaces in rat motor cortex. Proceedings of the 1st international IEEE EMBS Conference on Neural Engineering. Capri Island, Italy.

Papargeorgiou D., Bledsoe S.C., Gulari M., Hetke J.F., Anderson D.J., Wise K.D., 2001. A shuttered probe with in-line flowmeters for chronic in vivo drug delivery. In Proc. 14th IEEE Int. Conf. Micro. Electro. Mechanical Systems. (MEMS 2001), 212-215.

Pesaran B., Musallam S., Andersen R.A., 2006. Cognitive neural prosthetics. Curr Biol. 16(3), R77-80.

Polikov V.S., Tresco P.A., Reichert W.M., 2005. Response of brain tissue to chronically implanted neural electrodes. J. Neurosci. Methods. 148, 1-18.

Polishchuk A.Y., Zaikov G.E., Transport devices for controlled delivery, in: Multicomponent transport in polymer systems for controlled release, Gordon and breach science publishers, 1997, pp. 107-140.

Prior M.J., Brown A.M., Mavroudis G., Lister T., Ray D.E., 2004. MRI characterisation of a novel rat model of focal astrocyte loss. MAGMA. 17(3-6), 1251-32.

Properzi F., Asher R.A., Fawcett J.W., 2003. Chondroitin sulphate proteoglycans in the central nervous system: changes and synthesis after injury. Biochem. Soc. Trans. 31, 335-336.

Properzi F., Fawcett J.W., 2004. Proteoglycans and brain repair. News Physiol. Sci. 19, 33-38.

Raghavendra V., Tanga F., DeLeo J.A., 2003. Inhibition of Microglial Activation Attenuates the Development but Not Existing Hypersensitivity in a Rat Model of Neuropathy. J. Pharmacol. Exp. Ther. 306(2), 624-630.

Rathnasingham R., Kipke D.R., Bledsoe S.C. Jr, McLaren J.D., 2004. Characterization of implantable microfabricated fluid delivery devices. IEEE Trans Biomed Eng. 51(1), 138-145.

Retterer S.T., Smith K.L., Bjornsson C.S., Neeves K.B., Spence A.J., Turner J.N., Shain W., Isaacson M.S., 2004. Model neural prostheses with integrated microfluidics: a potential intervention strategy for controlling reactive cell and tissue responses. IEEE Trans Biomed Eng. 51, 2063-73.

Ridet J.L., Malhotra S.K., Privat A., Gage F.H., 1997. Reactive astrocytes: cellular and molecular cues to biological function. Trends Neurosci. 20(12), 570-577.

Robinson D.A., 1968. The electrical properties of metal microelectrodes, P IEEE. 56 (6), 1065-1071.

Richards J.H., The role of polymer permeability in the control of drug release, in: J. Comyn (Ed.), Polymer permeability, Elsevier applied science publishers, London and New York, 1985, pp. 217-268.

Ross J.D., O'Connor S.M, Blum R.A., Brown E.A., DeWeerth S.P., Multielectrode impedance tuning: reducing noise and improving stimulation efficacy. 26th Annual International Conference IEEE Engineering in Medicine and Biology Society (EMBS), September, 2004.

Rousche P.J., Normann R.A. 1998. Chronic recording capability of the Utah Intracortical Electrode Array in cat sensory cortex. J Neurosci Methods. 82, 1–15.

Rousche P.J., Pellinen D.S., Pivin D.P., Williams J.C., Vetter R.J., Kipke D.R., 2001. Flexible polyimide-based intracortical electrode arrays with bioactive capability. IEEE Trans Biomed Eng. 48, 361–371.

Salminen A., Liu P.K., Hsu C.Y., 1995. Alteration of transcription factor binding activities in the ischemic rat brain. Biochem Biophys Res Commun. 212(3), 939-944.

Saltzman W.M., Mak M.W., Mahoney M.J., Duenas E.T., Cleland J.L., 1999. Intracranial delivery of recombinant nerve growth factor: release kinetics and protein distribution for three delivery systems. Pharm Res. 16(2), 232-40.

Saltzman W.M., Drug delivery systems, in: Drug delivery engineering principles for drug therapy, Oxford university press, 2001, pp. 236-258.

Sanchez J.C., Carmena J.M., Lebedev, M.A., Nicolelis M.A.L., Harris J.G., Principle J.C., 2004. Ascertaining the importance of neurons to develop better brain-machine interfaces. IEEE Trans. Biomed. Eng. 51, 943-953.

Santhanam G., Ryu S.I., Yu B.M., Afshar A., Shenoy K.V., 2006. A high-performance brain-computer interface. Nature. 442, 195-198.

Sapan C.V., Lundblad R.L., Price N.C., 1999. Colorimetric protein assay techniques. Biotechnol Appl Biochem. 29, 99-108.

Schneider A., Stieglitz T., 2004. Implantable flexible electrodes for functional electrical stimulation. Med Device Technol. 15(1), 16-18.

Schreyer D.J., Jones E.G., 1987. Growth of corticospinal axons on prosthetic substrates introduced into the spinal cord of neonatal rats, Dev. Brain Res. 35, 291-299.

Schwartz A.B., 2004. Cortical neural prosthetics. Annu. Rev. Neurosci. 27, 487-507.

Shain W., Spataro L., Dilgen J., Haverstick K., Retterer S., Isaacson M., Saltzman M., Turner J.N., 2003. Controlling cellular reactive responses around neural prosthetic devices using peripheral and local intervention strategies. IEEE Trans. Neural. Syst. Rehabil. Eng. 11, 186-188.

Singh A., Ehteshami G., Massia S., He J.P., Storer R.G., Raupp G., 2003. Glial cell and fibroblast cytotoxicity study on plasma-deposited diamond-like carbon coatings. Biomaterials. 24, 5083–5089.

Slepko N., Levi G., 1996. Progressive activation of adult microglial cells in vitro. Glia. 16(3), 241-246.

Smith G.M., Strunz C., 2005. Growth factor and cytokine regulation of chondroitin sulfate proteoglycans by astrocytes. Glia. 52(3), 209-218.

Smoak K.A., Cidlowski J.A., 2004. Mechanisms of glucocorticoid receptor signaling during inflammation. Mech Ageing Dev. 125, 697-706.

Snow D.M., Lemmon V., Carrino D.A. , Caplan A.I., Silver J., 1990. Sulfated proteoglycans in astroglial barriers inhibit neurite outgrowth in vitro, Exp. Neurol. 109(1), 111-130.

Sola C., Casal C., Tusell J.M., Serratosa J., 2002. Astrocytes enhance lipopolysaccharide-induced nitric oxide production by microglial cells. Eur J Neurosci. 16(7), 1275-1283.

Spataro L., Dilgen J., Retterer S., Spence A.J., Isaacson M., Turner J.N., Shain W., 2005. dexamethasone treatment reduces astroglia responses to inserted neuroprosthetic devices in rat neocortex. Exp. Neurol. 194, 289-300.

Star R.A., Rajora N., Huang J., Stock R.C., Catania A., Lipton J.M. 1995. Evidence of autocrine modulation of macrophage nitric oxide synthase by alpha-melanocyte-stimulating hormone. Proc Natl Acad Sci U S A. 92(17), 8016-8020.

Starowicz K., Przewlocka B., 2003. The role of melanocortins and their receptors in inflammatory processes, nerve regeneration and nociception. Life Sci. 73(7), 823-847.

Stence N., Waite M., Dailey M.E., 2001. Dynamics of microglial activation: a confocal time-lapse analysis in hippocampal slices. Glia. 33(3), 256-266.

Szarowski D.H., Andersen M.D., Retterer S., Spence A.J., Isaacson M., Craighead H.G., Turner J.N., Shain W. 2003. Brain responses to micro-machined silicon devices. Brain Res. 983, 23-35.

Takeuchi A., Miyaishi O., Kiuchi K., Isobe K., 2001. Macrophage colony-stimulating factor is expressed in neuron and microglia after focal brain injury. J. Neurosci. Res. 65, 38-44.

Tanaka J., Fujita H., Matsuda S., Toku K., Sakanaka M., Maeda N., 1997. Glucocorticoid- and mineralocorticoid receptors in microglial cells: the two receptors mediate differential effects of corticosteroids. Glia. 20, 23-37.

Tang X., Davies J.E., Davies S.J.A., 2003. Changes in distribution, cell associations, and protein expression levels of NG2, neurocan, phosphacan, brevican, versican V2, and tenascin-C during acute to chronic maturation of spinal cord scar tissue. J. Neurosci. Res. 71, 427-444.

Tatsumi K., Haga S., Matsuyoshi H., Inoue M., Manabe T., Makinodan M., Wanaka A., 2005. Characterization of cells with proliferative activity after a brain injury. Neurochem. Int. 46, 381-389.

Tijssen P., 1993. Practice and Theory of Immunoassays, in: Laboratory Techniques in Biochemistry and molecular biology, 8th edition, Amsterdam, The Netherlands: Elsevier.

Tobias C.A., Han S.S., Shumsky J.S., Kim D., Tumolo M., Dhoot N.O., Wheatley M.A., Fischer I., Tessler A., Murray M., 2005. Alginate encapsulated BDNF-producing fibroblast grafts permit recovery of function after spinal cord injury in the absence of immune suppression. J Neurotrauma. 22(1), 138-156.

Toulmond S., Parnet P., Linthorst A.C., 1996. When cytokines get on your nerves: cytokine networks and CNS pathologies. Trends Neurosci. 19(10), 409-410.

Turner J.N., Shain W., Szarowski D.H., Andersen M., Martins S., Isaacson M., Craighead H., 1999. Cerebral astrocyte response to micromachined silicon implants. Exp Neurol. 156, 33-49.

Twycross R. 1994. The risks and benefits of corticosteroids in advanced cancer. Drug Saf. 11, 163-178.

Ughrin Y.M, Chen Z.J., Levine J.M., 2003. Multiple regions of the NG2 proteoglycan inhibit neurite growth and induce growth cone collapse. J. Neurosci. 23, 175-186.

Unsicker K., Strelau J., 2000. Functions of transforming growth factor-beta isoforms in the nervous system. Cues based on localization and experimental in vitro and in vivo evidence. Eur J Biochem. 267(24), 6972-6975.

Vetter R.J., Williams J.C., Hetke J.F., Nunamaker E.A., Kipke D.R., 2004. Chronic neural recording using silicon-substrate microelectrode arrays implanted in cerebral cortex. IEEE Trans Biomed Eng. 51(6), 896-904.

Vielmetter J., Stolze B., Bonhoeffer F., Stuermer C.A., 1990. In vitro assay to test differential substrate affinities of growing axons and migratory cells. Exp. Brain Res. 8, 283-287.

Waddell W.J., 1956. A simple ultraviolet spectrophotometric method for the determination of protein. J Lab Clin Med. 48(2), 311-314.

Wadhwa R., Lagenaur C.F., Cui X.T., 2006. Electrochemically controlled release of dexamethasone from conducting polymer polypyrrole coated electrode. J Control Release. 110(3), 531-541.

Wallis C., Melnick J.L., Gerba C.P., 1979. Concentrations of viruses from water by membrane chromatography, Annu. Rev. Microbio. 33, 413-437.

Williams J.C., Rennaker R.L., Kipke D.R., 1999. Long-term neural recording characteristics of wire microelectrode arrays implanted in cerebral cortex. Brain Res. Brain Res Protoc. 4(3), 303-13

Williams J.C. 2001. Performance of chronic neural implants: measurement, modeling and intervention strategies. PhD thesis. Ariz. State Univ.

Wolf P., 1983. A critical reappraisal of Waddell's technique for ultraviolet spectrophotometric protein estimation. Anal. Biochem. 129, 145-155.

Wong M.W., Tang Y.Y., Lee S.K., Fu B.S., 2005. Glucocorticoids suppress proteoglycan production by human tenocytes. Acta Orthop. 76(6), 927-31.

Wu V.W., Schwartz J.P., 1998. Cell culture models for reactive gliosis: new perspectives. J Neurosci Res. 51(6), 675-681.

Yamazaki T., Tukiyama T., Tokiwa T., 2005. Effect of dexamethasone on binding activity of transcription factors nuclear factor-kappaB and activator protein-1 in SW982 human synovial sarcoma cells. In Vitro Cell Dev Biol Anim. 41(3-4), 80-82.

Yang K., Mu X.S., Hayes R.L., 1995.Increased cortical nuclear factor-kappa B (NF-kappa B) DNA binding activity after traumatic brain injury in rats. Neurosci Lett. 197(2),101-104.

Zhong Y., McConnell G.C., Ross J.D., DeWeerth S.P., Bellamkonda R.V., 2005. A novel dexamethasone -releasing, anti-inflammatory coating for neural implants. Proceedings of the 2nd international IEEE EMBS Conference on Neural Engineering. Arlington, USA. 522-525.

Zhong Y., Bellamkonda R.V., 2005. Controlled release of anti-inflammatory agent alpha-MSH from neural implants. J Control Release. 106(3), 309-318.